



YAŞAR UNIVERSITY
GRADUATE SCHOOL OF NATURAL AND APPLIED SCIENCES

MASTER'S THESIS

**DESIGN AND MANUFACTURING OF A FEED SYSTEM
FOR KU BAND SATELLITE COMMUNICATION**

MUSTAFA EMRE ÇARKACI

THESIS ADVISOR: ASSOC. PROF. DR. MUSTAFA SEÇMEN

ELECTRICAL AND ELECTRONICS ENGINEERING

PRESENTATION DATE: 28.08.2018

BORNOVA / İZMİR
AUGUST 2018

We certify that we have read this thesis and that in our opinion it is fully adequate, in scope and in quality, as a thesis for the degree of Master of Science.

Jury Members:

Signature:

Assoc. Prof. Dr. Mustafa SEÇMEN
(Supervisor)

Yaşar University



Asst. Prof. Dr. Nalan ÖZKURT

Yaşar University

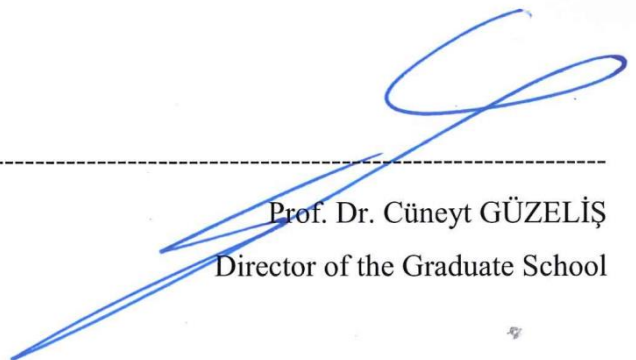


Prof. Dr. Korkut YEĞİN

Ege University



Prof. Dr. Cüneyt GÜZELİŞ
Director of the Graduate School



ABSTRACT

DESIGN AND MANUFACTURING OF A FEED SYSTEM FOR KU BAND SATELLITE COMMUNICATION

Çarkacı, Mustafa Emre

M.Sc., Electrical and Electronics Engineering

Advisor: Assoc. Prof. Dr. Mustafa SEÇMEN

August 2018

In this thesis, the design and realization of two critical components for the reflector antenna feeding system used for satellite communication or broadcasting applications are explained. One of these components is wide-band corrugated conical horn antenna that is commonly used in telemetry, satellite tracking, radar and remote sensing systems, and it is used as a direct radiator antenna in broadband measurements. The second one is a 3-port waveguide diplexer design which allows working of an antenna as receiver and transmitter simultaneously in different frequencies. The system works in Ku frequency band which is commonly preferred for satellite communication.

The antenna is designed with the circular to rectangular WR-62 waveguide transition structure to provide matching to diplexer and also it operates in 10-19 GHz frequency band and has a high return loss value of better than 20 dB and an antenna gain of 14.5-20 dBi within the given band.

The diplexer is designed to operate for the frequency band of 10.5-12.75 GHz at RX (receiving) band and 17.3-18.4 GHz at TX (transmit) band. The common port (feeding to antenna) and TX port of the structure have WR-62 rectangular waveguide and RX port has WR-75 rectangular waveguide cross sections. These ports are combined at T-junction by passing from transition sections. Possible to use in case of need, three different versions of the proposed diplexer are designed, simulated and implemented. The first one is the H-plane diplexer with vertical polarization and the second is the horizontal polarized E-plane diplexer. Finally, a dual-polarized diplexer that works both vertically and horizontally polarized is designed. The designed diplexers have better reflection loss than 15 dB in the RX and TX arms and isolation

values around 60-75 dB. At the same time, the designs have a good insertion loss value.

Regarding to manufacturing, one of the most important objectives of the thesis is to use three dimensional (3-D) printing technology and conductive spray coating method, which makes the prototypes of the designed structures much cheaper and produces in a shorter time than CNC manufacturing. Along with the results, it has been proven that the verification of the designs is also possible with this method.

Key Words: Satellite communication, direct broadcasting, reflector feeding, corrugated conical horn antenna, diplexer, Ku-Band, 3D printing technology



ÖZ

KU BAND UYDU HABERLEŞMESİ İÇİN BESLEME SİSTEMİ TASARIMI VE ÜRETİMİ

Çarkacı, Mustafa Emre

Yüksek Lisans Tezi, Elektrik Elektronik Mühendisliği

Danışman: Doç. Dr. Mustafa SEÇMEN

Ağustos 2018

Bu tezde, uydu haberleşme ya da medya yayıncılıkta kullanılmak üzere, reflektör besleme sisteminin birbirine entegre en önemli iki parçanın tasarımı, ölçümleri ve üretiminden bahsedilmektedir. Bunlardan biri, haberleşme, uydu takip, radar ve uzaktan algılama sistemlerinde yaygın olarak tercih edilen ve geniş bant ölçümlerinde doğrudan bir verici anten olarak da kullanılabilen oluklu konik boynuz (horn) antenin tasarımı, diğeri ise sistemdeki antenin, farklı frekanslarda, aynı anda hem alıcı hem de verici olarak kullanılmasını sağlayan ve bir frekans ayırıcı olan 3 girişli dalga kılavuzu çiftleyici (diplexer) tasarımıdır. Sistemde çalışma bandı olarak, uydu haberleşmede yaygın olarak tercih edilen Ku frekans bandı kullanılmaktadır.

Tasarlanan çiftleyici, RX (alım) bandında 10.5-12.75 GHz frekanslarında, TX (iletim) bandında ise 17.3-18.4 GHz frekanslarında çalışmaktadır. Yapının anteni besleyen ortak girişi ve TX girişi WR-62 dikdörtgen dalga kılavuzu boyutlarında olup, RX girişi WR-75 dalga kılavuzu boyutlarındadır. Bu üç girişin bulunduğu iletim hatları bir T-junction yapısı ve geçişler ile birleştirilmiştir. Önerilen çiftleyicinin, ihtiyaçlara göre kullanılabilen, farklı polarizasyonlarda üç versiyonu tasarlanmıştır. Bunlardan ilki dikey polarizasyonlu olan H-plane çiftleyici olup, ikincisi yatay polarize E-plane çiftleyicidir. Son olarak da hem yatay hem de dikey polarize çalışan (dual-polarized) çiftleyici tasarlanmıştır. Tasarlanan çiftleyicinin, RX ve TX bandındaki geri yansıma kayıpları 15 dB'den daha iyi olup, izolasyon değerleri 60-75 dB dolaylarındadır. Aynı zamanda tasarımlar iyi bir araya girme kaybı değerine sahiptir.

Anten, çiftleyici ile uyumlu hale gelmesi için daireselden dikdörtgen WR-62 dalga kılavuzuna geçişi sağlayan bir yapı ile birlikte tasarlanmıştır ve 10-19 GHz frekans bandında çalışmakta olup, 15 dB'den yüksek geri yansıma kaybı değerine ve bant boyunca 14.5-20 dBi kazanç değerlerine sahiptir.

Üretim için tezin önemli amaçlarından biri de, tasarlanan yapıların prototiplerinin CNC ile üretime kıyasla çok daha ucuz ve kısa sürede üretimini sağlayan üç boyutlu (3-D) baskı teknolojisi ve iletken spreyle kaplama yöntemi kullanılmasıdır. Alınan sonuçlarla birlikte, bu yöntemle de tasarımların doğrulanmasının mümkün olduğu kanıtlanmıştır.

Anahtar Kelimeler: Uydu haberleşmesi, medya yayıncılık, reflektör besleme, oluklu konik boynuz anten, diplexer, Ku-Bant, 3B baskı teknolojisi



ACKNOWLEDGEMENTS

I would first like to thank my supervisor Assoc. Prof. Dr. Mustafa SEÇMEN for his endless patience and guidance during our study.

I would also like to thank Prof. Dr. Korkut YEĞİN and SVS Telekom to present me the chance of carrying out a project in this area.

I would also like to thank Asst. Prof. Dr. Nalan ÖZKURT for contributing to the evaluation of this thesis.

I would like to express my enduring love to my parents, who are always devoted and supportive to me in my life.

I would like to special thank to Göksenin BOZDAĞ for his helps during the measurements of antenna radiation patterns in this study.

Finally, I would like to thank the members of Ege University RF/Microwave and Radar Research Group for their supports and helps.

Mustafa Emre ÇARKACI

İzmir, 2018

TEXT OF OATH

I declare and honestly confirm that my study, titled “DESIGN AND MANUFACTURING OF A FEED SYSTEM FOR KU BAND SATELLITE COMMUNICATION” and presented as a Master’s Thesis, has been written without applying to any assistance inconsistent with scientific ethics and traditions. I declare, to the best of my knowledge and belief, that all content and ideas drawn directly or indirectly from external sources are indicated in the text and listed in the list of references.

Mustafa Emre arkacı

Signature



August 28, 2018



TABLE OF CONTENTS

| | |
|---|-------|
| ABSTRACT | v |
| ÖZ | vii |
| ACKNOWLEDGEMENTS | ix |
| TEXT OF OATH | xi |
| TABLE OF CONTENTS | xii |
| LIST OF FIGURES | xiv |
| LIST OF TABLES | xviii |
| SYMBOLS AND ABBREVIATIONS | xix |
| CHAPTER ONE INTRODUCTION | 1 |
| 1.1. Scope of the Thesis | 1 |
| 1.2. Motivation and Literature Search | 2 |
| 1.3. Thesis Overview and Outline of the Thesis | 5 |
| CHAPTER TWO THE STRUCTURE OF SATELLITE COMMUNICATION SYSTEMS | 7 |
| 2.1. Configuration of Satellite Communication Systems | 7 |
| 2.2. Feed System Structure | 12 |
| 2.3. Horn Antennas | 16 |
| 2.3.1. Corrugated Horn Antennas | 17 |
| 2.3.2. General Antenna Parameters | 18 |
| 2.3.2.1. Radiation Pattern | 18 |
| 2.3.2.2. Return Loss | 20 |
| 2.3.2.3. Directivity and Gain | 20 |
| 2.3.2.4. Polarization | 21 |
| 2.4. Diplexer Structure | 22 |
| 2.4.1. Rectangular and Square Waveguides | 24 |
| 2.4.1.1. Propagation and Mode Theory in Rectangular Waveguides | 25 |
| 2.4.1.2. Dominant Modes in Rectangular and Square Waveguides | 26 |
| 2.4.2. Circular Waveguides | 27 |
| 2.4.3. Waveguide T-Junction | 28 |
| 2.4.4. Waveguide Filters | 29 |

| | |
|--|-----------|
| CHAPTER THREE CONICAL CORRUGATED HORN ANTENNA DESIGN | 32 |
| 3.1. Conical Corrugated Profile Design | 32 |
| 3.1.1. Optimization Works and Simulation Results..... | 35 |
| 3.2. Antenna Design with Transition | 36 |
| 3.2.1. Optimization Works and Simulation Results..... | 37 |
| CHAPTER FOUR WAVEGUIDE DIPLEXER DESIGN | 42 |
| 4.1. Iris Bandpass Waveguide Filter Theory For Diplexer Structure..... | 42 |
| 4.1.1. Iris Bandpass (RX Reject) Filter Design for Uplink/TX..... | 44 |
| 4.1.2. Iris Bandpass (TX Reject) Filter Design for Downlink/RX..... | 46 |
| 4.2. T-Junction Design..... | 48 |
| 4.2.1. H-Plane T-Junction Design and Simulation Results..... | 49 |
| 4.2.2. E-Plane T-Junction Design and Simulation Results..... | 52 |
| 4.3. Design of the Diplexers..... | 54 |
| 4.3.1. H-Plane Diplexer Design and Simulation Results..... | 55 |
| 4.3.2. E-Plane Diplexer Design and Simulation Results..... | 56 |
| 4.3.3. Dual-Polarized Diplexer Design..... | 58 |
| 4.3.3.1. OMT Design..... | 58 |
| 4.3.3.2. Simulation Results for Dual-Polarized Diplexer..... | 62 |
| CHAPTER FIVE MANUFACTURING AND RESULTS | 65 |
| 5.1. Manufacturing | 65 |
| 5.2. Measurements | 67 |
| 5.3. Results for Conical Corrugated Horn Antenna..... | 70 |
| 5.4. Results for Diplexers..... | 72 |
| 5.4.1. H-Plane Diplexer Results..... | 72 |
| 5.4.2. E-Plane Diplexer Results..... | 76 |
| 5.5. Results for Overall System..... | 79 |
| CHAPTER SIX CONCLUSIONS AND FUTURE RESEARCH..... | 83 |
| REFERENCES..... | 85 |

LIST OF FIGURES

| | |
|---|----|
| Figure 1.1. Shaped Reflector Antenna System (Rao, Sharma and Shafai, 2013)..... | 3 |
| Figure 2.1. Satellite Communication Segments (Maral and Bousquet, 2010)..... | 7 |
| Figure 2.2. Frequency Translation Transponder (Ippolito, 2008) | 8 |
| Figure 2.3. Sky Noise Contribution to Antenna Temperature as a Function of Operating Frequency and Pointing Angle. (Stutzman and Thiele, 2013)..... | 9 |
| Figure 2.4. Satellite Communication Frequency Bands (Elbert, 2004)..... | 10 |
| Figure 2.5. Average Atmospheric Attenuation versus Frequency (Pozar, 2012) | 11 |
| Figure 2.6. A Basic Reflector Antenna System (Antesky,2018)..... | 12 |
| Figure 2.7. An Example of Reflector Antenna Feed System..... | 13 |
| Figure 2.8. Examples of E-plane and H-plane Bends (Rao, Sharma and Shafai, 2013)..... | 13 |
| Figure 2.9. Various Transition Types (Rao, Sharma and Shafai, 2013)..... | 14 |
| Figure 2.10. Examples of Waveguide Filter Types (Rao, Sharma and Shafai, 2013)..... | 14 |
| Figure 2.11. Examples of Tees (Rao, Sharma and Shafai, 2013)..... | 15 |
| Figure 2.12. Typical Horn Antenna Configurations (a) E-plane (b) H-plane (c) Pyramidal (d) Conical (Balanis, 2005)..... | 16 |
| Figure 2.13. (a) Conical Corrugated Horn Antenna Structure (b) An example for a Conical Corrugated Horn Antenna (Balanis, 2005) | 17 |
| Figure 2.14. Spherical Coordinate System (Dybdal, 2009)..... | 18 |
| Figure 2.15. Radiation Pattern (a) Radiation Lobes and Beamwidths of An Antenna Pattern (b) Linear Plot of Power Pattern and Its Associated Lobes and Beamwidths. (Balanis, 2005)..... | 19 |
| Figure 2.16. Polarization (a) Rotation of Wave (b) Polarization Ellipse (Balanis, 2005) | 22 |
| Figure 2.17. General Waveguide Diplexer Types (a) E-plane type diplexer (b) H-plane type diplexer (Uher, Bornemann and Rosenberg, 1993). | 23 |
| Figure 2.18. Geometry of the Rectangular Waveguide (Pozar, 2012). | 24 |
| Figure 2.19. Field lines for dominant TE_{10} mode in rectangular waveguides (Pozar, 2012). | |

| | |
|--|----|
| | 26 |
| Figure 2.20. Geometry of a Circular Waveguide (Pozar, 2012). | 27 |
| Figure 2.21. Field Lines of Some Circular Waveguide Modes (Balanis, 2012).. | 28 |
| Figure 2.22. (a) H-plane (b) E-plane T-Junctions and Their Respective Equivalent Circuits (Sorrentino, Bianchi, 2010).. | 28 |
| Figure 2.23. Four Common Types of Filter Characteristics (Matthaei, Young and Jones, 1980). | 29 |
| Figure 2.24. Iris Waveguide Types (a) Shunt-Inductive Iris Waveguides (b) Shunt- Capacitive Iris Waveguides (Bianchi, 2007).. | 30 |
| Figure 2.25. Iris Waveguide Filters (a) Inductive Iris waveguide filter cross-section. (Uher, Bornemann and Rosenberg, 1993) (b) Capacitive Iris waveguide filter cross- section (Pozar,2012).. | 31 |
| Figure 3.1. Variable-depth slot type mode converter and parameters (Granet and James, 2005). | 33 |
| Figure 3.2. Output Radius-Flare Angle Graph (Olver, Clarricoats,Kishk and Shafai, 1994) | 34 |
| Figure 3.3. Designed Conical Corrugated Horn Antenna | 35 |
| Figure 3.4. Results of the Designed Antenna After the First Optimization (a) S_{11} (b) VSWR. | 36 |
| Figure 3.5. Designed antenna structure (a) with transition and parameters (b) Front and back views..... | 38 |
| Figure 3.6. Simulation Result of the Designed Antenna (a) S_{11} (b) VSWR (c) Gain. | 39 |
| Figure 3.7. Radiation Patterns of the Designed Antenna at (a) 10.5 GHz (b) 12 GHz (c) 14.5 GHz (d) 18.5 GHz..... | 41 |
| Figure 4.1. Shunt Inductive Loaded Filter (a) Equivalent Circuit (b) Top View of a Shunt Inductive Waveguide Filter (Bianchi, 2007).. | 42 |
| Figure 4.2. The Demonstration of the Synthesis, from top to bottom respectively low pass prototype, conversion of the bandpass prototype and shunt inductance loaded filter. (Bianchi, 2007).. | 43 |
| Figure 4.3. Geometry of the Waveguide Filters (a) Shunt-Inductive Iris (b) Shunt- Capacitive Iris (Bianchi, 2007). | 43 |

| | |
|--|----|
| Figure 4.4. The Designed H-plane Uplink Bandpass Filter (a) Perspective View (b) Cross Section View From the Top along with Parameters of Filter | 45 |
| Figure 4.5. Simulation Results of the Designed Uplink Bandpass Filter | 46 |
| Figure 4.6. The Designed E-plane Downlink Bandpass Filter (a) Perspective View (b) Cross Section View From the Top along with the Parameters of Filter | 47 |
| Figure 4.7. Simulation Results of the Designed Downlink Bandpass Filter. | 48 |
| Figure 4.8. The Designed H-Plane T-Junction Structure (a) Perspective View (b) Cross-Section from the Top along with the Parameters (c) Cross-Section from the side along with parameters..... | 50 |
| Figure 4.9. Simulation Results for the designed H-Plane T-Junction (a) Results for Port 2 (S_{21} - S_{22}) (b) Results for Port 3 (S_{31} - S_{33})..... | 51 |
| Figure 4.10. The Designed E-Plane T-Junction Structure (a) Perspective View (b) Cross-section from the Top along with the Parameters (c) Cross-Section from the side along with the Parameters..... | 53 |
| Figure 4.11. Simulation Results for the designed E-Plane T-Junction (a) Results for Port 2 (S_{21} - S_{22}) (b) Results for Port 3 (S_{31} - S_{33})..... | 54 |
| Figure 4.12. Designed H-Plane Diplexer (a) Perspective View (b) Inner Structure..... | 55 |
| Figure 4.13. Simulation Results of the Designed H-Plane Diplexer. | 56 |
| Figure 4.14. Designed E-Plane Diplexer (a) Perspective View (b) Inner Structure | 57 |
| Figure 4.15. Simulation Results of the Designed E-Plane Diplexer..... | 58 |
| Figure 4.16. Wave Propagation Modes for OMT (a) Port 1 (Common Port) (b) Port 2 (TX) (c) Port 3 (RX) | 59 |
| Figure 4.17. Designed OMT (a) Outer Structure (b) Inner Structure. | 60 |
| Figure 4.18. Simulation Results of the Designed OMT (a) S_{33} - S_{31} (Downlink/Vertical Pol.) (b) S_{22} - S_{12} (Uplink/Horizontal Pol.) (c) S_{23} - S_{32} (Isolation). | 62 |
| Figure 4.19. The Designed Dual-Polarized Diplexer (a) Perspective View and (b) Inner Structure..... | 63 |
| Figure 4.20. Simulation Results of the Designed Dual-Polarized Diplexer. | 64 |
| Figure 5.1. Printed Structures..... | 65 |
| Figure 5.2. Coated Structures After Printing Process (a) Nickel Coated Corrugated horn | |

| | |
|--|----|
| antenna (b) Nickel Coated H-Plane diplexer (c) Silver Coated E-Plane Diplexer (d) Silver Coated H-Plane Diplexer. | 66 |
| Figure 5.3. (a) Assembled Antenna and (b) H-plane Diplexer Structures by Adjustable Clamp System | 67 |
| Figure 5.4. Measurement Setup (a) H-Plane Diplexer Measurement (b) Antenna Measurement (c) E-Plane Diplexer Measurement. | 69 |
| Figure 5.5. Return Loss and Gain Results (a) Return Loss Value (b) Gain..... | 70 |
| Figure 5.6. Normalize Radiation Patterns of Produced Antenna at (a) 10.5 GHz (b) 14.5 GHz (c) 18 GHz. | 72 |
| Figure 5.7. Return Loss and Insertion Loss Results of the Fabricated H-Plane Diplexer (a) S_{11} (b) S_{21} (c) S_{22} (d) S_{31} (e) S_{33} | 75 |
| Figure 5.8. S_{32} (Isolation) Graph of the Fabricated H-Plane Diplexer. | 76 |
| Figure 5.9. Return Loss and Insertion Loss Results of the Fabricated E-Plane Diplexer (a) S_{11} (b) S_{21} (c) S_{22} (d) S_{31} (e) S_{33} | 78 |
| Figure 5.10. S_{32} (Isolation) Graph of the Fabricated E-Plane Diplexer. | 79 |
| Figure 5.11. Integrated Feeding System Structure..... | 80 |
| Figure 5.12. Gain Results of the Fabricated Feeding System with PEC Material and Nickel Coated Diplexer (a) RX side (b) TX side. | 81 |
| Figure 5.13. Gain Results of the Fabricated Feeding System with PEC Material and Silver Coated Diplexer (a) RX side (b) TX side..... | 82 |

LIST OF TABLES

| | |
|---|----|
| Table 2.1. Waveguide Characteristics (WR-75 & WR 62)..... | 27 |
| Table 3.1. Corrugated horn antenna parameters. | 33 |
| Table 3.2. Values of the Antenna Parameters After the First Optimization. | 35 |
| Table 3.3. Final dimensions of designed antenna..... | 37 |
| Table 4.1. The Dimensions of the Uplink Filter. | 46 |
| Table 4.2. The Dimensions of the Downlink Filter. | 48 |
| Table 4.3. The Dimensions of Designed H-Plane T-Junction. | 51 |
| Table 4.4. The Dimensions of Designed E-Plane T-Junction..... | 53 |



SYMBOLS AND ABBREVIATIONS

ABBREVIATIONS:

| | |
|------|---------------------------------------|
| GEO | Geostationary Orbit |
| PIM | Passive Intermodulation |
| RF | Radio Frequency |
| CNC | Computerized Numerical Control |
| CCM | Computer Controlled Precision Milling |
| FSS | Fixed Satellite Service |
| BSS | Broadcast Satellite Service |
| PRA | Parabolic Reflector Antenna |
| SRA | Shaped Reflector Antenna |
| BFN | Beamforming Networks |
| OMT | Orthomode Transducer |
| SLM | Selective Laser Melting |
| SLA | Stereolithography |
| FDM | Fused Deposition Modeling |
| ABS | Acrylonitrile butadiene styrene |
| PLA | Polylactic acid |
| MSS | Mobile Satellite Service |
| TTC | Tracking Telemetry and Command |
| VSAT | Very Small Aperture Terminals |
| TX | Transmission Arm |
| RX | Receiving Arm |
| DTH | Direct to Home |
| DBS | Direct Broadcasting Service |
| TE | Transverse Electric |

TM Transverse Magnetic
TEM Transverse Electromagnetic
PEC Perfect Electric Conductor



CHAPTER ONE

INTRODUCTION

1.1. Scope of the Thesis

The idea of communication by using satellites was first presented in May 1945 by the famous English scientist Arthur C. Clarke. Nowadays, the last point reached in communication systems is the satellite systems. These systems have come about as a result of efforts to create faster, high-capacity but at the same time lower-cost systems in the field of communication.

Satellite communication systems are used for commercial applications in a wide range of fields such as TV, telephone, data transfer, radio and Internet. In addition to these applications, it can also be used in the military to exchange information and communicate between the different units of the armed forces. Most communication satellites are located in a GEO and often use reflector antennas to transmit and receive RF signals at the same time by using separate downlink and uplink frequency bands to communicate with the antennas on Earth. The reflector antennas are directly or indirectly, via a sub-reflector, supported by the feed system to provide high gain coverage at certain locations on Earth. The most important hardware in a satellite antenna is the feeding system. This system is directly related to bandwidth, polarization, power handling, PIM levels, and illumination on the reflector. It also separates the various frequency bands and providing a good match to the free space. The system usually consists of a horn, orthomode transducer, filters or diplexers, polarizers, transitions, combining/dividing networks. For satellite communication antennas, while reflector provides desired gain and beam shape on the ground, feeding system is effective in determining important parameters such as insertion loss, return loss, axial ratio or cross-polar isolation, bandwidth and high power handling. Today, the most frequently used frequencies of satellite communication are C, Ku and Ka bands. Feeding at these frequencies can be achieved by waveguide structures in a compact size. In addition to its size advantages, these structures are

low-loss, resistant to high power and reliable for satellite communications. (Rao, Sharma and Shafai, 2013)

In this thesis, it is mainly focused on the design and production of an integrated system combining the components of corrugated conical horn antenna and waveguide diplexers in three different versions as H-plane, E-plane and dual-polarized to be used as a feed in Ku band satellite communication systems. The corrugated conical horn antenna is preferred due to its low side lobe level, polarization purity and high gain features. Besides, the diplexer which is an important part of feeding system is used to separate or combine the transmitted and receiving signals in horn antenna.

It is aimed to manufacture the prototypes of the designed structures at the shortest time and with the least cost, thus 3D printing technology, which is more advantageous than CNC/CCM machine technology is preferred. The fabricated structures are coated with conductive spray painting method, and the feasible prototype work is proven by using this 3D technology with compatible results.

1.2. Motivation and Literature Search

The application areas of satellite communication are increasing day by day with the development of technology. As a result of this situation, some different kinds of features are sought for the demanded products in this area, such as high power capability, light weight, compact design and low cost.

The primary sources used in satellite communication are the reflectors and its feed system which is designed and produced for Ku band satellite communication in this thesis. The different satellite services demands different types of antennas in order to meet the varying performance requirements. In the 1960s and 1970s, reflector antennas were first used to provide higher gain over coverage areas in communication satellites such as Echo 1, Telstar, Syncom III, and Early Bird.

Significant improvements have been made in satellite communication antennas and ground station antennas late 1970s and 1980s. Very large earth-station antennas have been deployed in order to communicate with GEO communication satellites in C and Ku band frequencies in many regions of Japan, the United States and Europe. In these earth-stations, shaped dual-reflector antennas and fixed-feed beam waveguide

technologies were used to improve the overall efficiency of the antenna system and the ability to track various satellites in orbit.

Another important development in the 1980s was the innovations in the form of the shaped reflector antennas used for contoured beam coverage in the C and Ku bands. As a result of these innovations, cost and schedule reductions of satellite payloads were provided significantly by eliminating the conventional beam-forming networks. In the 1970s and 1980s, cluster feeds were used with parabolic reflectors to create shaped beams, and key issues were mutual coupling among feeds in arrays and complexity of the beam-forming networks that combine the RF signals from all feeds. The success and adoption of shaped reflectors allowed single feed that eliminated the drawbacks of earlier designs (Rao, Sharma and Shafai, 2013).

Contoured beam antennas are also called shaped beam antennas are commonly used for FSS and BSS payloads. These antennas provide uplink, downlink, or both up/downlinks where the beam is broadened from high gain spot beam to a medium gain beam that is synthesized to fit the coverage region. There are two methods used to generate contoured beams, first one is PRA with a feed array and high-level beam-forming network method and the other one is with a single feed SRA method shown in figure below (see Figure 1.1).

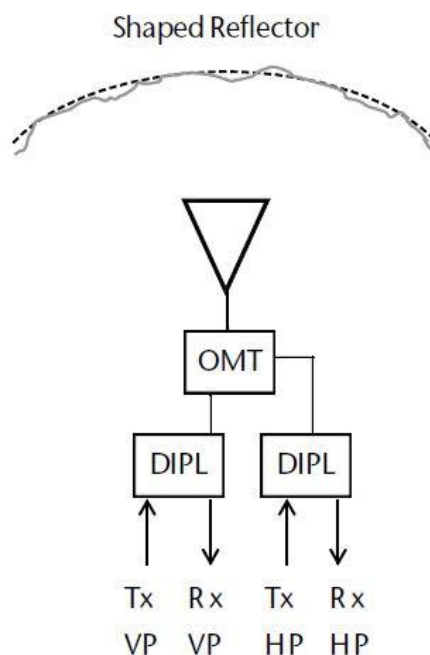


Figure 1.1 Shaped Reflector Antenna System (Rao, Sharma and Shafai, 2013)

The SRA technology provides both transmission and reception of contoured beams through a single antenna over a single wideband feed system, without the need for the use of BFNs. In the system, the two separate frequency bands to be used in reception and transmission are separated by the use of diplexer/s, and polarization is changed by OMT (Rao, Sharma and Shafai, 2013). According to the design of the diplexer, both the polarization changing and the frequency separation process can be achieved with only a diplexer even without having to use an OMT.

With the all these developments, the demand for such waveguides (diplexers, OMT's, filters, bends, etc.) structures has increased and the needs have changed accordingly. When such designs are realized, a prototype is primarily needed and the product is developed or marketed in accordance with the results obtained. For these reasons, it is aimed that prototype production can be realized both quickly and by low cost. Since, these structures are complicated in their geometric shapes, high precision is required in the production process. Nowadays, CNC/CCM machines are often used for the production of these complex structures. However, it can be stated that CNC/CCM process is challenging, long-running and very high-cost from the point of view of a product which is designed and will be produced as a prototype. Thanks to development of additive manufacturing technology, prototype production has become possible with much lower cost as well as in a much shorter time by using 3-D printing machines. Although there are other technologies in 3-D printing such as SLA, polyjet and others, most of 3-D printers on the market work with FDM technology due to its advantages in terms of cost of the machine and materials used in the production, compact size of the machine, common usage and easy operation in production process. FDM based 3-D printers can produce a desired structure by melting various plastic materials such as ABS or PLA and extruding layer by layer (Noorani, 2018).

Another advantage of FDM technology is that the printing sensitivity settings could be changed by the user's preference. Many parameters, such as layer height, print speed and infill density can be adjusted with the desired precision by user to create better quality prints.

In this thesis with this motivation, a prototype of Ku band reflector feed system combining a corrugated conical horn antenna and waveguide diplexers are verified by using 3D FDM/PLA printing technology and conductive aerosol painting method.

Since the production of antennas and electromagnetic structures with 3D printing technology becomes a hot topic due to their low cost and low production time, there are many studies in recent years (almost all after 2016) in literature, which presents the verification of horn antennas or microwave components such as diplexers/OMTs at different frequency bands with 3D printing technology (J.C.S. Chieh et al., 2014; A. Genc et al., 2017; J.R. Silva et al., 2017; A.T. Castro, B. Babakhani and S.K. Sharma, 2017; V. Midtbøen, K.G. Kjelgård and T.S. Lande, 2017; H.Yao et al., 2017; M.Mirzaee et al., 2015; B.Zhang and H.Zirath, 2016; A.Bhutani et al., 2016; E.Menargues et al., 2017; E.Laplanche et al., 2017; A.I. Dimitriadis et al., 2017; X.Shang et al., 2016; E.Menargues et al., 2017). However only one component either a horn antenna by using of the ABS material with FDM technology (J.C.S. Chieh et al., 2014; A. Genc et al., 2017; J.R. Silva et al., 2017; A.T. Castro, B. Babakhani and S.K. Sharma, 2017; H.Yao et al., 2017) or a diplexer/OMT by using more expensive SLM or metal printing (B.Zhang and H.Zirath, 2016; A.Bhutani et al., 2016), SLA and Polyjet techniques (E.Menargues et al., 2017; E.Laplanche et al., 2017; A.I. Dimitriadis et al., 2017; X.Shang et al., 2016; E.Menargues et al., 2017) is usually shown for the demonstration such that the integration of a corrugated horn antenna with a waveguide diplexer in a feed system manufactured with 3D printing technology, which is realized at Ku band, is carried out in this study for the first time in literature. Some of the mentioned studies in literature use SLM, SLA or Polyjet techniques where FDM is preferred in this study in order to obtain the prototype with as low cost and low production time as possible. Besides, the ones using FDM technology produce their structures with ABS material where less expensive PLA is selected in this study due to its advantages over ABS in the manufacturing process to be described later.

1.3. Thesis Overview and Outline of the Thesis

In this thesis, the design and manufacturing of a reflector feeding system, which consists of a conical corrugated horn antenna and diplexer by using additive manufacturing technology, are proposed for Ku band satellite communication. Besides, three different versions of the diplexer as H-plane, E-plane and dual-polarized are proposed to design. The configuration of each structure is given and all theoretical information are explained for designs. Followed by determining the effective parameters of the initial structures are obtained with the given theoretical

information, parametric drawings of these structures are made in CST Microwave Studio software program and optimization studies are carried out. The optimization process continues until the desired system results are achieved. After the optimization process, designed corrugated horn antenna, H-plane and E-plane diplexer prototypes are manufactured by using a 3-D printer and these structures coated by conductive aerosol paint spray. The measurements of these prototypes are performed at Yasar University Antenna and Microwave Laboratory and TUBITAK BILGEM Antenna and Research Center. Measurements, and simulation results are compared with measurement results for the verification of results.

The thesis consists of six chapters in summary.

In Chapter 2, it is included the configuration of satellite communication systems, feed system structure and components, required system parameters and electromagnetic mode conversions.

Chapter 3 includes the theoretical information and design steps about conical corrugated horn antenna.

Chapter 4 explains the diplexer design which includes also the two iris band pass filter design with three different versions.

Chapter 5 gives the manufacturing process and compared simulation and measurement results.

Chapter 6 concludes the thesis.

CHAPTER TWO

THE STRUCTURE OF SATELLITE COMMUNICATION SYSTEMS

2.1. Configuration of Satellite Communication Systems

Satellite communication system consists of three different segments which are shown in figure below (see Figure 2.1). These are space segment, a control segment and ground segment. The communication between these segments is provided through over the uplink/downlink operations by transmit/receive antennas. If it needs to be defined, uplink is the transmission from earth stations to the satellites, and downlink is the transmission from satellites to the earth stations.

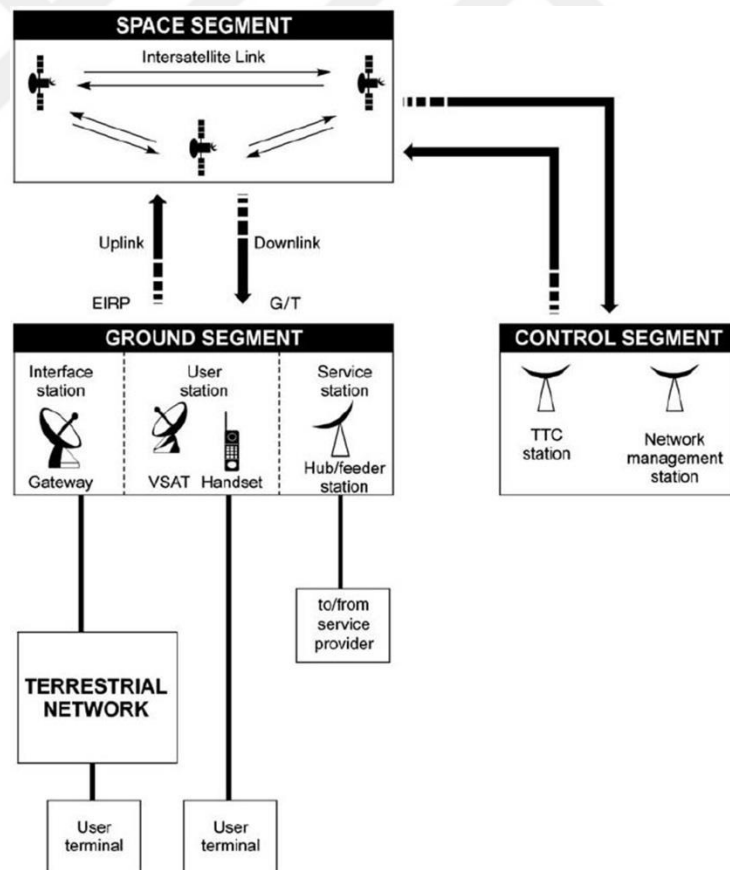


Figure 2.1. Satellite Communication Segments (Maral and Bousquet, 2010).

Space segment contains one or more active and backup satellites, which are

organized into a constellation. Control segment, also called TTC stations are responsible for the control and monitoring of satellites. Ground segment also includes all the traffic from earth stations.

The space segment can be divided in two parts, payload and platform. The most important and key component of payload structure is transponder. Transponder is the series of various electronic components which provides a communication channel or a link between the transmitted downlink signal by a downlink antenna and received uplink signal by an uplink antenna.

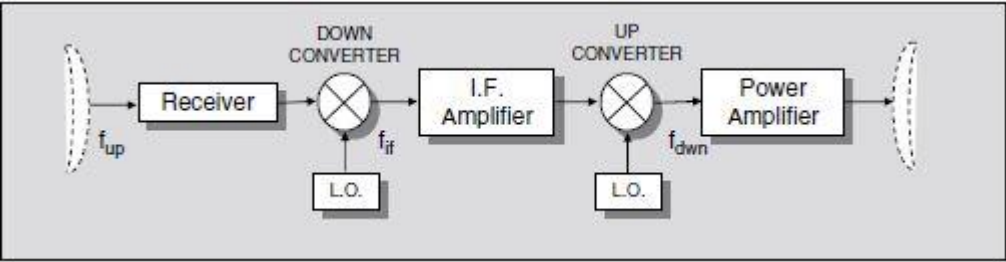


Figure 2.2. Frequency Translation Transponder (Ippolito, 2008)

The frequency translation transponder, which is shown in figure above (see Figure 2.2) is used for FSS, BSS and MSS applications. As it can be seen from the figure, the received uplink radio frequency, f_{up} is converted to an intermediate lower frequency, f_{if} , amplified, and then converted back up to the downlink RF frequency, f_{down} , for transmission to the earth (Ippolito, 2008).

For the ground segment, the earth stations can be divided in three sections as user stations, interface stations and service stations. Handsets, mobile stations, portables and VSATs can be given as examples for user stations, which provide direct access to space segment. Besides, the interface stations of the earth stations are known as gateways that connect the space segment and terrestrial networks. Service stations are hub / feeder stations that distribute or collect the information from user stations to space segment or space segment to user stations. In this way, the connection between service provider and user is provided by a hub (for collecting services) or a feeder station (for broadcasting services). A connection to a user terminal from a gateway, hub, or feeder station is called a forward connection. The opposite of this case is also called return connection. Both the return and forward connections require an uplink and a downlink.

The frequency bands used for communications are determined by the International Telecommunication Union (ITU), headquartered in Geneva / Switzerland. Members of the Union include every government on the planet. The most attractive portion of the radio spectrum, which is allocated by ITU for satellite communication, lies between 1 and 30 GHz because the electromagnetic noise level in nature is small over this frequency range shown in figure below (see Figure 2.3). (Stutzman and Thiele, 2013).

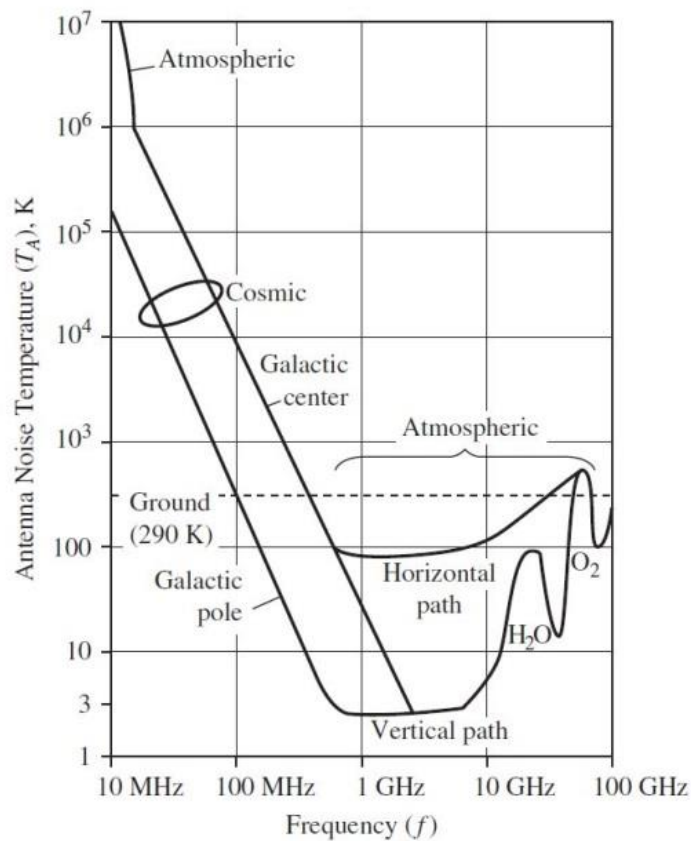


Figure 2.3. Sky Noise Contribution to Antenna Temperature as a Function of Operating Frequency and Pointing Angle. (Stutzman and Thiele, 2013)

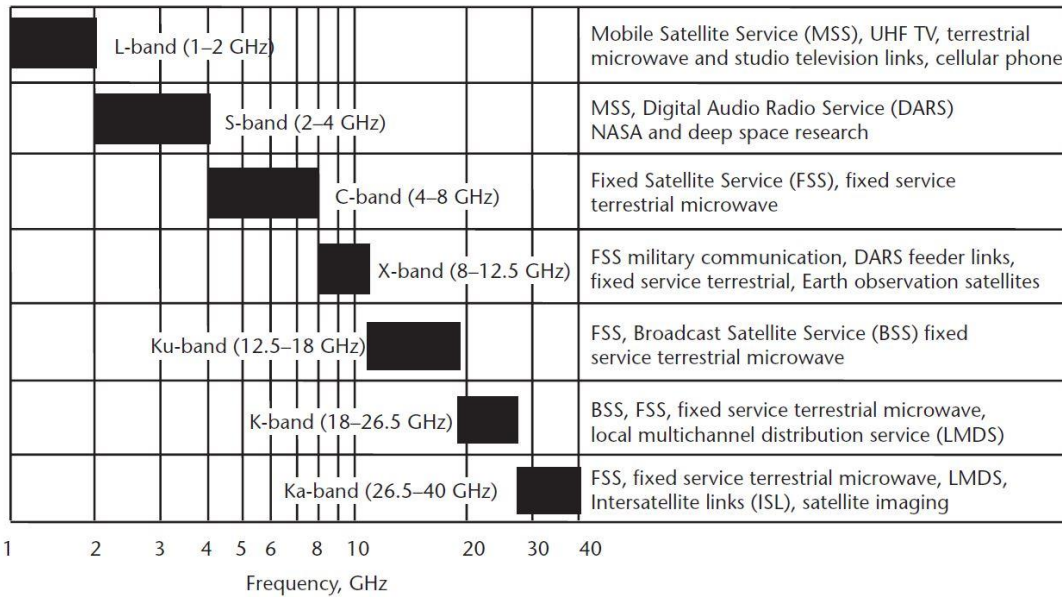


Figure 2.4. Satellite Communication Frequency Bands (Elbert, 2004)

The frequency bands which are used in satellite communication are shown in figure above (see Figure 2.4). Today, most commonly used microwave frequencies C, X and Ku bands in the range of 3-18 GHz. These bands provide a wider range than the L and S bands. In addition to the classification in Figure 2.4, the range of 10.7-18.4 GHz is accepted as Ku-band. This frequency range actually includes part of the X-band (8-12 GHz). In fact, many Ku-band systems include X band frequencies. The X-band is frequently used in military applications and deep space communications. (Umar, 2004)

C band is generally used in cable TV in North America, and satellite DTH in Asia. In addition, it is used for local and international telephone services in some countries around the world. Also, the Ku band was previously used in intercity trunking links between North America and Europe. However, later it was accepted in Western Europe for local services, especially for TV distribution. Today, it is preferred for DBS and VSAT networks in many countries. (Elbert, 2008)

In satellite communications, reflector antennas and their associated feeding systems are generally used in ground stations. For this reason, it is necessary to explain uplink and downlink operations according to the ground station in this thesis. For the uplink, signal is transmitted to the satellite by the ground station, so the uplink

frequency band is considered as TX band. Also, for the downlink, the signal which is transmitted from the satellite is received by ground station antenna, so the downlink frequency band is considered as RX band.

The other important detail needed to be known about satellite communication is that high frequency values are always used to communicate from ground to the satellites. The reason of this situation is that the ionosphere layer in the atmosphere contains ionized gas particles that can reflect or block lower frequency waves. For this reason, high frequency is preferred when transmitting the signals. Besides, the downlink frequency is always lower than the uplink frequency bands due to the atmospheric attenuation characteristics shown in Figure 2.5.

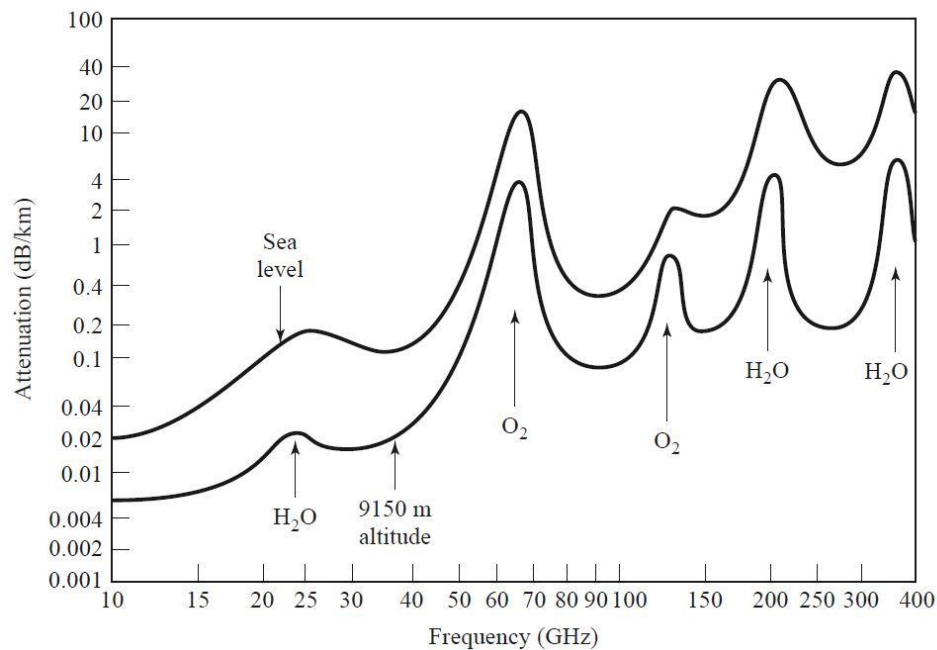


Figure 2.5. Average Atmospheric Attenuation versus Frequency (Poazar, 2012)

As it can be seen from the figure above, the minimum attenuation level is in the range of 10-20 GHz. As a result, because of a low-power signal transmission in the downlink process where the signal is transmitted from the satellite to the earth, the 10.5-12.75 GHz range is generally used as downlink frequency to avoid attenuation for Ku-band. In the uplink, a frequency band which is slightly above this determined range (10.5-12.75 GHz) is preferred. This operation is more resistant to attenuation since there is a high-power transmission from the earth station to the satellite.

In this thesis, by using all these information, the operating frequency band is preferred for RX as 10.5-12.75 GHz, and for TX as 17.3-18.4 GHz to be used in Ku band feeder station of DBS/BSS systems.

2.2. Feed System Structure

Today, the frequencies commonly used for satellite communications are the C, X, Ku, and Ka frequency bands. The most important requirements of the systems which used in these frequency bands have low loss, high power handling capability and to be very reliable. The structures that can provide all these features are waveguides. Designed and produced waveguides must also be in compact size and light weights for the feeding system. In addition, the systems such as FSS, where uplink and downlink operations are performed with the same feed system over a single antenna, require very large bandwidth and dual-band feed designs.

Antenna systems, which have a critical place in the realization of uplink and downlink operations in satellite communication, basically consist of a reflector and a feeding system shown in Figure 2.6.

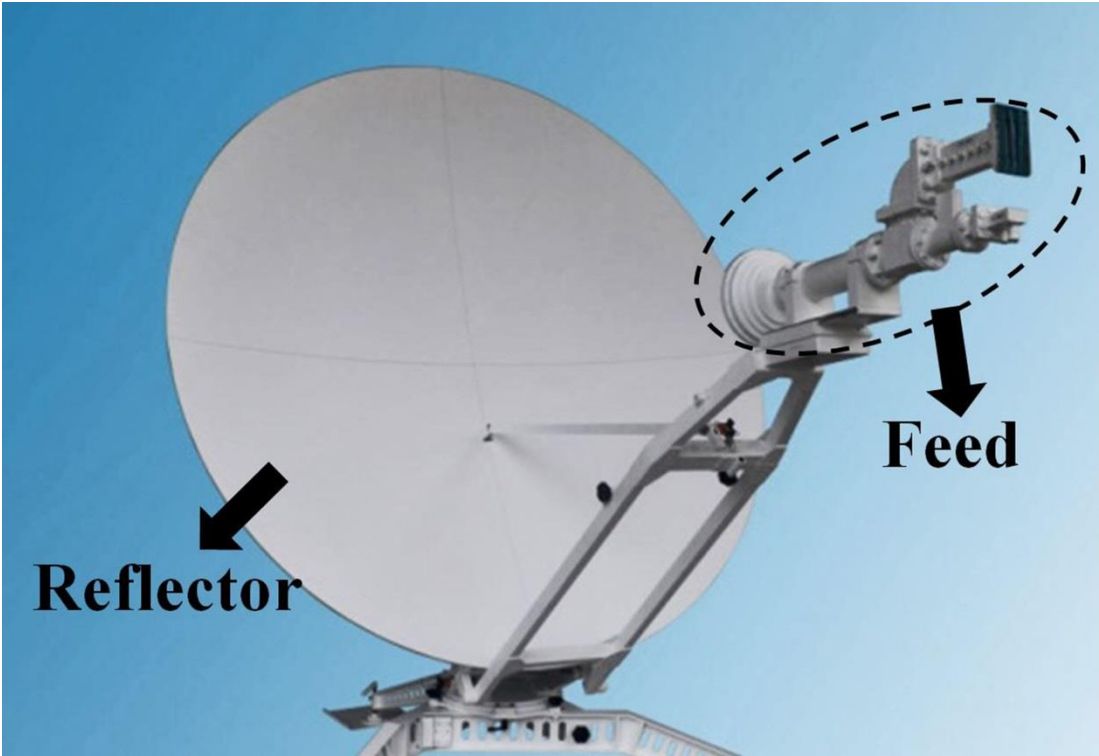


Figure 2.6. A Basic Reflector Antenna System (Antesky, 2018)

The detailed feed structure shown in figure below (see Figure 2.7), it is generally made up of one or more orthomode transducers and diplexers which support a corrugated horn antenna. However, these mentioned structures also contain many essential components in themselves. If the feed components used in a satellite system are summarized, these are bends, transitions, filters, e-plane/h-plane magic tees or T-junctions, OMT's, polarizers and horn structures.

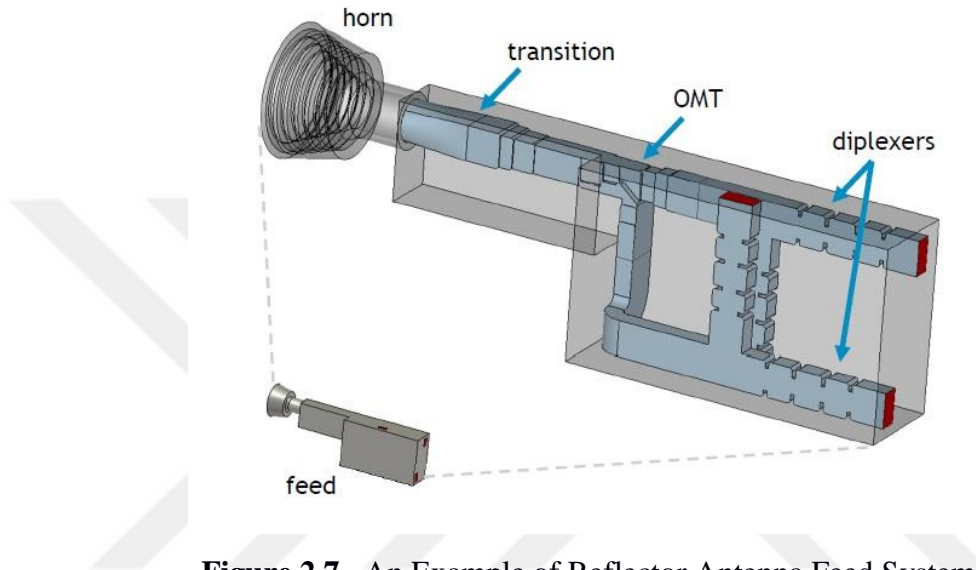


Figure 2.7. An Example of Reflector Antenna Feed System

These components can be explained briefly as follows;

Bends: These structures often used in waveguide feed systems for changing the wave propagation direction. They can be used in two different types, E-plane and H-plane, as shown in figure below (see Figure 2.8). There is a positive effect on system the return loss value.

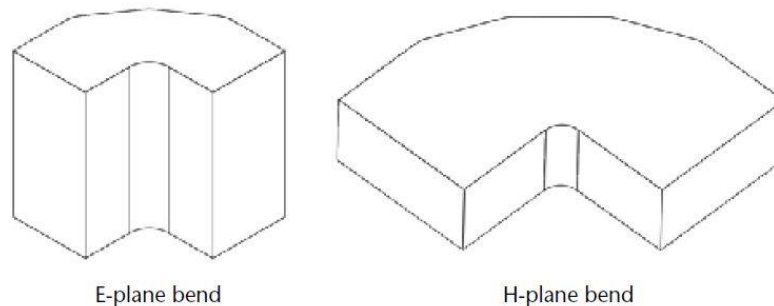


Figure 2.8. Examples of E-plane and H-plane Bends (Rao, Sharma and Shafai, 2013)

Transitions: Waveguide feeding components cannot be always designed in standard sizes to achieve more efficient results and providing an ideal performance. These structures can be generally designed as rectangular, square, circular, ridged or coaxial, depending on their application areas. Transitions are required to minimize reflections and provide an impedance matching for connections between these non-standard sized waveguide sections. A transition typically consists of steps that gradually change the cross section between the two waveguide sections to be combined. Various transition types are shown in Figure 2.9.

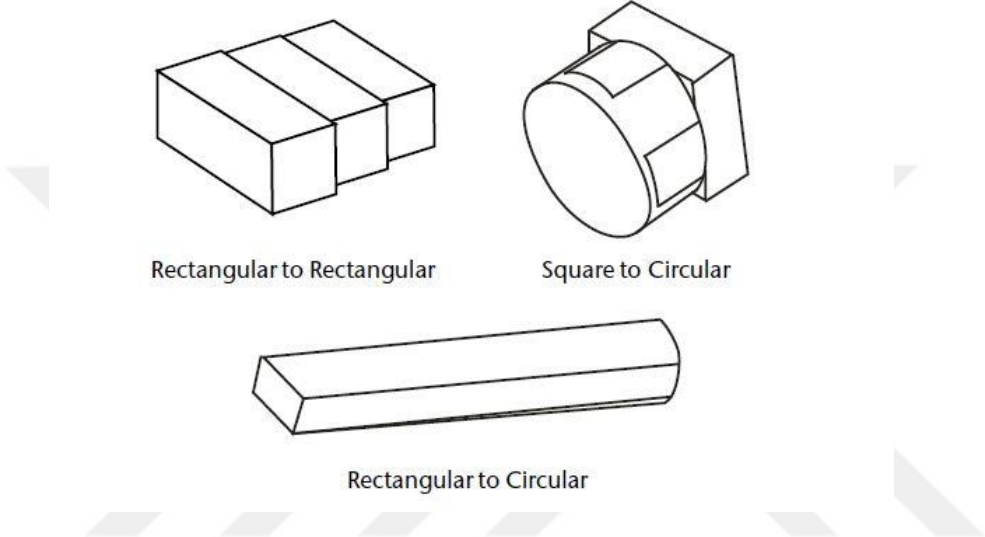


Figure 2.9. Various Transition Types (Rao, Sharma and Shafai, 2013)

Filters: They are highly important in antenna feeds and waveguide structures where received and transmitted signals are combined, particularly where broadband performance is required. Passing and rejecting performances between TX and RX bands are provided by filters. These filters can be classified as low-pass, band-pass, and high-pass. While low-pass filters are usually designed with corrugated sections, inductive iris type structures are preferred in bandpass filters. Different types of filter structures are shown in Figure 2.10.

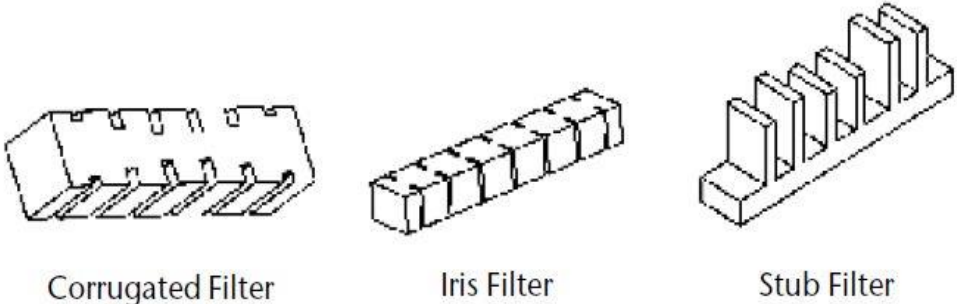


Figure 2.10. Examples of Waveguide Filter Types (Rao, Sharma and Shafai, 2013)

E-plane, H-plane and Magic Tees: It can be said that the most basic element in the feeding systems is a power divider / combiner. The simplest version of this structure is a three-port component that divides a signal equally into two paths or combines two signal into one path and is often referred to as tee. The structure with 180-degree phase shift between the two outputs is known as E-plane, and the structure with 0-degree phase shift is known as H-plane. Also, magic tee is a 4-port combination of these two types of tee. These structures can be observed from the figure below (see Figure 2.11).

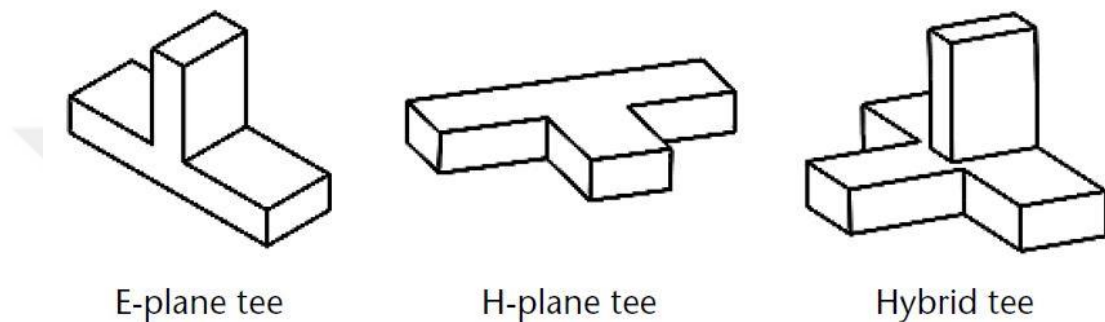


Figure 2.11. Examples of Tees (Rao, Sharma and Shafai, 2013)

Orthomode Transducers: OMT's are used in feed systems that require dual polarization. These structures allow the dividing or combining of two dominant mode orthogonal signals. In addition, it provides a good isolation value between the vertical and horizontal ports.

Diplexer: Diplexers are used in feed system as a frequency separator. They allow working of an antenna as receiver and transmitter simultaneously in different frequencies. The detailed information is given in section 2.4 and design methods are explained in Chapter 4.

Horns: Horns are the most important components for feeding structure. They present high gain performance, good cross-polarization and return loss levels. The detailed information is given in section 2.3 and design methods are explained in Chapter 3.

In this thesis, the design of a feed system to be used in Ku band satellite communication systems was realized, and the designed feed system consists of a

wide band corrugated horn antenna and diplexer which supports it. The diplexer consists of two iris band pass filters which are used to carry out the uplink and downlink operations of the system. The transition structures are designed to provide matching between the antenna and the diplexer. In the following sections of the thesis, these structures and their important parameters will be defined separately and the applied design methods will be explained.

2.3. Horn Antennas

The horn antennas are widely used as a feed component in many areas such as, radio astronomy, satellite tracking, and communication dishes. Besides, its usage as a feed for reflectors and lenses, it is a commonly used component for standard calibration and gain measurements of other high gain antennas. (Balanis, 2005)

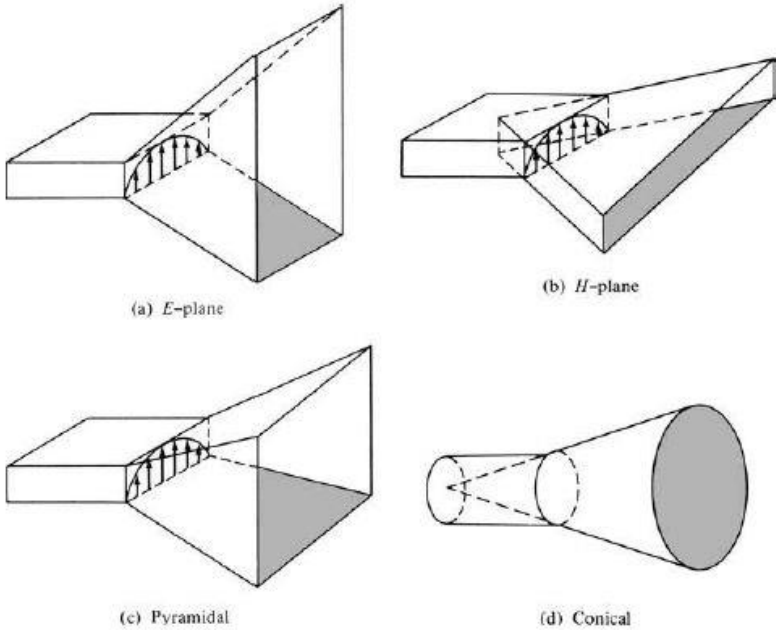


Figure 2.12. Typical Horn Antenna Configurations (a) E-plane (b) H-plane (c) Pyramidal (d) Conical (Balanis, 2005)

Horns are also the most significant component of the feed system. In modern communication satellites, hybrid or multimode horns which consisting of corrugated or smooth-walled inner structure are used in different configuration that shown in figure above (see Figure 2.12). Corrugated feed horns provide the best cross-polarization, return loss, and broadband performance in spite of aperture efficiency, manufacturing complexity, and mass. Moreover, smooth-walled structures can provide very high efficiency, and they have some advantages such as easy

manufacturing, lower mass in spite of poor cross-polarization level. (Handbook of reflector antennas and feeds system.)

2.3.1. Corrugated Horn Antennas

The corrugated horn antennas can be designed in different configurations which are given in Figure 2.12. However, the conical type of corrugated horns is used for dual or circular polarization applications where the satellite communication is also one of them. These type of horn antennas which have slots and teeth in its inner surface are used as a feed for reflectors in communication satellites, radar and remote sensing systems and also they are used as direct radiator antennas for broadband measurements. The antenna is preferred because of providing high directivity and gain as well as low cross-polarization level, low side and back lobe levels and good return loss value. All these advantageous features of the antenna results from the fact that inner surface is in a corrugated structure. Corrugated horn antennas basically consist of four main sections. As it can be seen in figure below (see Figure 2.13(a)) respectively; input waveguide, mode converter, corrugated profile and antenna aperture sections.

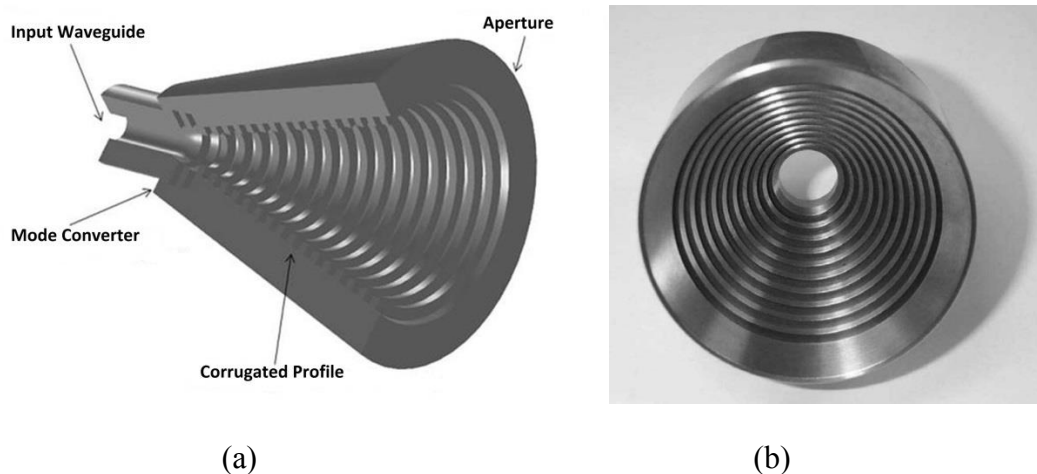


Figure 2.13. (a) Conical Corrugated Horn Antenna Structure (b) An example for a Conical Corrugated Horn Antenna (Balanis, 2005)

When there is TE_{11} mode propagation in the input waveguide section, which is a smooth and flat walled structure, TE_{11} and TM_{11} modes propagation starts from the moment the wave passes to the corrugated surface. However, the corrugated surface of the antenna behaves like a mode converter, and this situation provides the

propagation of the both electric and magnetic field components of the TE and TM modes at the same velocity as a single hybrid (HE_{11}) mode.

Hybrid mode propagation provides extremely good beam symmetry in radiation patterns with low cross-polarization levels, with a high beam efficiency. For these reasons, corrugated horns provide good wide-bandwidth performance.

Due to all these of positive features, a corrugated horn antenna is preferred to be used as a reflector antenna feed in this thesis. The theoretical information and design process of this structure are explained in "Corrugated Horn Antenna Design" chapter of the thesis.

2.3.2. General Antenna Parameters

In order to clearly define the performance of a designed or produced antenna, some important parameters need to be known and determined at the desired level. In this part of the thesis, some of these antenna parameters will be briefly described.

2.3.2.1. Radiation Pattern

As mentioned previously, horn antennas, which are aperture type antennas, are widely used in satellite communication systems. The propagation performance of these types of antennas is investigated through the spherical coordinate system shown in Figure 2.14.

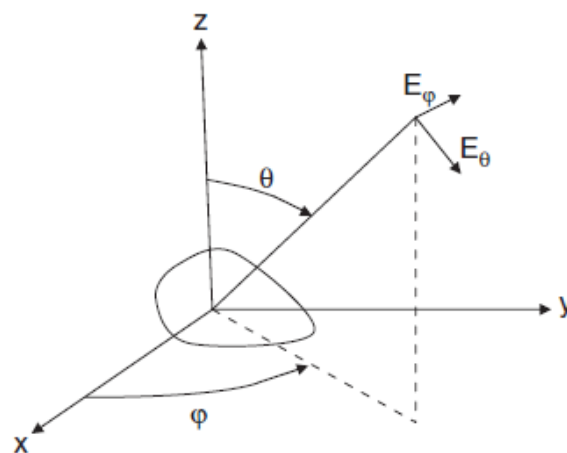


Figure 2.14. Spherical Coordinate System (Dybdal, 2009).

In these coordinates, the antennas are generally assumed to be located in the XY plane and propagate in the +z direction. In this case, XY plane in the figure is scanned by Φ angle ($0 \leq \Phi \leq 360$), and called azimuth plane. The other fundamental plane is represented with θ angle ($0 \leq \theta \leq 180$), and called as elevation plane.

A radiation pattern is an indication of the direction in which the antenna is propagated and how much power it propagates. An antenna pattern consists of radiation lobes, as shown in Figure 2.15.

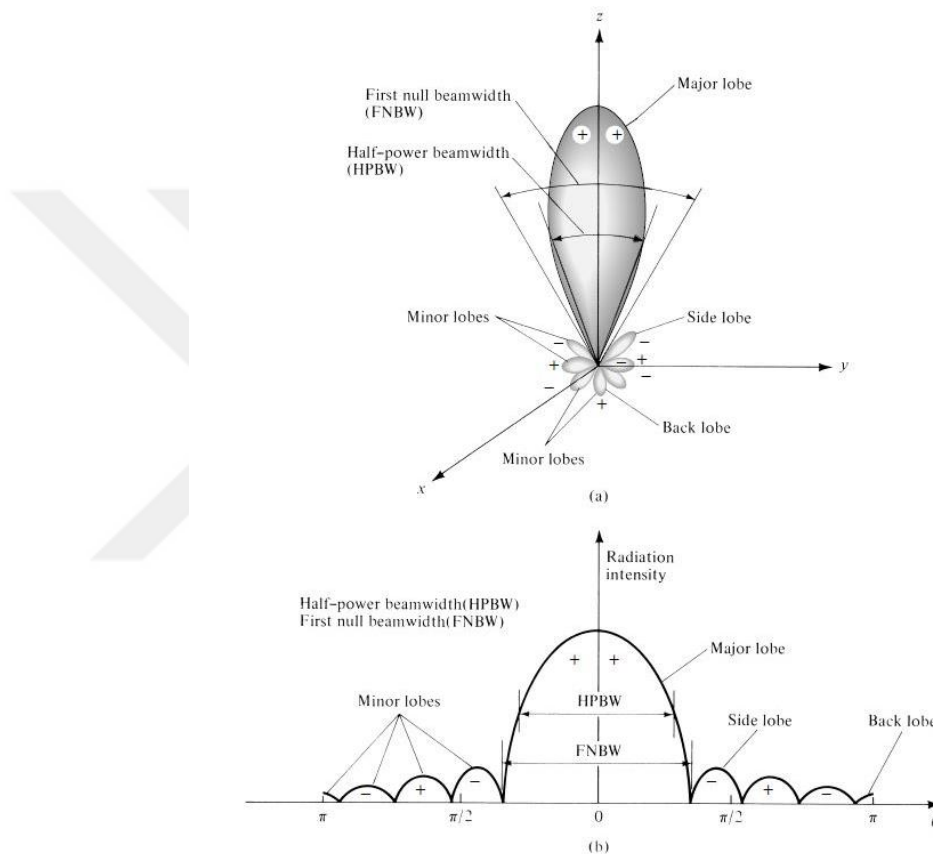


Figure 2.15. Radiation Pattern (a) Radiation Lobes and Beamwidth of an Antenna Pattern (b) Linear Plot of Power Pattern and Its Associated Lobes and Beamwidth. (Balanis, 2005).

Major lobe (main beam) can be defined as the radiation lobe containing the direction of maximum radiation. Also the half power beamwidth (HPBW) is the angle between the half-power (-3 dB) points of the main lobe, when referenced to the peak effective radiated power of the main lobe.

2.3.2.2. Return Loss

In satellite communication systems, it is aimed that transmitted and received signals have low loss as much as possible. This loss in the system depends on the impedance matching between the antenna and transmission line to which antenna is connected. It means, to deliver maximum power for the system, impedance of components that connected to each other must be well matched. The parameter, which describes numerically how well the matching between components of the system is, is the voltage standing wave ratio (VSWR) measure. VSWR is a function of reflection coefficient and it describes how much power reflected from the antenna. It defined by the following formula where the reflection coefficient is given by Γ ;

$$VSWR = \frac{1+|\Gamma|}{1-|\Gamma|} \quad (1)$$

The reflection coefficient is also known as return loss or S_{11} . S_{11} is a scattering matrix parameter and the relation between impedances and S_{11} parameter is expressed as;

$$S_{11} = \frac{V_o^-}{V_o^+} = \frac{Z_L - Z_o}{Z_L + Z_o} \quad (2)$$

Return loss in dB expressed in terms of S_{11} parameter as;

$$RL(dB) = -20 \log(|S_{11}|) \quad (3)$$

2.3.2.3. Directivity and Gain

Two of the most important parameters for antenna systems in satellite communication are that gain and directivity. The directivity of an antenna, D , can be defined as “The ratio radiation intensity in a given direction from the antenna to radiation intensity averaged overall directions” (Balanis, 2005). The maximum directivity is mathematically expressed as

$$D_{\max} = \frac{U_{\max}}{U_0} = \frac{4\pi U_{\max}}{P_{\text{rad}}} \quad (4)$$

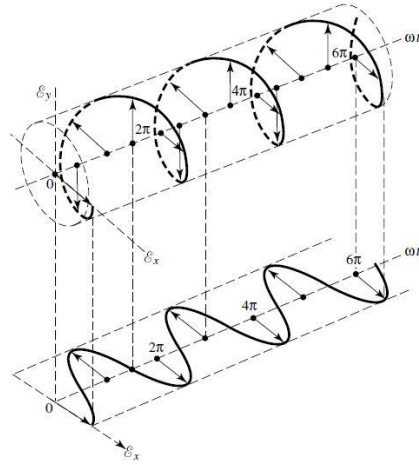
Here, in order to find average radiation intensity (U_0) in equation (4), total radiated power (P_{rad}) in equation (4) is divided by 4π .

The gain is defined as “the increase in strength realized in concentrating the radiowave energy, either in transmission or reception, by the antenna system.” (J. Ippolito, 2008). Gain is usually expressed as in dBi, decibels above an isotropic antenna, which is an antenna that radiates uniformly in all directions. The ratio between the radiated power from the antenna of a system to transmit (generated) power of antenna gives total system efficiency. The system efficiency represents with a coefficient, which is e_0 . Gain of antenna is calculated with directivity of antenna in given direction.

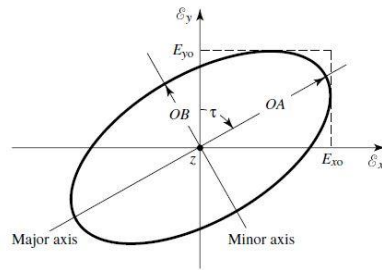
$$G = e_0 D \quad (5)$$

2.3.2.4. Polarization

The wave radiated by the antenna consists of electric and magnetic field components. These two components are orthogonal and perpendicular to the propagation direction of the wave, and also vary according to the frequency of the wave. As a rule, the polarization of the wave is defined by the direction of the electric field. Polarization can be classified into three different types, linear, circular and elliptical. In general, it can be said that the electric field traces are an ellipse and they are actually elliptical polarized. Accordingly, it can be said that linear and circular polarization is a special case of elliptical polarization.



(a)



(b)

Figure 2.16. Polarization (a) Rotation of Wave (b) Polarization Ellipse (Balanis, 2005)

The polarization type is determined by an antenna parameter called axial ratio. Axial ratio can be expressed as;

$$AR = \left| \frac{E_{\max}}{E_{\min}} \right| \quad (6)$$

Generally, elliptically polarization is the ration of major axis to minor axis. If this ratio value is zero ($AR=1=0$ dB), the polarization will be circular. If the value of ratio is going to infinity ($AR=\infty$), the polarization will be linear. But In the literature, if the radiated electromagnetic wave has an axial ratio between 0 dB to 3 dB, it is considered to be circular polarized.

2.4. Diplexer Structure

The feeding system of satellite communication required with high performance

structures to combine reception and transmission in a common antenna. These structures are known as multiplexers/diplexers that they can be used as frequency separator. Multiplexers generally have three or more ports and they consist of different types of filters which provide working at separated frequency bands as receive and transmit channels.

Receive/transmit channel multiplexers for satellite or space communication systems must provide high isolation between the bands, due to the high difference of receive and transmit signal levels. Moreover, these structures have to provide low insertion loss, mass, size and high power handling capability (sometimes more than several kW) features. Waveguide diplexers/multiplexers are preferred due to providing these features. Different filters can be combined a T-junction in these multiplexer structures.

Waveguide diplexers classified as two main types which they are shown in figure below (see Figure 2.17) as, E-plane, H-plane. A 3-port diplexer which is designed in this thesis consists of a common port, a TX port and a RX port. TX port comes from the transmit channel and comprises a RX reject filter and the RX port goes to receive channel and comprises a TX reject filter. Also, common port supports the feed horn and provides to transmission of the channels RX/TX. The connection of all these ports is provided by a T-Junction structure. The most important point for common port is that its dimensions should be chosen by single mode propagation capability in the operating frequency of the system.

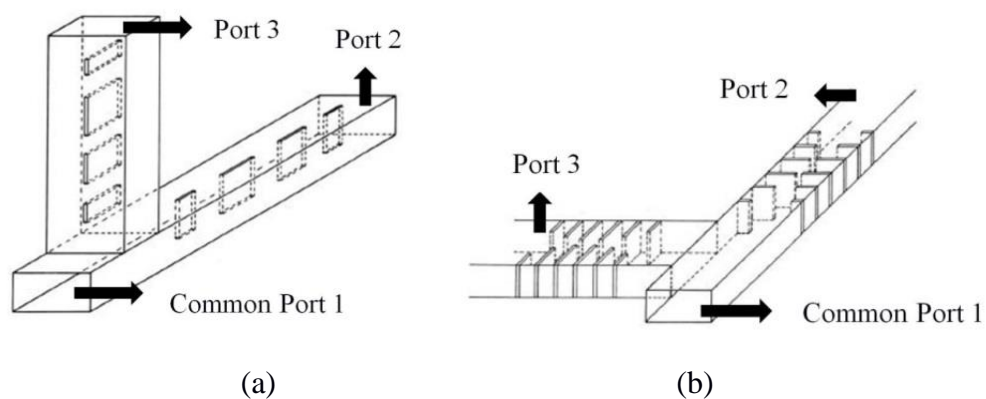


Figure 2.17. General Waveguide Diplexer Types (a) E-plane type diplexer (b) H-plane type diplexer (Uher, Bornemann and Rosenberg, 1993)

For different applications or requirements, dual-polarized diplexers, which contain E-plane and H-plane lines together in separate ports, can be sometimes designed.

In this thesis, three port waveguide diplexers are designed in three different versions. The operating band is determined as Ku frequency band, and the receiving channel is determined between 10.5 and 12.75 GHz, also transmit channel is determined between 17.3 and 18.4 GHz. For these reasons, proposed diplexer requires different filters to provide band pass between receiving and transmitting channels. Theoretical information and design steps of the diplexers are explained in chapter 4.

2.4.1. Rectangular and Square Waveguides

Waveguides are metal pipes guiding electromagnetic waves and can propagate electromagnetic energy above a certain frequency. They are the transmission lines commonly used in many areas such as, high power systems, millimeter wave applications, satellite systems and some precision test applications. Hollow metal pipes, coaxial cables and fiber optical cables can be given as example of the waveguides. (Uher, Bornemann and Rosenberg, 1993)

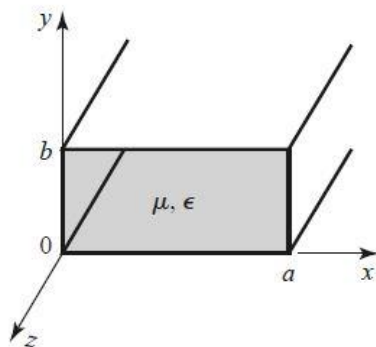


Figure 2.18. Geometry of the Rectangular Waveguide (Pozar, 2012)

There are two main geometries of waveguides. These are rectangular and cylindrical structures. Also, square type waveguides can be used for dual-polarized applications. Rectangular waveguides are the most commonly used propagation medium in antenna feed systems. They have some advantages such as being durable, having low loss and high power handling capability. Their sizes cause disadvantageous at lower frequencies. However, they are often used in the frequency range between 6 and 140

GHz, and for these frequencies the sizes of rectangular waveguides can be compact dimensions. Figure 2.18 where the long and short edges of the waveguide respectively given as a and b show the structure of basic rectangular waveguide.

In this thesis, rectangular and square type waveguide structures are used for diplexer design. Therefore, in the next section of this chapter, “Propagation and Mode Theory in Rectangular Waveguides” are explained.

2.4.1.1. Propagation and Mode Theory in Rectangular Waveguides

Theoretically, there are three modes of propagation in waveguide and transmission lines by solving Maxwell’s equations. These modes are TE, TM and TEM waves. In rectangular waveguides only TE_{mn} and TM_{mn} modes can be excited. Here, m and n are two integers. They can take on all values from zero to infinity, and represent the number of half sine wave variations of the field component in the x and y directions respectively. If the propagation direction is assumed to be “+z” by Figure 2.18, for TE waves, there is no E-field so, the E-field vectors are always perpendicular to the direction of propagation. In TM mode, there is no component of H-field vector along the propagation direction; therefore, H-field vectors are always perpendicular to the direction of propagation.

Each mode (each combination of m and n) has a cutoff frequency $f_{c,mn}$ given by;

$$f_{c,mn} = \frac{k_c}{2\pi\sqrt{\mu\varepsilon}} = \frac{1}{2\pi\sqrt{\mu\varepsilon}} \sqrt{\left(\frac{m\pi}{a}\right)^2 + \left(\frac{n\pi}{b}\right)^2} \quad (7)$$

According to (7), cutoff frequency depends on the dielectric material, the waveguide dimensions and the considered mode, no electromagnetic energy propagates. The other important point about the TE and TM modes in waveguides, that all TE and TM modes have the same cutoff frequency, except from the TE modes with subscripts m or n equal to zero.

To sum up, the advantages provided by waveguide mode theory are the determination of the cutoff frequency and the operating frequency range.

2.4.1.2. Dominant Modes in Rectangular and Square Waveguides

The dominant mode is the mode with lowest cutoff frequency. From the equation (7), the dominant mode always TE_{10} in rectangular waveguides as shown in figure (see Figure 2.19). As known, unlike rectangular waveguide, the square waveguide has two equal edges. For this reason, two dominant modes of TE_{10} and TE_{01} should be considered in structure with square waveguide. Its cutoff frequency can be written as;

$$f_c = \frac{c}{2a\sqrt{\mu\epsilon}} \quad (8)$$

By all these information, considering the operating frequency band of the diplexer (10-19 GHz), the most suitable standard waveguides to work with are WR-75 and WR-62, whose characteristics are detailed in a table (see Table 2.1). The frequency band is 10.5-12.75 GHz for RX, and 17.3-18.4 GHz for TX. According to these frequency bands, the usable frequency range of the WR-75 is appropriated for RX port and the usable frequency range of WR-62 is appropriated for TX port. Also, owing to lowest cutoff frequency of the WR-62 waveguide, it is used again for common port dimensions because, it covers operating frequency band of the system.

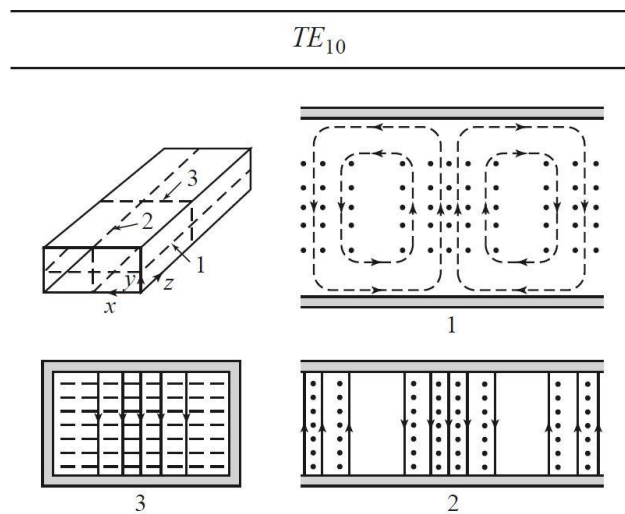


Figure 2.19. Field lines for dominant TE_{10} mode in rectangular waveguides (Pozar, 2012)

Table 2.1. Waveguide Characteristics (WR-75 & WR 62)

| Waveguide Type | Inner dimensions a x b (in millimeters) | Usable Frequency Range (GHz) | TE ₁₀ Cutoff Frequency (GHz) |
|----------------|---|------------------------------|---|
| WR-75 | 19.05 - 9.525 | 10 - 15 | 7.869 |
| WR-62 | 15.7988 – 7.8994 | 12.4 - 18 | 9.488 |

2.4.2. Circular Waveguides

Circular waveguides are generally used in some specific applications where the circular symmetry is utilized, such as in a rotary joint, or in specific components, such as phase shifter or dual mode filters (Bianchi, 2007). In this thesis, the designed conical corrugated horn antenna has an input waveguide structure in a circular geometry. Besides, due to the rectangular geometry of the diplexer, a rectangular-to-circular waveguide transition is needed to provide connection of the antenna and diplexer structure together.

These waveguides are hollow metal pipes that support TE and TM modes. According to cylindrical coordinates, the geometry of a circular waveguide is shown in figure below (see Figure 2.20) with inner radius a .

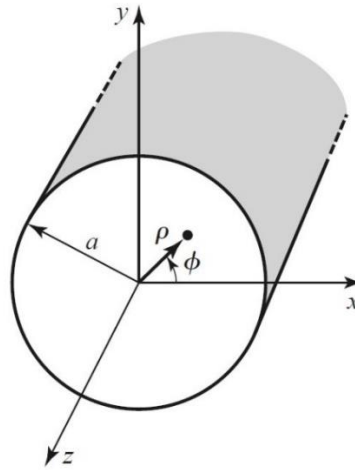


Figure 2.20. Geometry of a Circular Waveguide (Pojar, 2012)

The operating frequency and the modes which can travel inside of the circular waveguide are determined by the inner radius since the radius value is the most effective parameter for the determination of cutoff frequency. The cutoff frequency for circular waveguides is defined as;

$$f_{c_{mn}} = \frac{\rho_{mn} c}{2\pi a \sqrt{\mu\epsilon}} \quad (9)$$

where c is the speed of light. TE_{11} is the dominant mode for the circular waveguides. Field lines for some different modes in circular waveguide are shown in Figure 2.21.

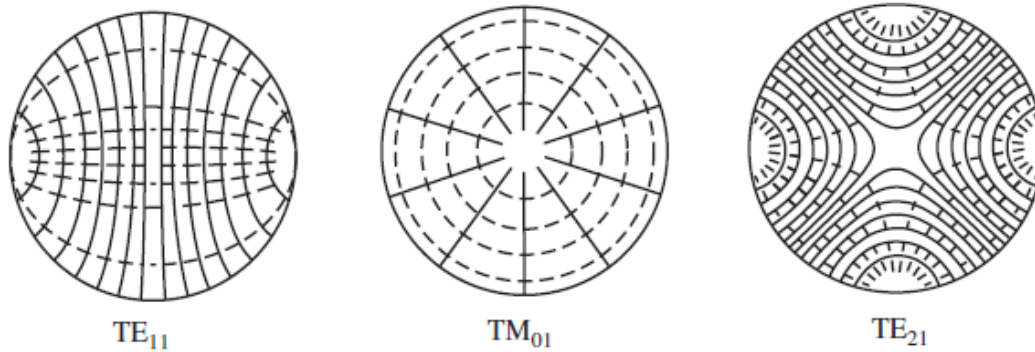


Figure 2.21. Field Lines of Some Circular Waveguide Modes (Balanis, 2012).

2.4.3. Waveguide T-Junction

In many microwave systems it is necessary to provide a connection between two or more transmission lines. In rectangular waveguide structures, this process is realized by waveguide T-junctions. These structures can be divided into two types as H-Plane and E-Plane as shown in Figure 2.22.

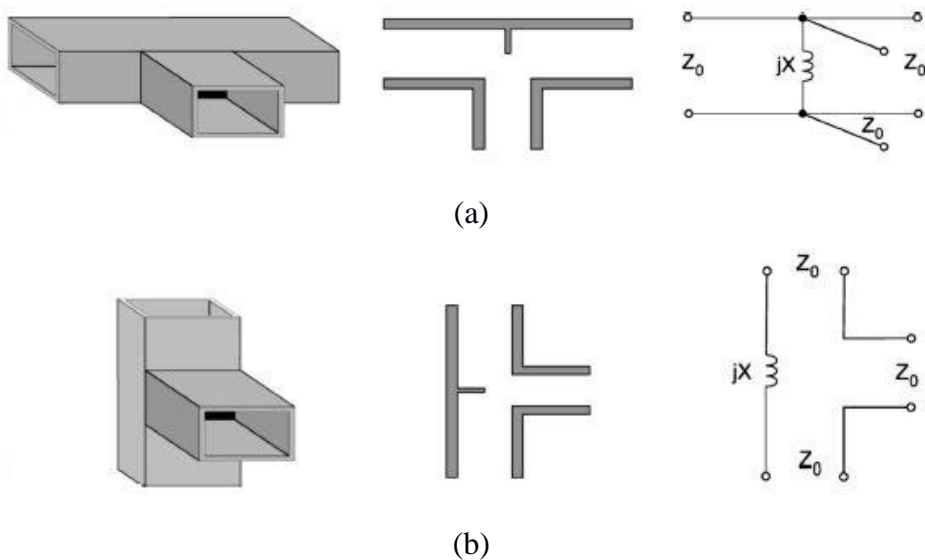


Figure 2.22. (a) H-plane (b) E-plane T-Junctions and Their Respective Equivalent Circuits (Sorrentino, Bianchi, 2010)

E plane junction corresponds to the series connection of the branch line, while the H plane junction corresponds to the shunt connection. This is easily understood by focusing attention on the waveguide longitudinal currents, which flow at the center of the wider waveguide walls. In order to reduce the mismatch, and thus the reflections that a simple junction produces, suitable metal elements can be inserted in the junction region to compensate for the reactance values associated with the discontinuity (Sorrentino, Bianchi, 2010).

2.4.4. Waveguide Filters

Filter structures are generally used to reject undesired frequencies in the system, or to adjust the desired operating frequency. For filtering process, low loss, high isolation, band-passing and compact sized structures are sought. These requirements can only be achieved with waveguide filters. They are often preferred in RF/microwave technologies and satellite communication systems due to these features. Today, widely used filter types are low-pass, high-pass, band-pass and band-stop filters; which are named according to their pass band responses, and their characteristics are shown in Figure 2.23. (Uher, Bornemann and Rosenberg, 1993).

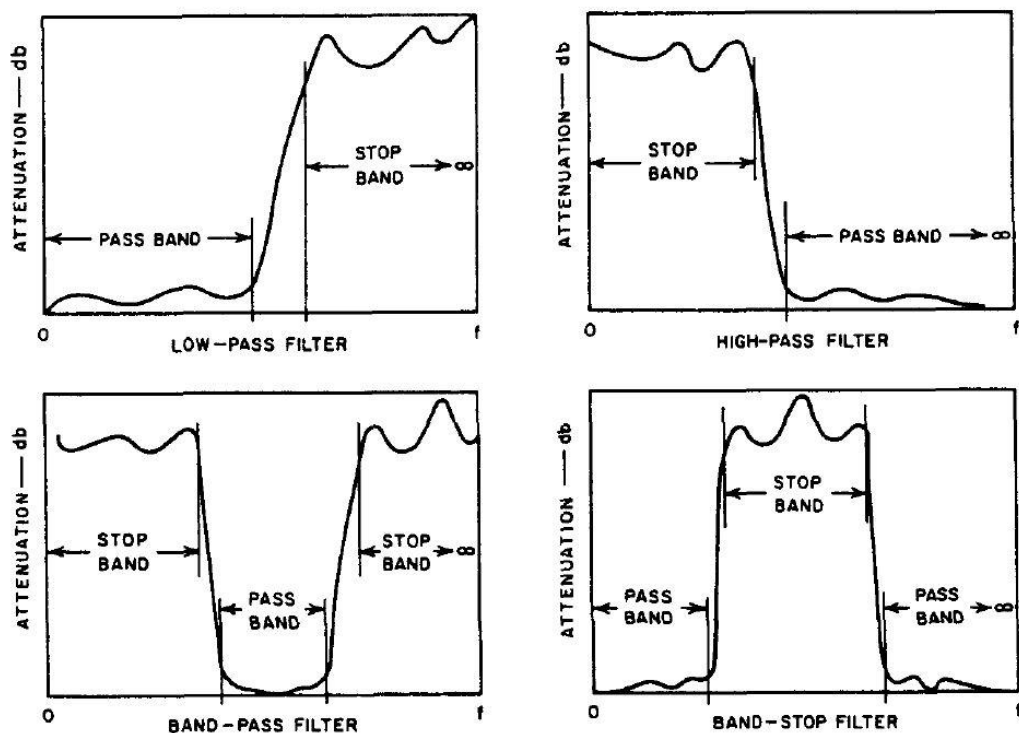


Figure 2.23. Four Common Types of Filter Characteristics (Matthaei, Young and Jones, 1980)

The system designed in this thesis will work on a wide range of band such as 10-19 GHz and since the receive band covers 10.5-12.75 GHz and the transmission band covers specific band ranges such as 17.3-18.4 GHz, two separate waveguide band pass filters are used for receiving/transmitting operation in diplexer structure.

In the designed band pass filter, iris and corrugated structure are preferred and low-pass Chebyshev prototype filter theory is used. These irises/obstacles can be ordered symmetrically or non-symmetrically according to the positive effects in system and they are used to provide impedance matching. These elements can be classified as shunt-capacitive and shunt-inductive structure that shown in Figure 2.24. If the edges of the iris are perpendicular to the electric plane (E-plane), the capacitive effect is observed. However, if the edges of the iris perpendicular to magnetic plane (H-plane), the inductive effect is observed (Bianchi, 2007).

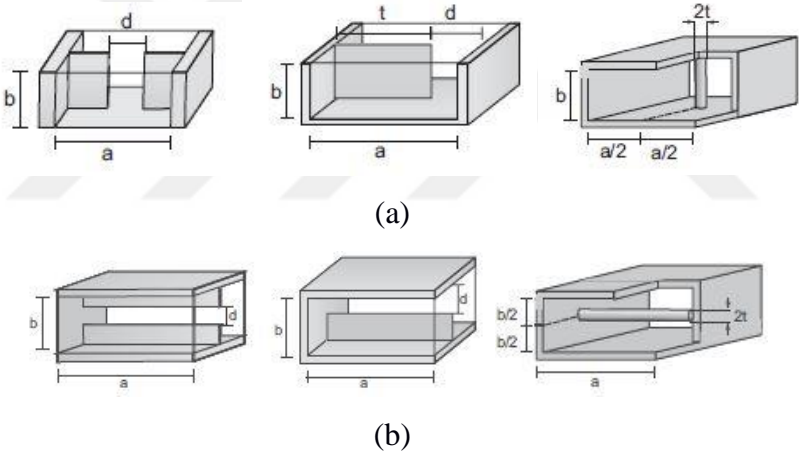
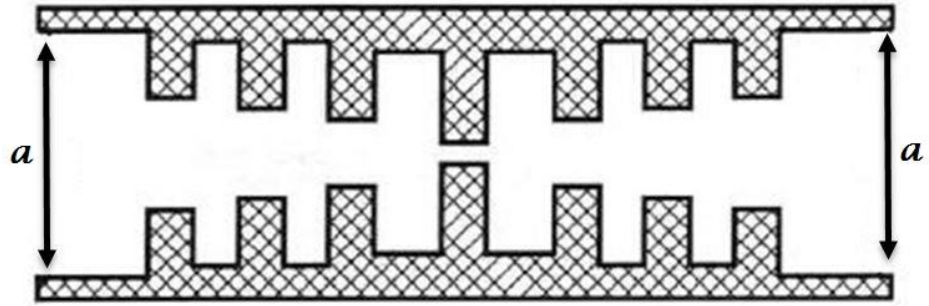
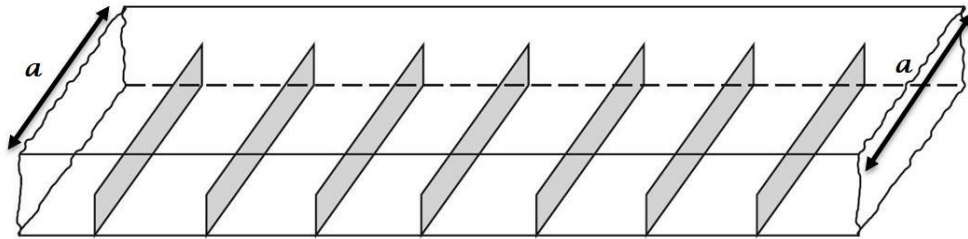


Figure 2.24. Iris Waveguide Types (a) Shunt-Inductive Iris Waveguides (b) Shunt-Capacitive Iris Waveguides (Bianchi, 2007)

Besides, the inductive iris waveguide filter and capacitive iris waveguide filter examples are shown in Figure 2.25. Here, each iris corresponds to either an inductance for Figure 2.25(a) or capacitance for Figure 2.25(b).



(a)



(b)

Figure 2.25. Iris Waveguide Filters (a) Inductive Iris waveguide filter cross-section. (Uher, Bornemann and Rosenberg, 1993) (b) Capacitive Iris waveguide filter cross-section (Pozar,2012)

CHAPTER THREE

CONICAL CORRUGATED HORN ANTENNA DESIGN

3.1. Conical Corrugated-Profile Design

In many different applications, dual linear or circular polarization is used. However, for a horn antenna in a smooth-walled structure, the beamwidth values in two different planes are not equal because the aperture geometry of these antennas is only square or circular. When we feed a reflector with such horn antennas, unequal phase centers appear in the orthogonal plane, as a result, high sidelobe level and back lobe are obtained in E-plane and H-plane. This is an undesirable situation for the system. If we convert the smooth-walled horn antenna profile to the corrugated antenna profile, then these disadvantages are prevented (Milligan, 2005). For these reasons, the corrugated-profile horn antenna is preferred to feed in this thesis.

It should be noted that, in our study, the minimum frequency (f_{min}) is 10 GHz, the maximum frequency (f_{max}) is 19 GHz, and depending on these frequencies, our operating band is determined as 10-19 GHz. Since this specified operating band provides the broadband application condition of (9), the center frequency (f_c) value is calculated almost 12 GHz, according to (10) and (11).

$$1.4f_{min} \leq f_{max} \leq 2.4f_{min} \quad (10)$$

$$f_c \approx 1.2f_{min} \quad (11)$$

As mentioned in section 2.3.1 of thesis, the antenna consists of input waveguide, mode converter, corrugated profile and aperture parts. Although they are named separately, the mode converter and corrugated profile are designed as a whole. This is because the mode converter type also determines the profile of the corrugated structure. The choice of the mode converter type is an important factor in the design of the antenna, because this structure is determined by the operating frequency band. There are 3 types of mode converter as, variable-depth, ring-loaded and variable-

pitch-to-width slots, and each of them provides a different bandwidth (Granet and James, 2005). In this study, the variable depth slot mode converter which provides our operating frequency band 10-19 GHz and shown in Figure 3.1 is chosen to be used for the design of the corrugated antenna profile.

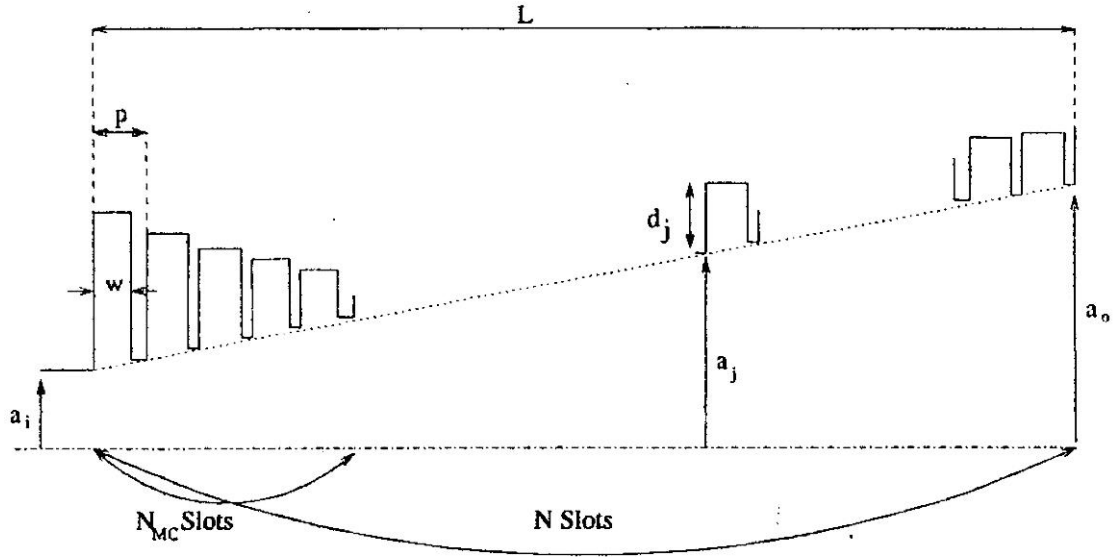


Figure 3.1. Variable-depth slot type mode converter and parameters (Granet and James, 2005)

The bandwidth which is provided by variable depth slot mode converter is given by;

$$f_{\max} \leq 1.8 f_{\min} \quad (12)$$

After determining the mode converter type and corrugated profile structure, the parameters shown in Figure 3.1 are calculated as given in Table 3.1.

Table 3.1. Corrugated horn antenna parameters

| Parameter | Definition |
|-------------------------------|---------------------------|
| a_i | Input radius |
| a_o | Output radius |
| L | Length |
| N | Total number of slots |
| $P=L/N$ | Slot pitch |
| w | Slot width |
| $\delta=w/p$ | Slot pitch to width ratio |
| $(p-w)=(1-\delta)p$ | Width of the sloth teeth |
| d_j where $1 \leq j \leq N$ | Depth of the j th slot |

For the calculation of parameters firstly, a reference input radius value is obtained for the input waveguide using the formula given in (13).

$$a_i = \frac{3\lambda_c}{2\pi} \quad (13)$$

As a result, the calculated reference input radius (a_i) value is determined as 11.94 mm. The reference output radius (a_o) value is obtained by the way of the graphic in the figure (see Figure 3.2), from the literature knowledge that the optimum flare (taper) angle value for the corrugated feed horns is about 19-20 degrees.

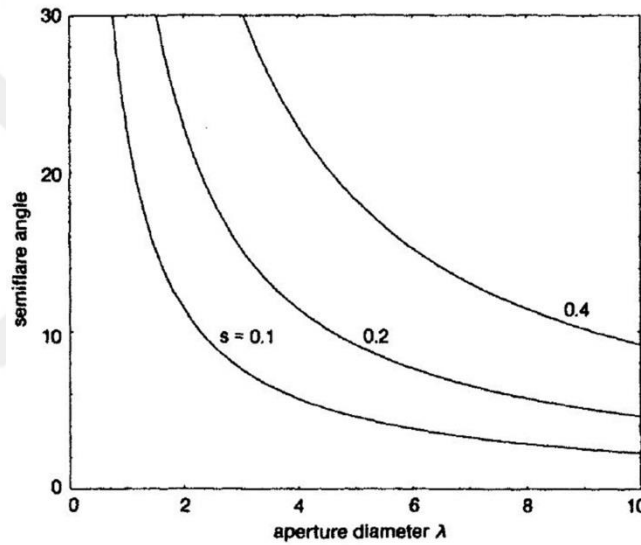


Figure 3.2. Output Radius-Flare Angle Graph (Olver, Clarricoats, Kishk and Shafai, 1994)

In this way, the reference a_o value is determined almost $1.8\lambda_c \approx 45$ mm.

$$\frac{\lambda_c}{10} \leq p \leq \frac{\lambda_c}{5} \quad (14)$$

Another important parameter which is the total value of the slot width and ridge width is the slot pitch (p) value. For the determination of this parameter, the range that given in (14) was taken into consideration and optimization study is carried out accordingly.

The depths of the slots are generally determined between $\lambda_{min}/4$ and $3\lambda_{max}/4$ along the band in the literature, and the smallest and largest depth values of the designed antenna were obtained as 4.94 mm to 9.85 mm. Another important consideration for antenna design in such applications is that the antenna is in a compact size. For this reason, it is aimed to set the flare length of antenna to be between 75-85 mm in this study. As a result, the number of slots (N) are determined approximately 15.

3.1.1. Optimization Works and Simulation Results

The antenna is designed and optimized with *CST Microwave Studio* software using all these reference dimensions calculated in the previous section. In order to get fast results in the first stage, *PEC* was selected as the material in the *CST* and the simulations were done by *Time Domain Solver*. The values obtained after the optimization studies are given in Table 3.2, and the designed antenna structure with these parameter values is shown in Figure 3.3.

Table 3.2. Values of the Antenna Parameters after the First Optimization

| Parameter | Value (mm) |
|-----------------|------------|
| a_i | 12.64 |
| a_o | 40.55 |
| L | 72 |
| N | 15 |
| $P=L/N$ | 4.79 |
| w | 3.47 |
| $p-w$ | 1.33 |
| Max. slot depth | 9.86 |
| Min. slot depth | 4.94 |

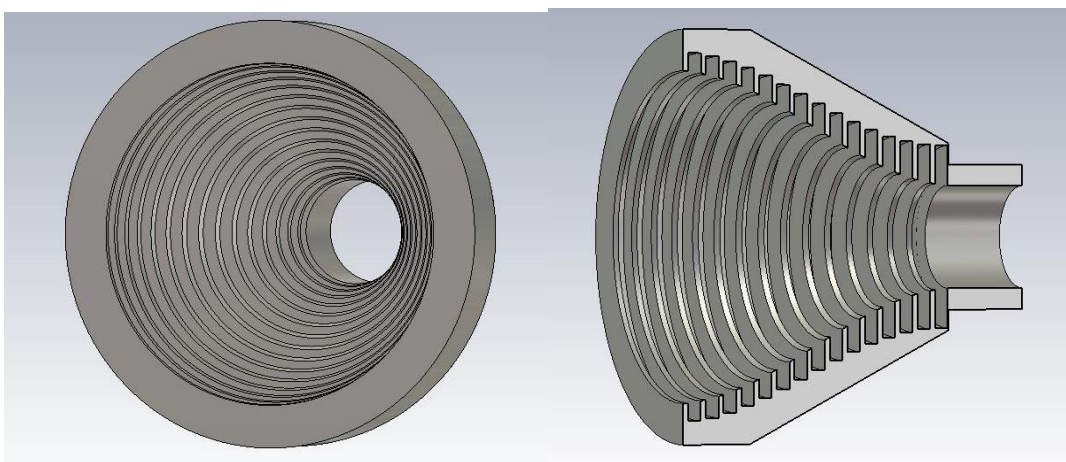


Figure 3.3. Designed Conical Corrugated Horn Antenna

The simulation results of the return loss (S_{11}) and VSWR value in the operating frequency band of the designed antenna are shown in Figure 3.4.

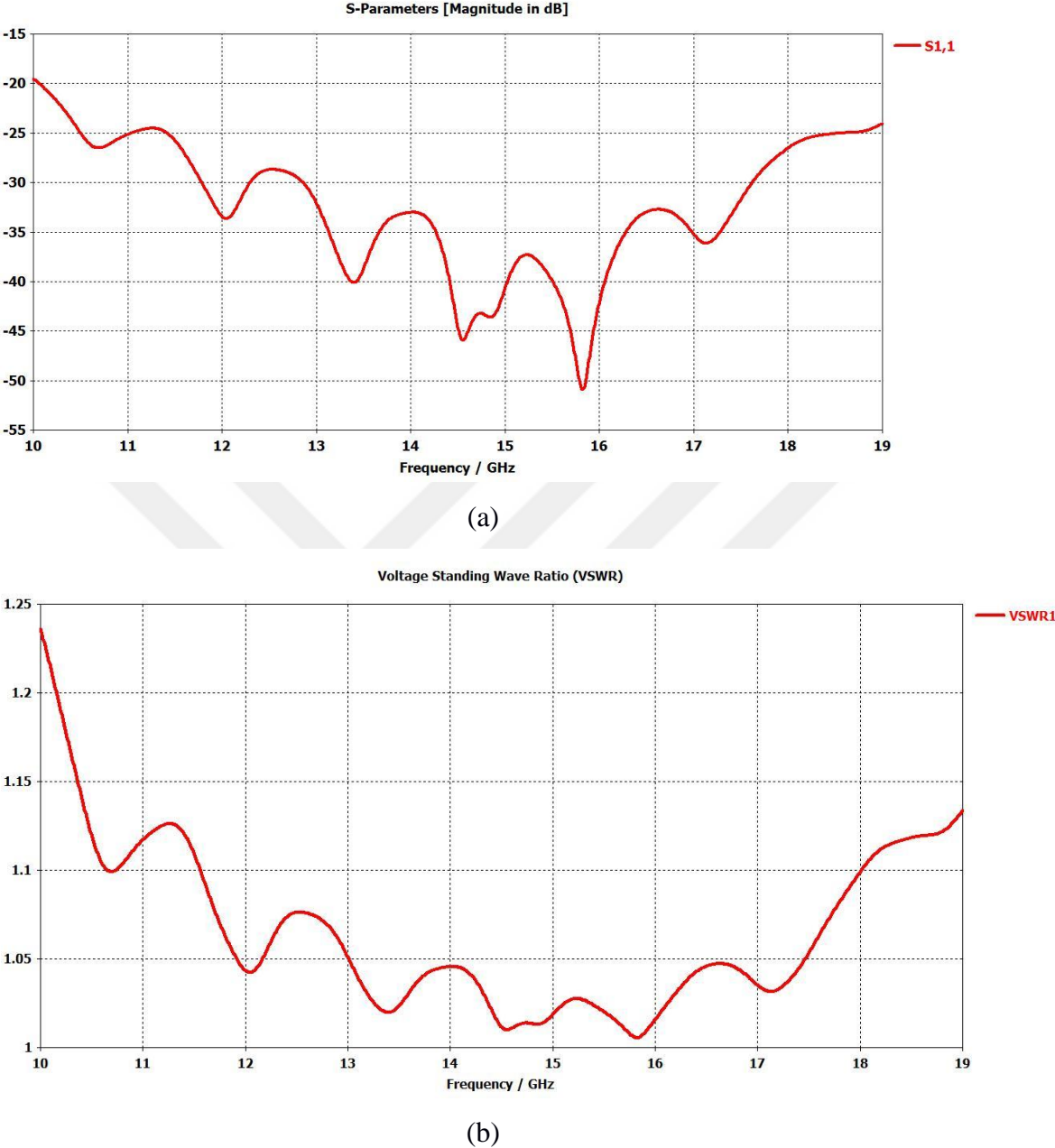


Figure 3.4. Results of the Designed Antenna After the First Optimization (a) S_{11}
(b) VSWR

3.2 Antenna Design with Transition

Since the antenna structure is used to feed a reflector in satellite communication systems, a diplexer waveguide will be supported behind the antenna; therefore, a circular to rectangular transition waveguide is needed in the feeding section of the

antenna. The transition section converts the dominant TE₁₀ mode in rectangular waveguide to TE₁₁ dominant mode in circular waveguide and vice-versa. To avoid unexpected dimensional changes and generation of higher order modes, the minimum length of the transition should be $2\lambda_g$, where λ_g is guided wavelength given as;

$$\lambda_g = \frac{\lambda_0}{\sqrt{1 - \left(\frac{f_c}{f_0}\right)^2}} \quad (15)$$

For transition, the dimensions of the rectangular section are determined according to the standard WR62 waveguide given in Table 2.1, which corresponds to the operating frequency of the antenna. Also, for the circular section, the input radius value is used for the cutoff frequency calculations.

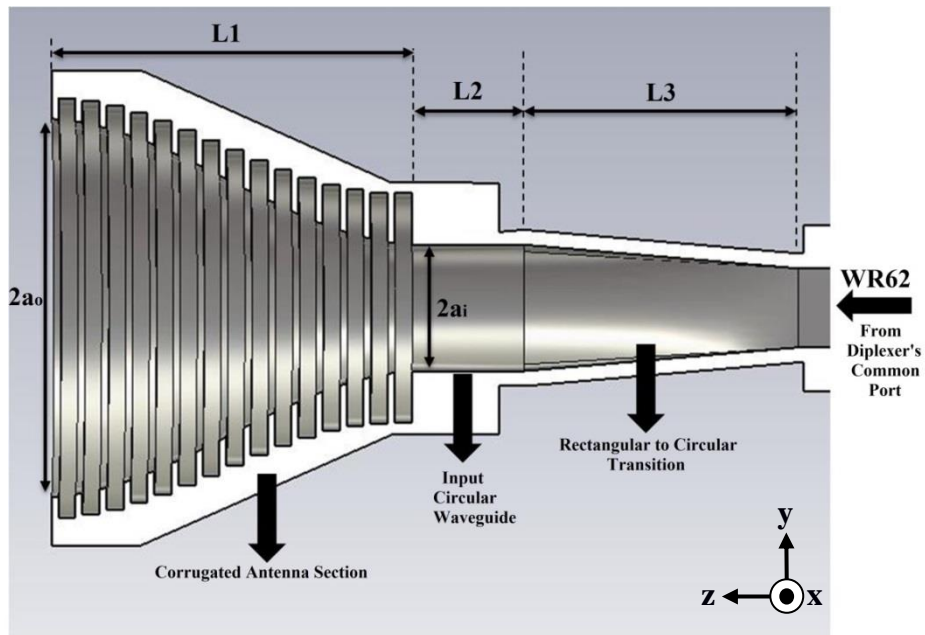
In equation (15), f_c is taken as a mean value 8.22 GHz which is the average cutoff frequency of our circular and rectangular waveguides and also f_0 is taken as 14.5 GHz center frequency. As a result, the λ_g value is determined as 50.48 mm.

3.2.1. Optimization Works and Simulation Results

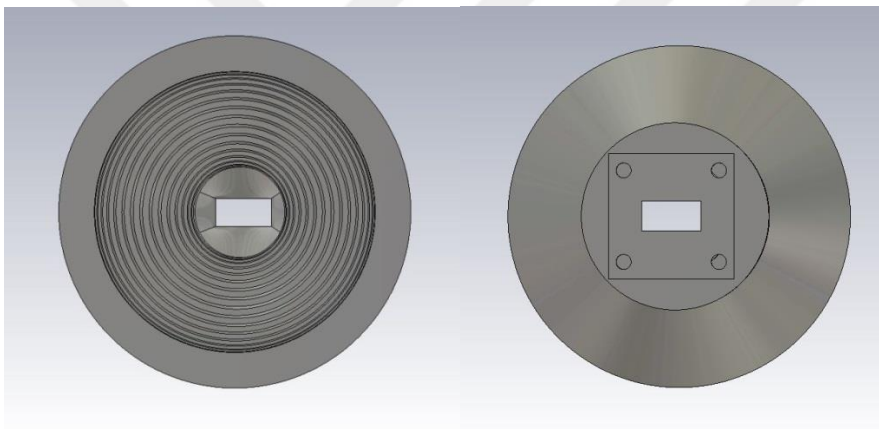
By adding a transition to the antenna structure designed in the previous section, the antenna parameters and transition length have been optimized a second time. During the optimization run, the values of the transition length are determined according to the condition of (minimum length $\geq 2\lambda_g$). The parameter values of the designed antenna after the last optimization are given in Table 3.3, and the structure of antenna are depicted in Figure 3.5.

Table 3.3. Final dimensions of designed antenna

| Parameter | Dimension (mm) |
|-----------------|----------------|
| a_i | 12.64 |
| a_o | 37.88 |
| $L1$ | 72 |
| $L2$ | 22.5 |
| $L3$ | 55 |
| N | 15 |
| $P=L/N$ | 4.8 |
| w | 3.4 |
| $p-w$ | 1.4 |
| Max. slot depth | 10.35 |
| Min. slot depth | 4.68 |



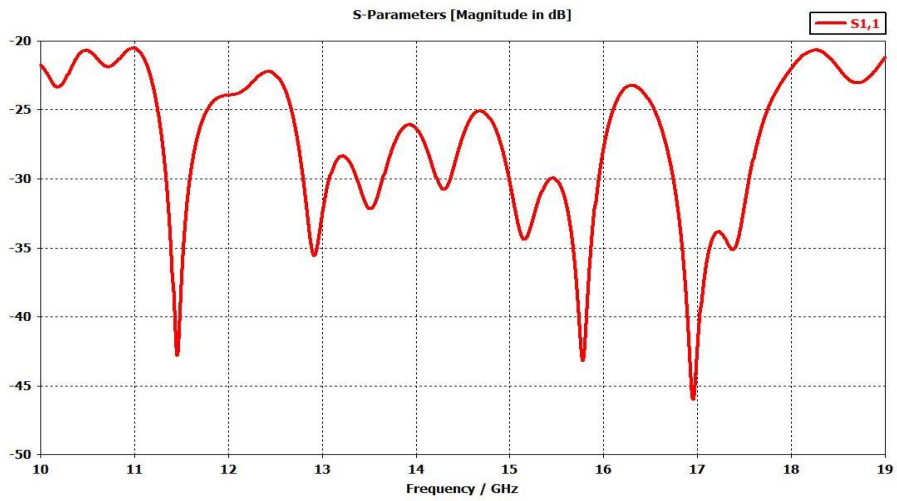
(a)



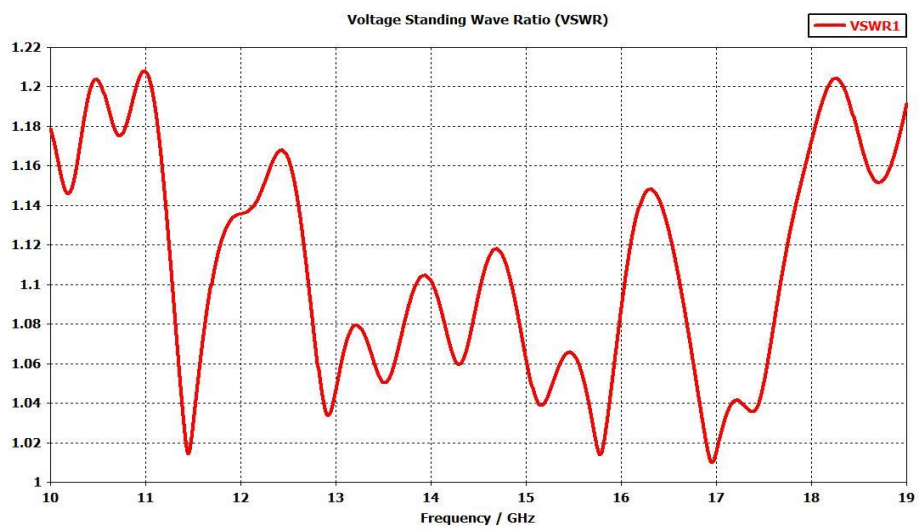
(b)

Figure 3.5. Designed antenna structure (a) with transition and parameters (b) Front and back view

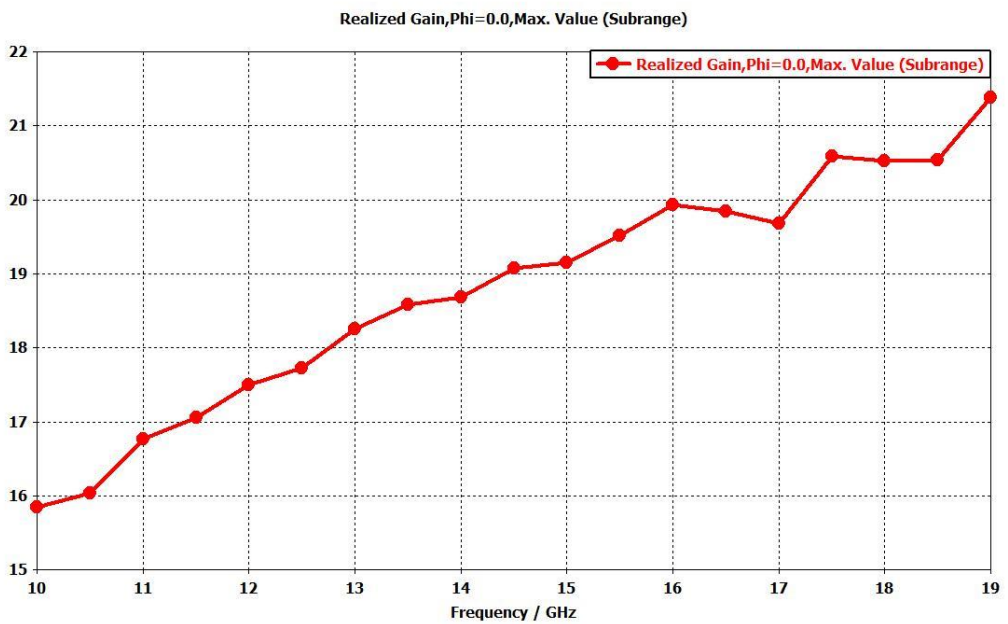
As a result, simulated S_{11} values are lower than -20 dB from 10 to 19 GHz, and the simulated gain values are between 15.9-21.4 dBi for 10-19 GHz. These results are shown in Figure 3.6.



(a)



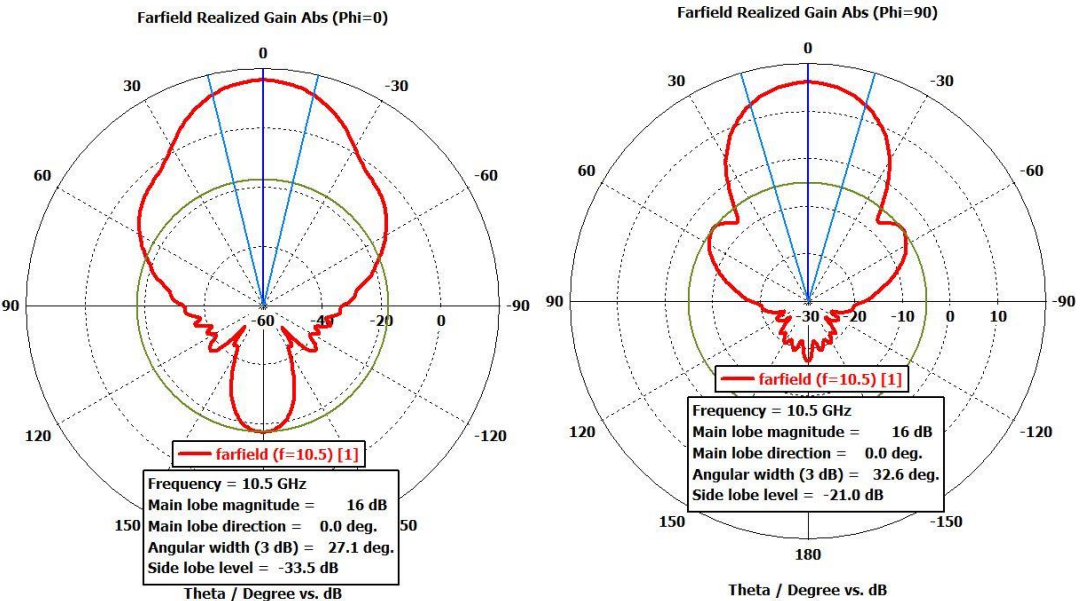
(b)



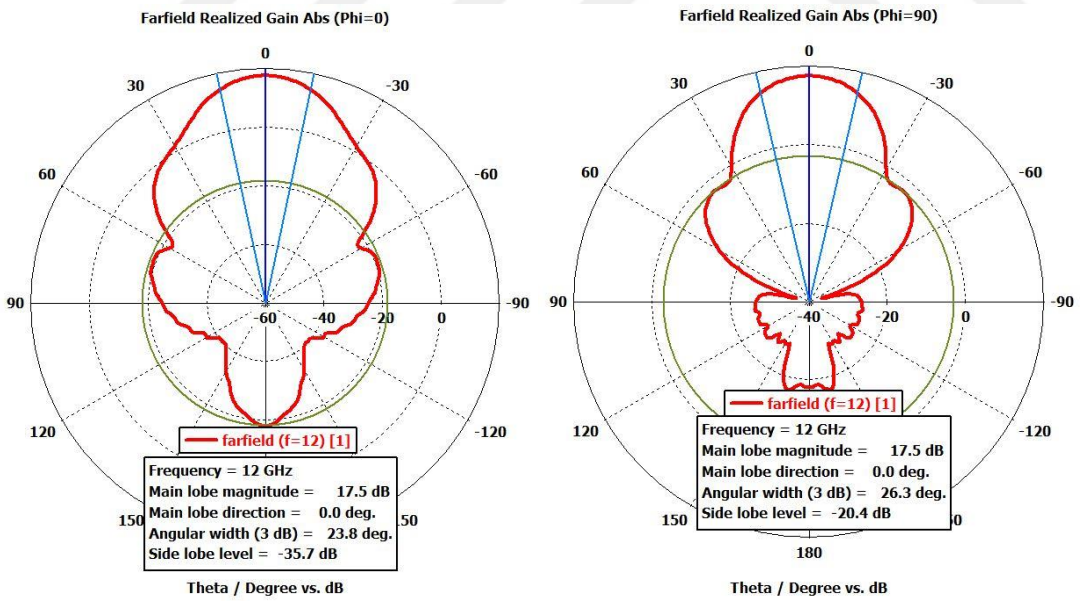
(c)

Figure 3.6. Simulation Results of the Designed Antenna (a) S_{11} (b) VSWR (c) Gain

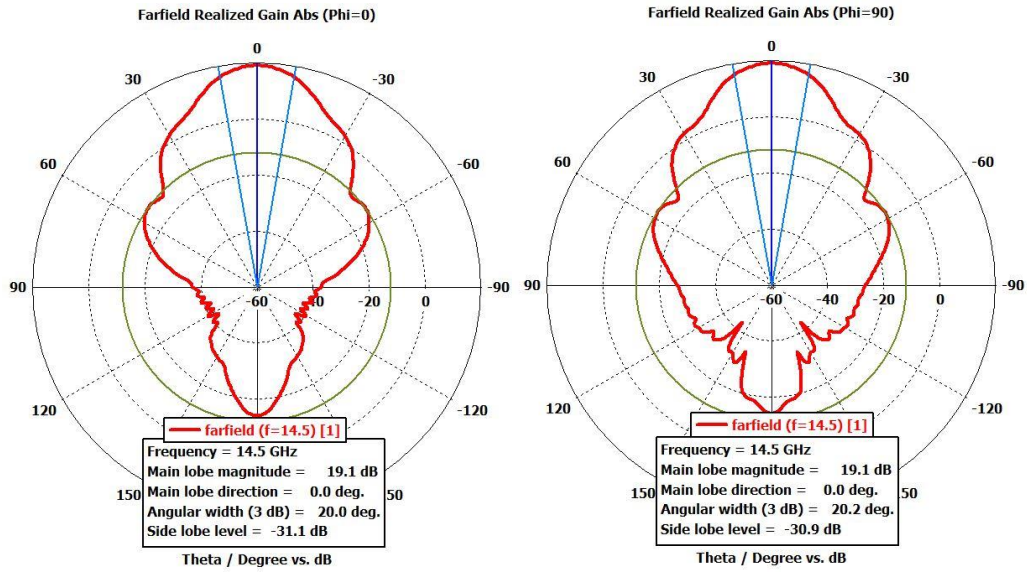
The radiation patterns of the designed antenna at 10.5, 12, 14.5 and 18.5 GHz are given in Figure 3.7 for the azimuth ($\phi = 0^\circ$) and elevation ($\phi = 90^\circ$) planes. As it can be seen from the figures respectively, the antenna has 21 dB, 20.4 dB, 30.9 dB and 23.5 dB side lobe levels in the given frequency bands, which are quite enough.



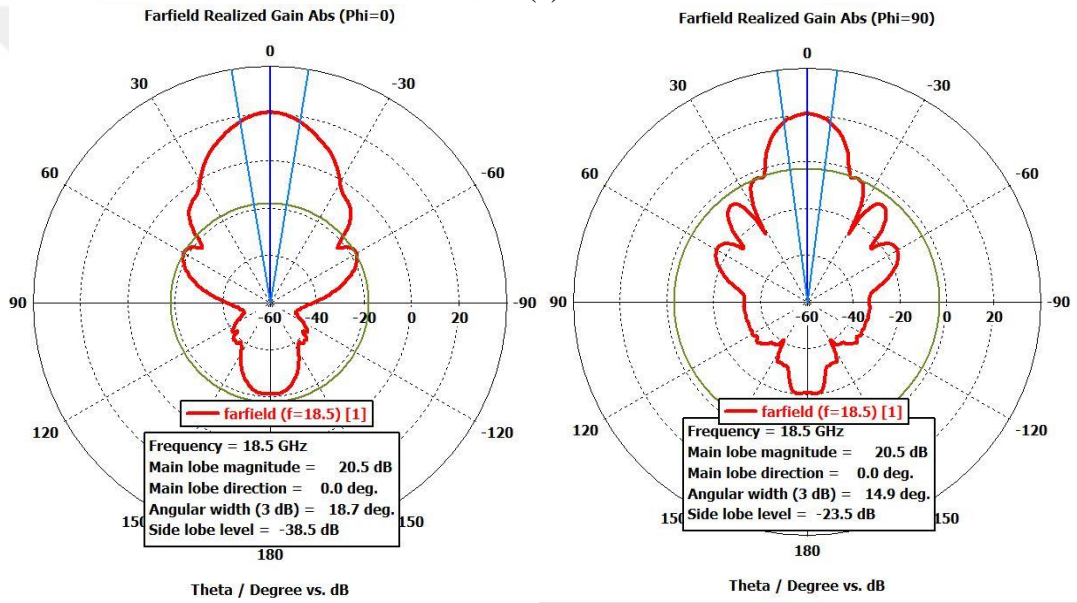
(a)



(b)



(c)



(d)

Figure 3.7. Radiation Patterns of the Designed Antenna at (a) 10.5 GHz (b) 12 GHz (c) 14.5 GHz (d) 18.5 GHz

CHAPTER FOUR

WAVEGUIDE DIPLEXER DESIGN

4.1 Iris Bandpass Waveguide Filter Theory for Diplexer Structure

The most common type of band-pass waveguide filters are shunt inductive or shunt capacitive loaded filters. These type of filters consist of waveguide sections loaded with shunt inductive/capacitive discontinuities, irises or posts which are explained with their advantages before in section 2.4.4. These filters also classified as direct coupled filters. The equivalent circuit of a shunt inductive loaded waveguide filter is shown in figure below (see Figure 4.1), consisting of N transmission line sections loaded with $N+1$ shunt inductances.

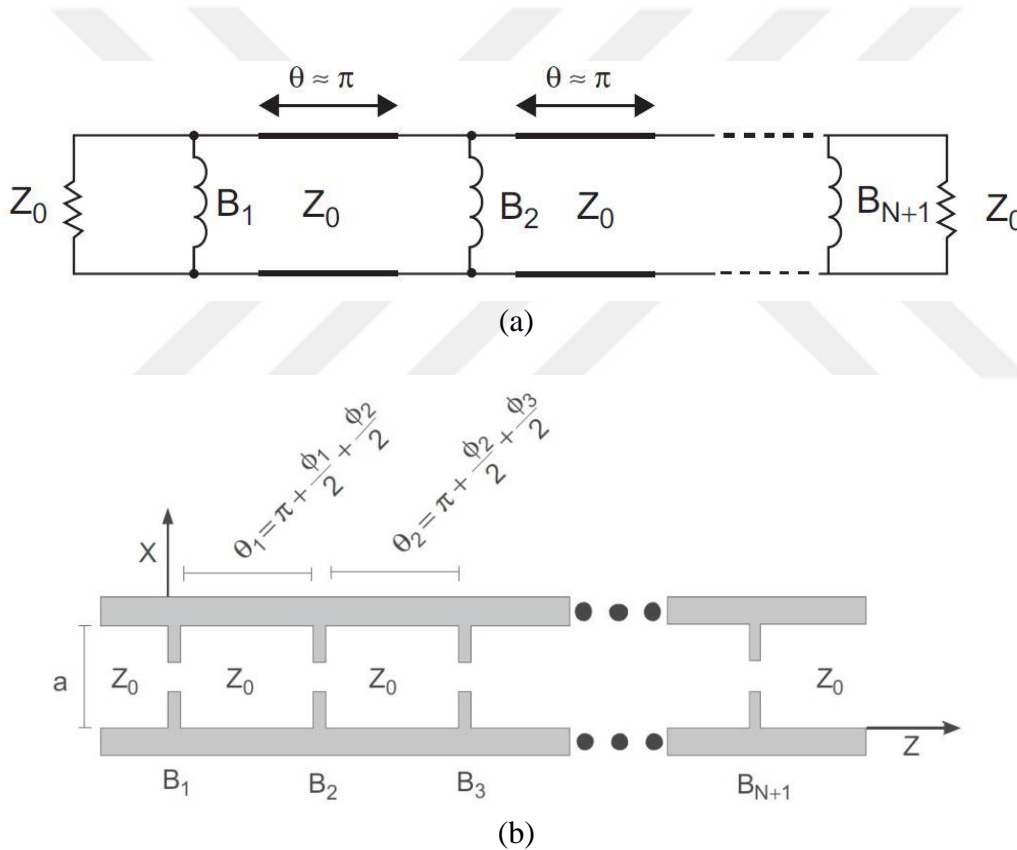


Figure 4.1. Shunt Inductive Loaded Filter (a) Equivalent Circuit (b) Top view of a Shunt Inductive Waveguide Filter (Bianchi, 2007)

The design of these filters consists of four main steps and these are the synthesis of the low-pass prototype, the synthesis of the band-pass filter, design of the waveguide filter structure and optimization works. The synthesis and their equivalent circuits are shown in Figure 4.2.

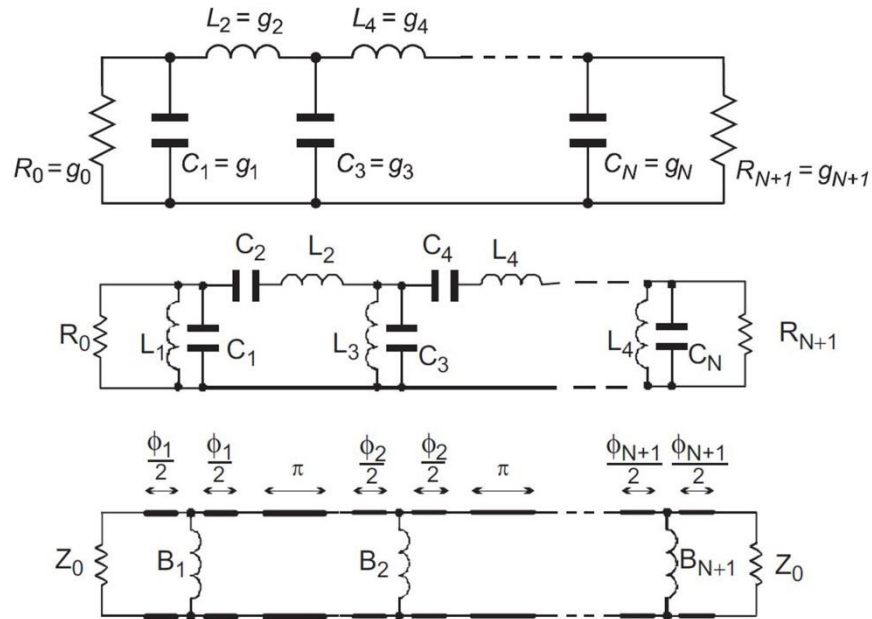


Figure 4.2. The Demonstration of the Synthesis, from top to bottom respectively low pass prototype, conversion of the bandpass prototype and shunt inductance loaded filter (Bianchi, 2007).

For the band-pass filter, the N^{th} order low-pass prototype circuit is transformed into the ladder band-pass filter prototype by using the low-pass to band-pass frequency transform in the literature (Bianchi, 2007). After all these synthesis, waveguide filters have some important parameters as shown in Figure 4.3.

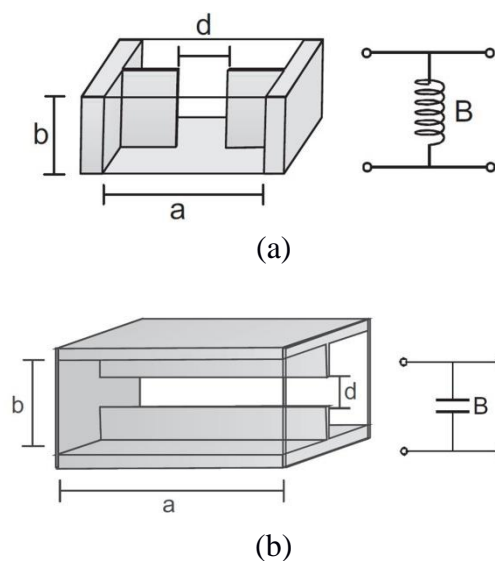


Figure 4.3. Geometry of the Waveguide Filters (a) Shunt-Inductive Iris (b) Shunt-Capacitive Iris (Bianchi, 2007)

The width of each iris is determined by inversion of the formulas from (16) to (20) as given below.

$$B_{ind} = \frac{2\pi}{\beta a} \cot^2\left(\frac{nd}{2a}\right) \left[1 + \frac{a\gamma_3 - 3\pi}{4\pi} \sin^2\left(\frac{nd}{a}\right) \right] \quad (16)$$

$$B_{cap} = \frac{2\beta b}{\pi} \left\{ \ln \left[\csc\left(\frac{\pi d}{2b}\right) \right] + \left[\frac{2\pi}{b\gamma_2} - 1 \right] \cos^4\left(\frac{\pi d}{2b}\right) \right\} \quad (17)$$

$$\beta = \sqrt{(\omega^2 \varepsilon \mu) - \left(\frac{\pi}{a}\right)^2} \quad (18)$$

$$\gamma_2 = \sqrt{\left(\frac{2\pi}{b}\right)^2 - \beta^2} \quad (19)$$

$$\gamma_3 = \sqrt{\left(\frac{3\pi}{a}\right)^2 - \omega^2 \varepsilon \mu} \quad (20)$$

From Figure 4.1(b), the length of the i -th waveguide section between the sequential irises i and $i+1$ is quickly computed by the corresponding electrical length θ_i at the center frequency, ω_0 .

$$l_i = \frac{\lambda_{g0}}{2\pi} \theta_i = \frac{\lambda_{g0}}{2\pi} \left(\pi + \frac{\phi_i}{2} + \frac{\phi_{i+1}}{2} \right) \quad (21)$$

where λ_{g0} is the guided wavelength at center frequency. Besides, it should be noted that if ϕ_i and ϕ_{i+1} are negative, the waveguide length should be shorter than $\lambda_{g0}/2$.

4.1.1. Iris Bandpass (RX Reject) Filter Design for Uplink/TX

In the design of the diplexer, the parts that need to be most sensitive are the filters. Especially in the design of the filter which will work in the uplink band for satellite

communication, it is expected that the return loss value will be at 20 dB levels and at the same time the filter will reject the other bands at higher levels because of the signal transmission at the very high power level from the ground stations.

In this thesis, the target specifications for the uplink filter are to have 17.3-18.4 GHz pass-band, have a low insertion loss value, provide a return loss value better than 20 dB, and reject the downlink band with a minimum level of 70 dB.

Depending on these features, an iris band pass filter which has $N = 5$ sections in accordance with the theoretical information given in section 4.1 is designed by optimizing the parameters that shown in figure below (see Figure 4.4) by using CST Microwave Studio software program.

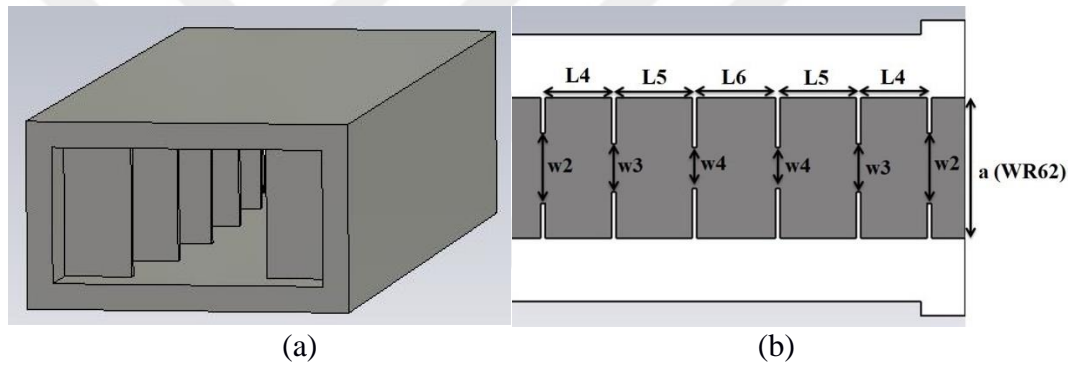


Figure 4.4. The designed H-plane Uplink Bandpass Filter (a) Perspective View and (b) Cross Section View From the Top along with Parameters of Filter

The dimensions of the input and output ports of the filter are selected according to the dimensions of the standard WR-62 waveguide in order to be compatible with the operating frequency. After the optimization studies, the final dimensions of the designed filter are obtained as shown in Table 4.1. The corresponding simulation results for the given parameter values in Table 4.1 are shown in Figure 4.5 where S_{11} - S_{22} (return loss) and S_{12} - S_{21} (insertion loss) values are given.

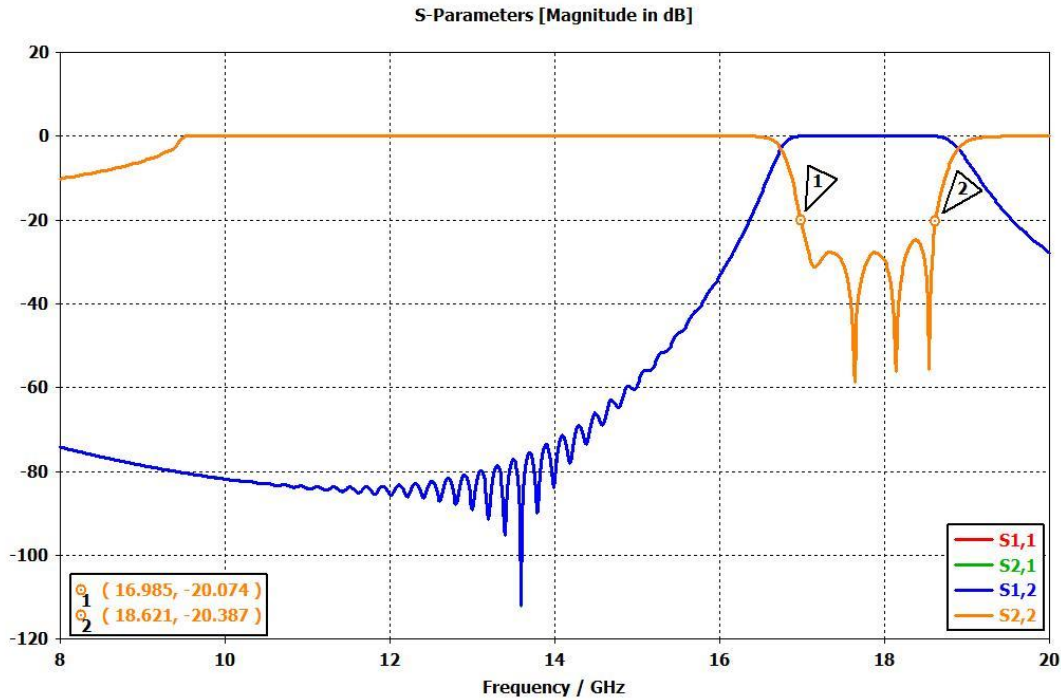


Figure 4.5. Simulation Results of the Designed Uplink Bandpass Filter.

As a result of this simulation, it can be observed that the designed filter for uplink operates in the frequency band of 17.3-18.4 GHz, has better return loss than 20 dB and rejects RX band at 75-80 dB levels.

Table 4.1. The Dimensions of the Uplink Filter

| Parameter | Dimension (mm) |
|------------|----------------|
| w_2 | 7.92 |
| w_3 | 5.34 |
| w_4 | 4.69 |
| L_4 | 7.47 |
| L_5 | 8.64 |
| L_6 | 8.84 |
| a (WR62) | 15.79 |

4.1.2. Iris Bandpass (TX Reject) Filter Design for Downlink/RX

For the downlink filter, the targeted features are to have 10.5-12.75 GHz pass-band, have a low insertion loss value, provide a return loss value better than 20 dB and reject the uplink frequency band at the level of minimum 65 dB.

According to these features, another iris bandpass filter having $N = 9$ sections is designed by optimizing the parameters as shown in Figure 4.6 by using CST Microwave Studio software program.

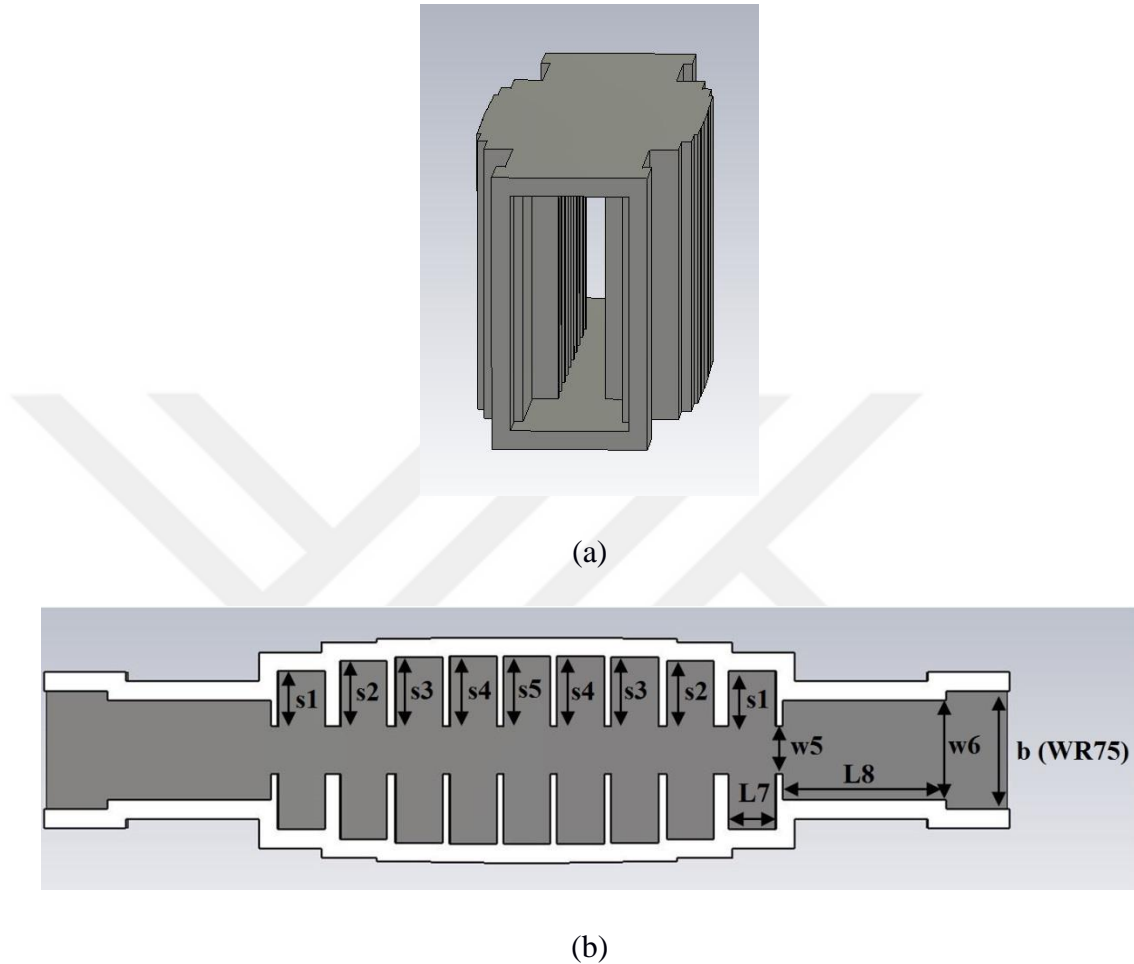


Figure 4.6. The designed E-plane Downlink Bandpass Filter (a) Perspective View and (b) Cross Section View From Top along with the Parameters of Filter

The dimensions of input and output ports of the filter are designed in standard WR-75 waveguide sizes with the symmetric transition structures in order to make compatible with operating frequency. After the optimization studies, the final dimensions of the designed filter are given in Table 4.2, and the corresponding simulation results are shown in Figure 4.7.

Table 4.2. The Dimensions of the Downlink Filter

| Parameter | Dimension (mm) |
|------------|----------------|
| $w5$ | 3.81 |
| $w6$ | 8.05 |
| $L7$ | 3.81 |
| $L8$ | 13.22 |
| $s1$ | 4.47 |
| $s2$ | 5.26 |
| $s3$ | 5.58 |
| $s4$ | 5.62 |
| $s5$ | 5.66 |
| b (WR75) | 9.525 |

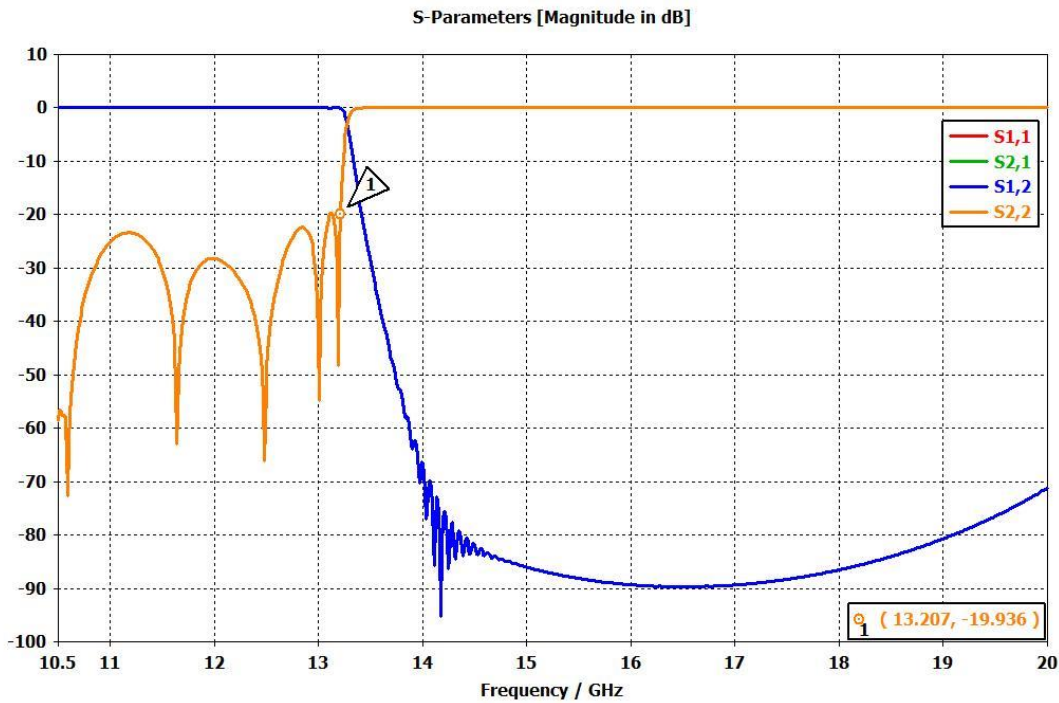


Figure 4.7. Simulation Results of the Designed Downlink Bandpass Filter.

From the results in Figure 4.7, it can be observed that the designed filter for downlink covers 10.5-12.75 GHz frequency band, has better return loss value than 20 dB and rejects TX frequency band at 80-85 dB levels.

4.2. T-Junction Design

As explained in Section 2.4.3, a T-junction design is needed to connect two or more waveguide transmission lines. In this thesis, a three-port T-junction structure was

needed to provide the transmission between uplink, downlink and common lines of the diplexer to be designed. In addition, since two of the diplexers to be designed will be in two different structures as H-plane and E-plane, the junctions are designed in two types; H-plane and E-plane.

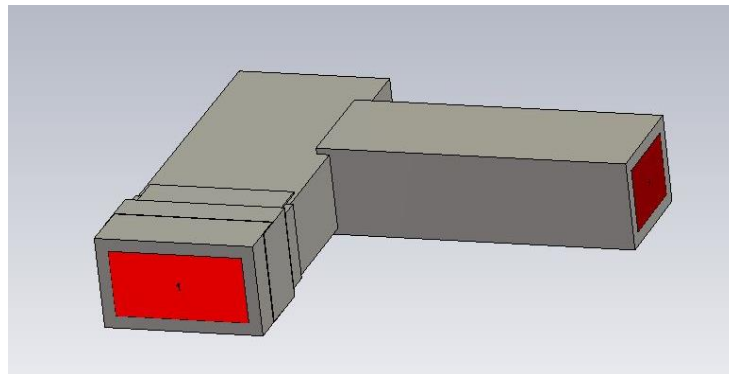
The first one of two most important parameters in a junction design is the distance from the common port to the small ridged structure that separates the three lines/ports from each other, and the other parameter is the dimensions of the window-like structure that separates the TX and RX lines from each other.

Before the optimization work, the initial dimensions of the window-like structure are determined according to the cutoff frequency formula given in (8).

The one of the main aim in junction design is to provide minimum loss for the transmission of the wave in the TX and RX lines from the common port. Afterwards, minimum loss is achieved by the addition of the filters where the insertion loss levels are significantly reduced to about 0.1 dB, and rejection between uplink / downlink will be provided.

4.2.1. H-Plane T-Junction Design and Simulation Results

The H-plane junction structure was designed by optimizing the parameters that described in the previous section in CST Microwave Studio software program and it is shown in the Figure 4.8 with the optimized parameters.



(a)

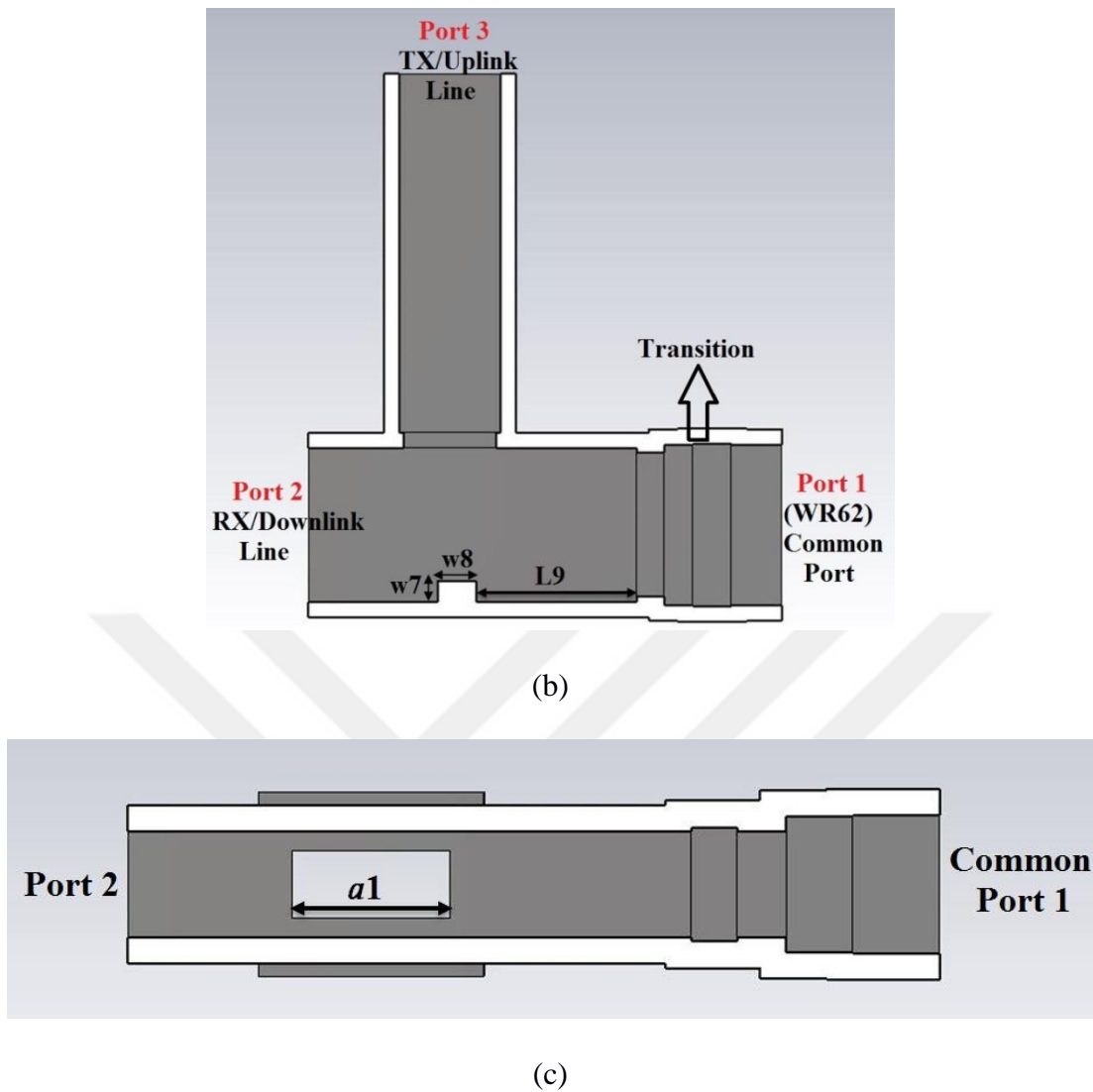
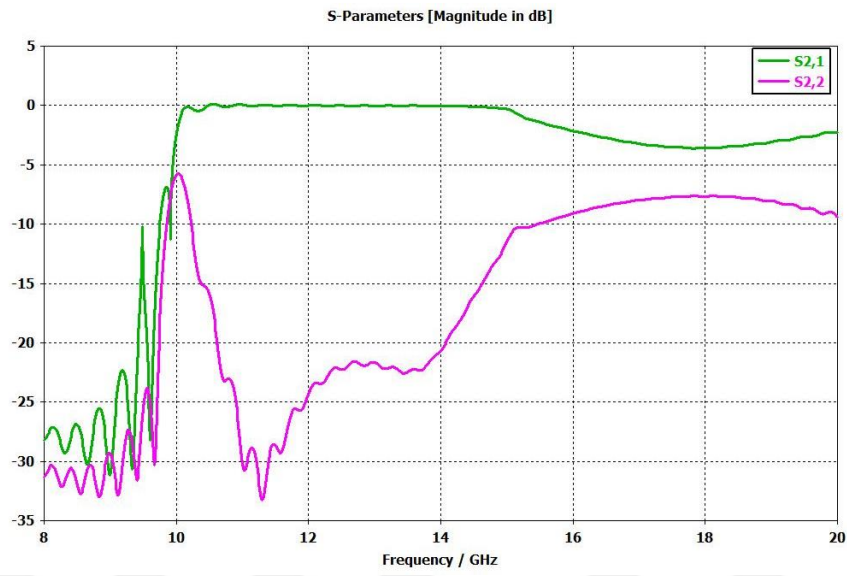


Figure 4.8. The designed H-Plane T-Junction Structure (a) Perspective View (b) Cross-Section from the Top along with the parameters (c) Cross-Section from the side along with parameters

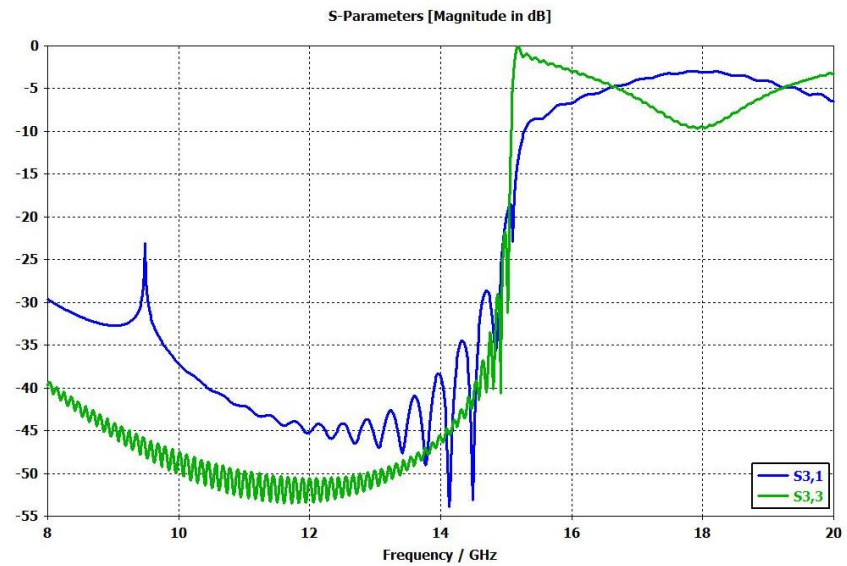
In the designed structure, port 1 is designated as common port. Port 2 and Port 3 are divided for RX/downlink and TX/uplink lines, respectively. Since the common port has the dimensions of WR-62 waveguide, the transition for the T-junction structure that is not in the standard waveguide dimensions is designed to provide matching to WR-62. The corresponding simulation results obtained after optimization are shown in Figure 4.9, and the dimensions of the designed structure are given in Table 4.3 with the parameters.

Table 4.3. The Dimensions of Designed H-Plane T-Junction

| Parameter | Dimension (mm) |
|-----------|----------------|
| $a1$ | 9.09 |
| $w7$ | 2.07 |
| $w8$ | 3.78 |
| $L9$ | 15.8 |



(a)



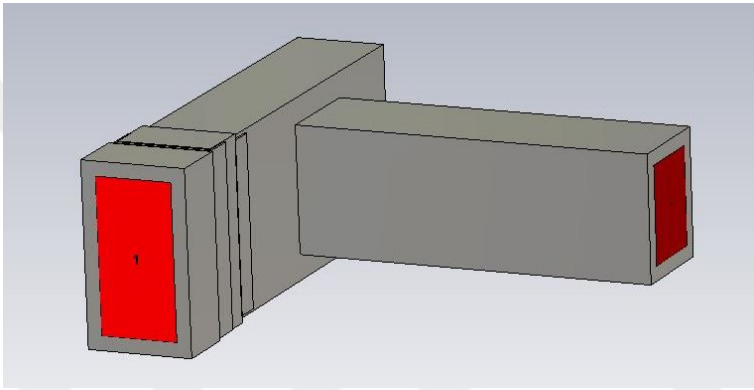
(b)

Figure 4.9. Simulation Results for the designed H-Plane T-Junction (a) Results for Port 2 (S_{21} - S_{22}) (b) Results for Port 3 (S_{31} - S_{33}).

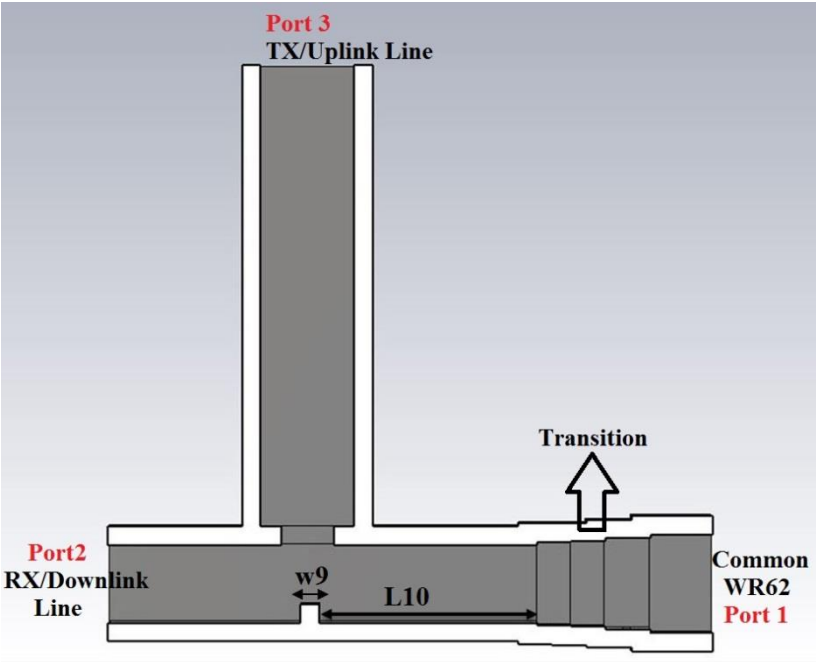
According to these results, it can be observed that the transmission from common port is provided to downlink (10.5-12.75 GHz) frequency band and to uplink (17.3-18.4 GHz) frequency band separately. Furthermore, it is observed that the window-like structure rejects the downlink band at a sufficient level by acting as a high-pass filter due to lower cutoff frequency of the dimensions obtained after optimization.

4.2.2. E-Plane T-Junction Design and Simulation Results

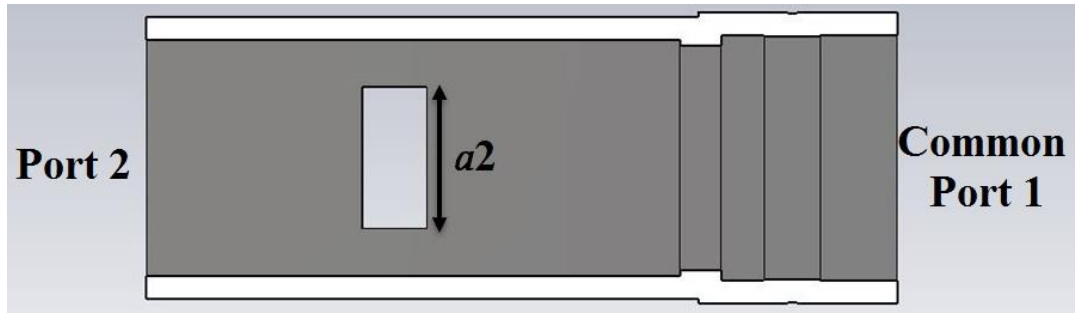
In E-plane junction design, the same method as H-Plane is used and optimization is applied. The designed structure and important parameters are given in Figure 4.10.



(a)



(b)



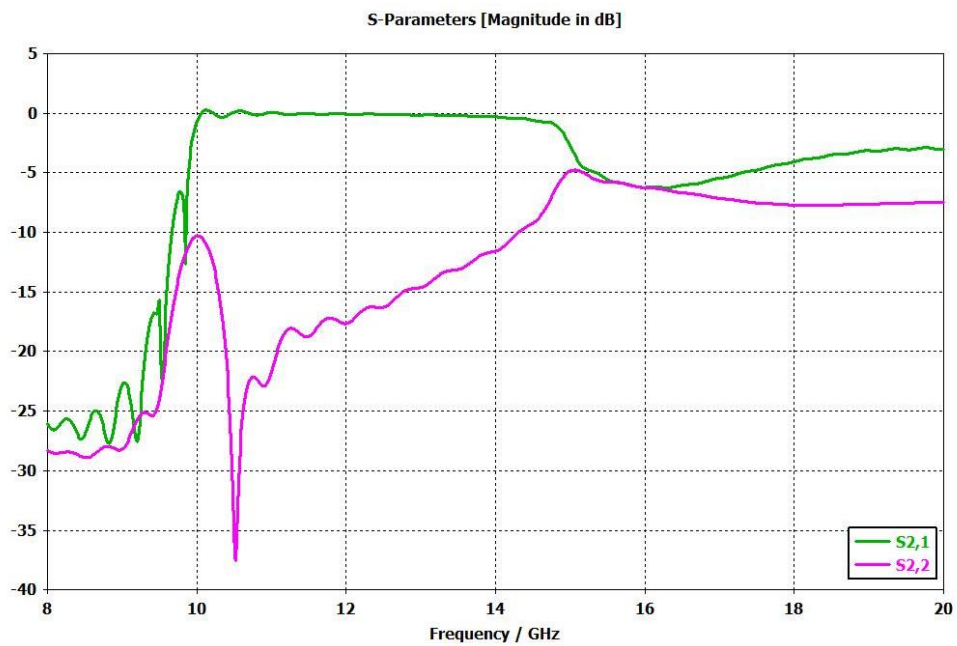
(c)

Figure 4.10. Designed E-Plane T-Junction Structure (a) Perspective View (b) Cross-section from the Top and Parameters (c) Cross-Section from the Side and Parameters

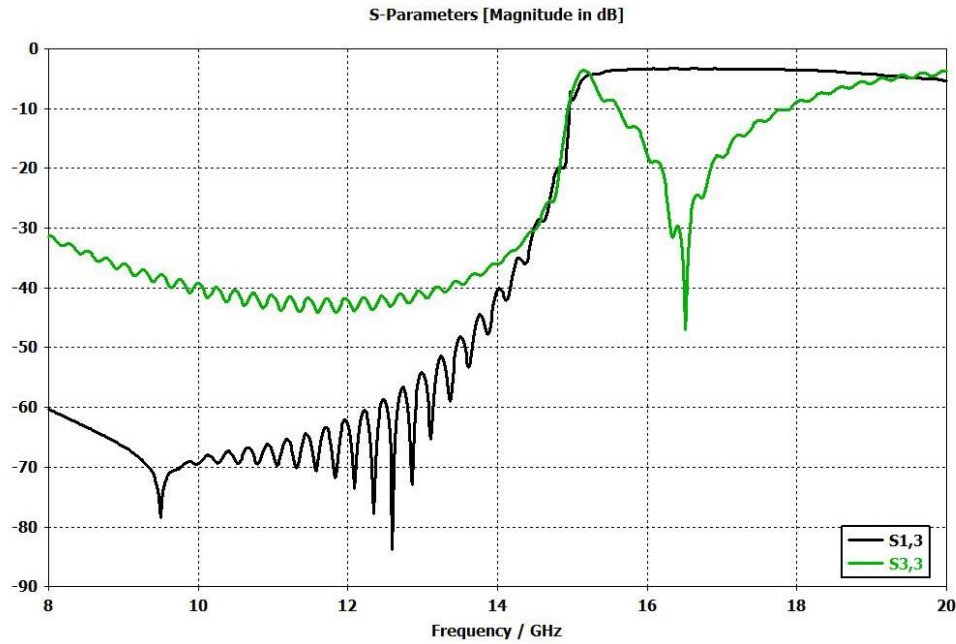
The simulation results obtained after the optimization are shown in Figure 4.11, and the dimensions of the designed structure are given in Table 4.4.

Table 4.4. The Dimensions of Designed E-Plane T-Junction

| Parameter | Dimension (mm) |
|-----------|----------------|
| $a2$ | 9.16 |
| $w9$ | 1.5 |
| $L10$ | 17.55 |



(a)



(b)

Figure 4.11. Simulation Results for the designed E-Plane T-Junction (a) Results for Port 2 (S_{21} - S_{22}) (b) Results for Port 3(S_{31} - S_{33}).

The results are almost identical to the H-plane results and again it can be observed that the transmission from common port is provided to downlink (10.5-12.75 GHz) frequency band and to uplink (17.3-18.4 GHz) frequency band, separately.

4.3. Design of the Diplexers

As explained previously in this thesis, the diplexer is designed to operate for the frequency range of 10.5-12.75 GHz at RX/downlink band, and 17.3-18.4 GHz at TX/uplink band. Diplexer structure was created in three different types as H-plane, E-plane and dual-polarized by combining of the designed filters, T-junctions and OMT structures together. The common (feeding port to the antenna) and TX ports have WR-62 rectangular waveguide and RX port has WR-75 rectangular cross sections. Also in the design process, different transition structures are designed and optimized to provide matching between filters and T-junction/OMT.

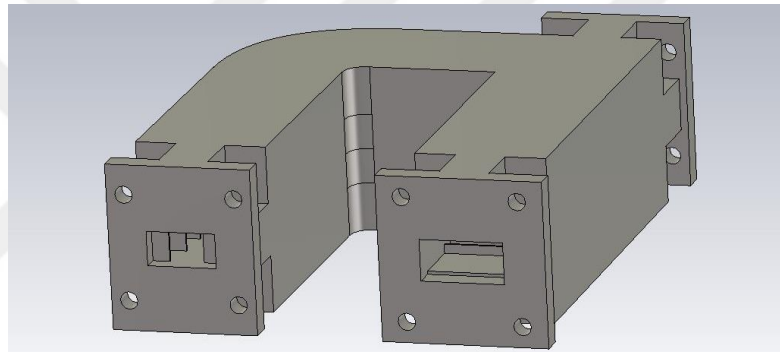
If the working principle of the diplexer is simply explained, it provides to separate the uplink and downlink frequency bands from each other and allows both reception and transmission over a single antenna at the same time. Also, RX filter provides

isolation (rejection) for TX frequencies (17.3-18.4 GHz) at RX port, and TX filter provides isolation (rejection) for RX frequencies (10.5-12.75 GHz) at TX port.

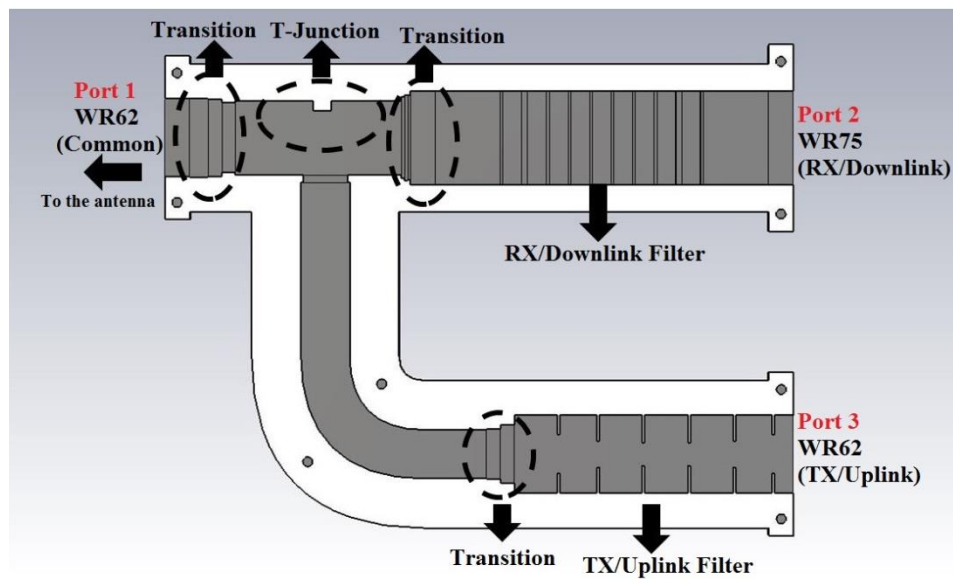
All of the simulation and optimization studies for the designs are performed at the high mesh level with PEC material by using “Time Domain Solver” in CST Microwave Studio computer software.

4.3.1. H-Plane Diplexer Design and Simulation Results

Diplexer is designed by combining filters with T-junction. In addition, transitions are designed and optimized to provide matching between the lines. The designed H-plane diplexer structure is shown in Figure 4.12 with its inner structure.



(a)



(b)

Figure 4.12. Designed H-Plane Diplexer (a) Perspective View (b) Inner Structure

The results obtained after the optimization studies on transitions are given in Figure 4.13.

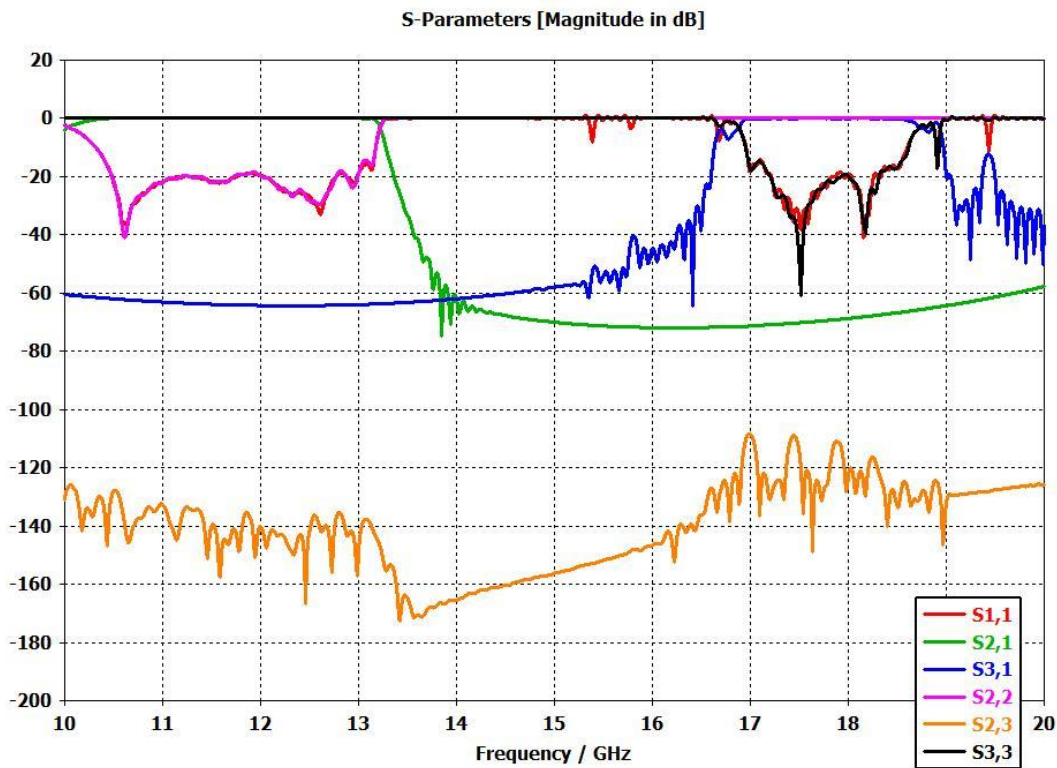
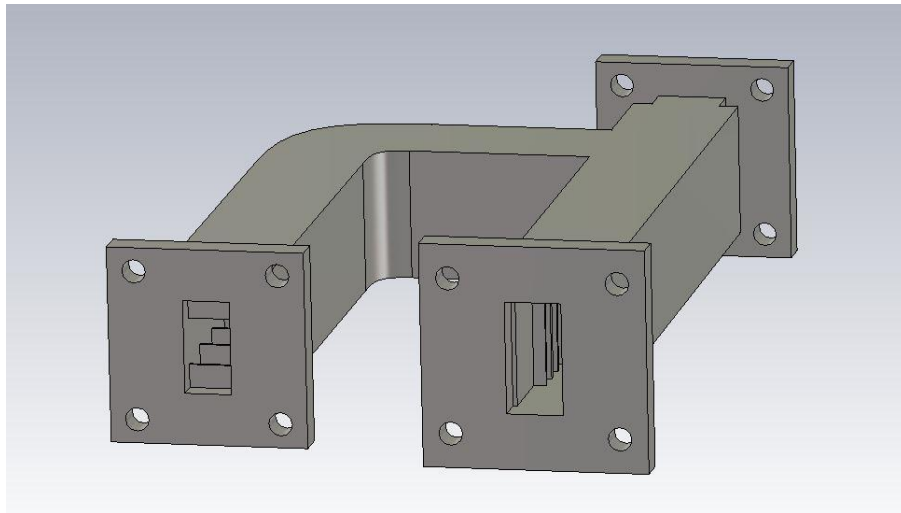


Figure 4.13. Simulation Results of the Designed H-Plane Diplexer

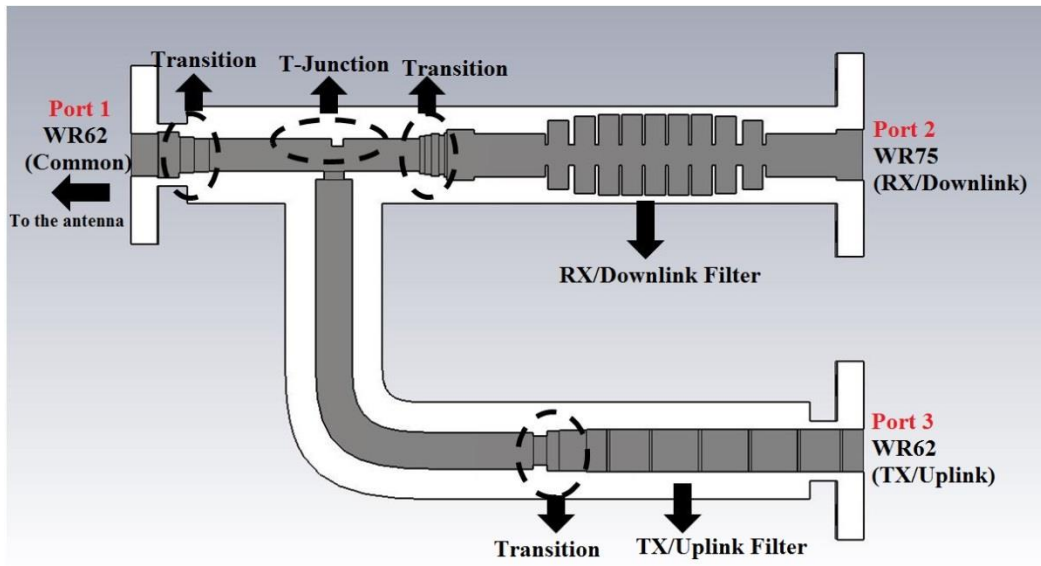
As seen from the results, the return loss values are higher than 20 dB for both downlink (10.5-12.75 GHz) and uplink (17.3-18.4 GHz) frequency bands as expected. Also, the RX reject value of the uplink side is min 60 dB and the TX reject value of the downlink side is min 70 dB levels. However, these rejection values can vary by the simulation method and mesh number. The other important parameter, S_{23}/S_{32} isolation value, is also in sufficient levels.

4.3.2. E-Plane Diplexer Design and Simulation Results

The designed E-plane diplexer is shown in figure below (see Figure 4.14) with its inner structure. For the design procedure, the same method in the H-plane has been applied.



(a)



(b)

Figure 4.14. Designed E-Plane Diplexer (a) Perspective View (b) Inner Structure

The results obtained after the optimization studies on transitions are given in Figure 4.15.

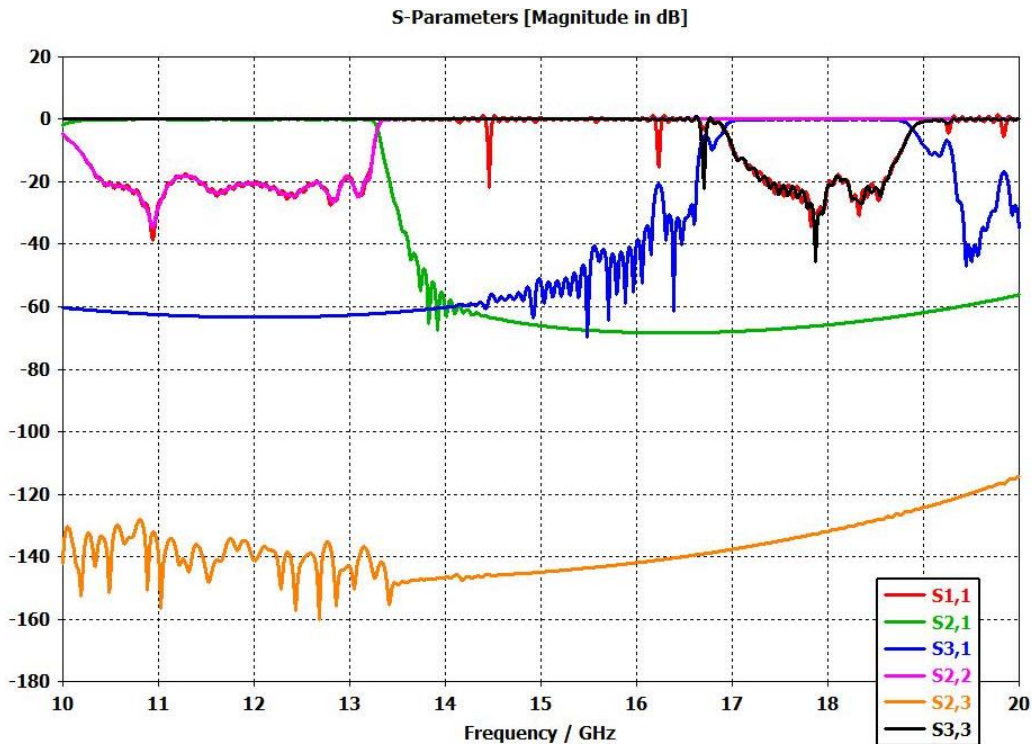


Figure 4.15. Simulation Results of the Designed E-Plane Diplexer

As in the H-plane, the return loss values are higher than 20 dB for both downlink (10.5-12.75 GHz) and uplink (17.3-18.4 GHz) frequency bands as expected. Also, the RX reject value of the uplink side is min 60 dB and the TX reject value of the downlink side is min 70 dB levels.

4.3.3. Dual-Polarized Diplexer Design

Dual polarization means that while the wave propagation is transmitted vertically on one side, on the other side this transmission is carried out horizontally. In waveguides, OMTs are needed to make this type of propagation. As explained in Section 2.2, OMTs allow dividing or combining of two dominant orthogonal signals.

For this reason, in order to combine the designed filters, an OMT is designed firstly.

4.3.3.1. OMT Design

In OMT designs, the common port usually consists of square or circular waveguides according to the geometry of the antenna to be supported. In this design, it was

decided to use square waveguide for common port. From the dimensions in Table 2.1 and equation (8) given in Section 2.4.1.2, according to the operating frequency band of the system, an edge length of the common port which is the square waveguide is determined by the long edge length (a) of the WR62 waveguide.

For the design and simulation of the structure, CST Microwave Studio program is used and PEC material is selected again. Unlike the simulations of other designs, excitation is performed in two separate modes for horizontal and vertical polarization by setting the polarization angle 90 degrees for the common port (Port 1) in OMT. The wave propagation modes in the ports are shown in Figure 4.16.

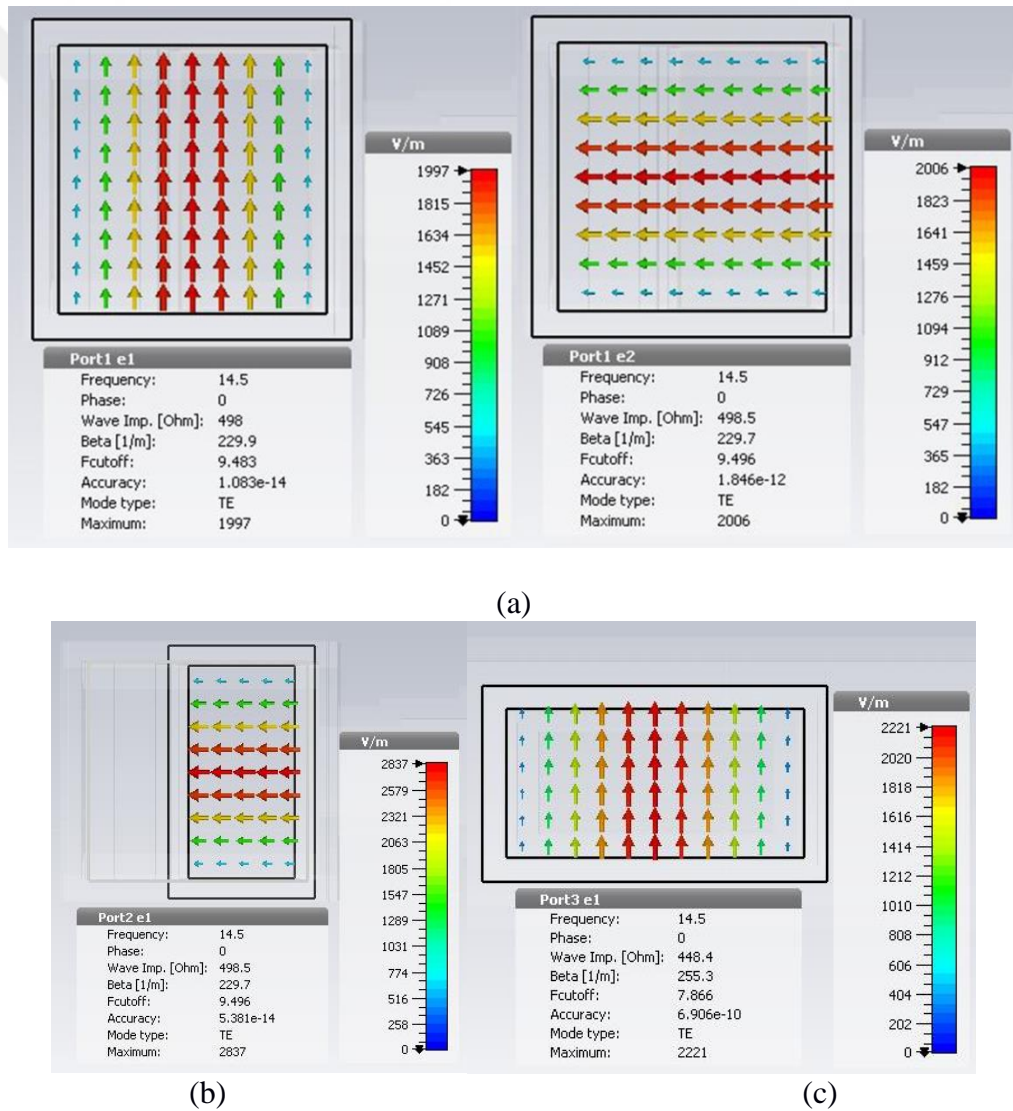
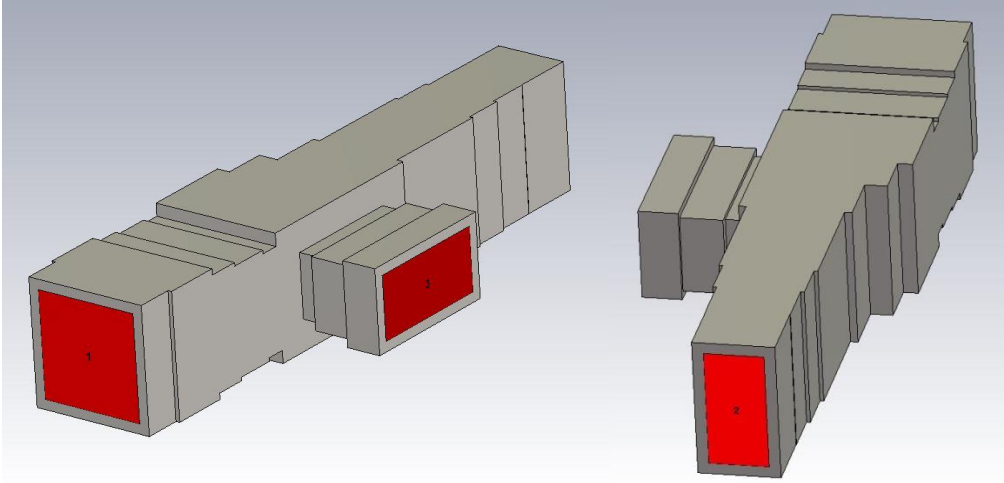


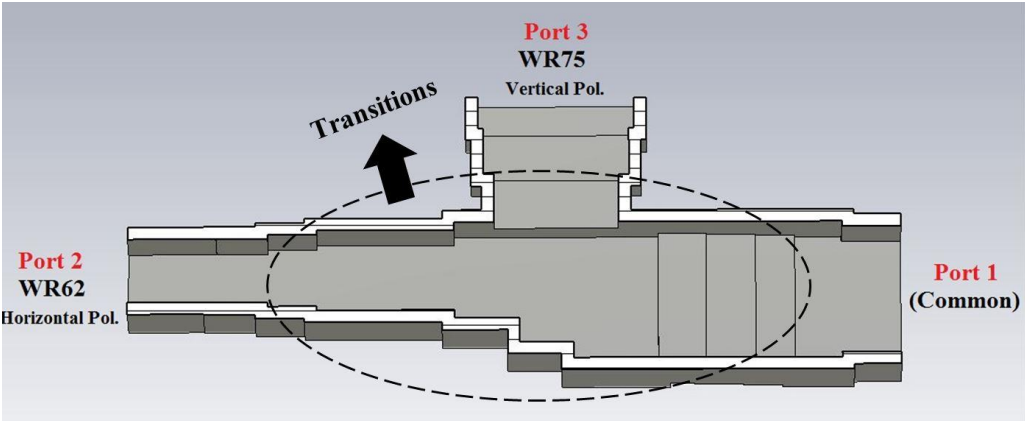
Figure 4.16. Wave Propagation Modes for OMT (a) Port 1 (Common Port) (b) Port 2 (TX) (c) Port 3 (RX)

WR-75 and WR-62 standard dimensions are used for the Port 3 (RX) and Port 2 (TX) respectively, as in the other designs.

There are also gradual transitions are used to provide matching between the ports. Then, the design is completed by optimizing the dimensions of these transitions. The designed OMT is given Figure 4.17.



(a)

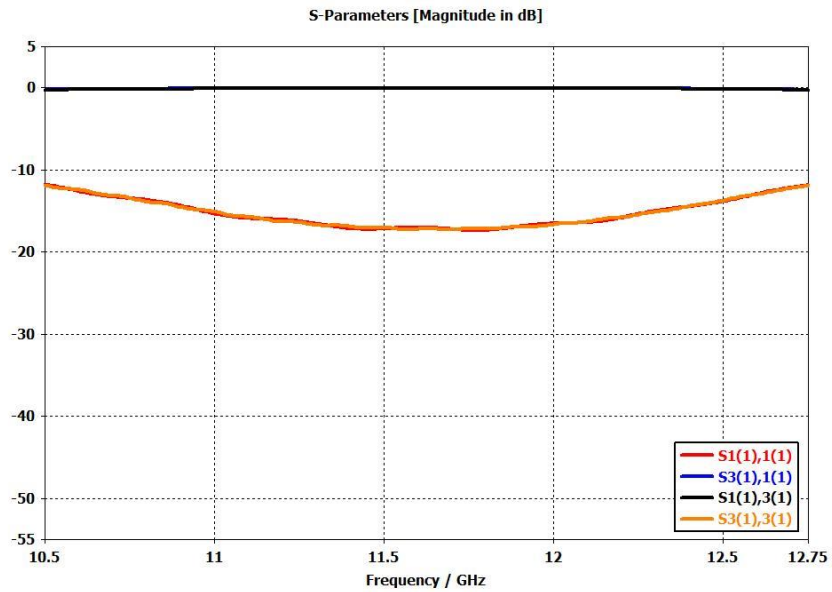


(b)

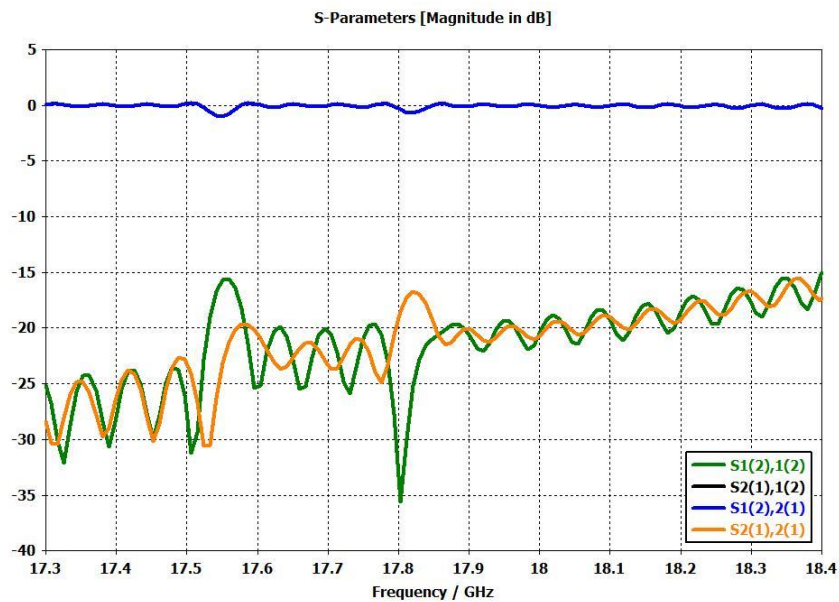
Figure 4.17. Designed OMT (a) Outer Structure (b) Inner Structure

In the simulations, mode 1 represents vertical polarization and mode 2 represents horizontal polarization for Port 1 (common). In addition, the wave propagation is

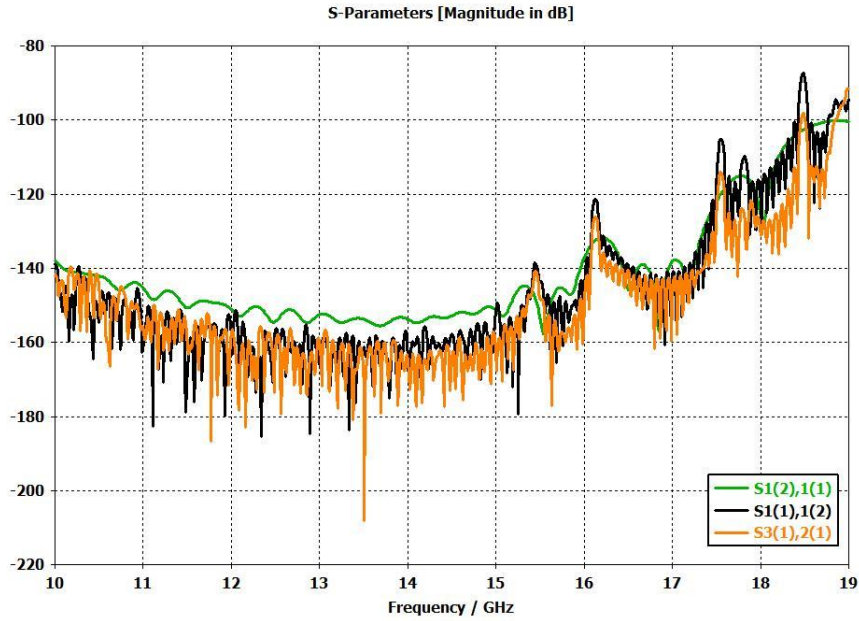
horizontal polarization for Port 2 (TX) and there is wave propagation in vertical polarization for Port 3 (RX). For these reasons, $S_{3(1)1(1)}$ insertion loss value should be considered for transmission in the vertical polarization and also $S_{1(2)2(1)}$ insertion loss value should be considered for the transmission in the horizontal polarization. Simulation results of the designed OMT are given in figure below (see Figure 4.18).



(a)



(b)



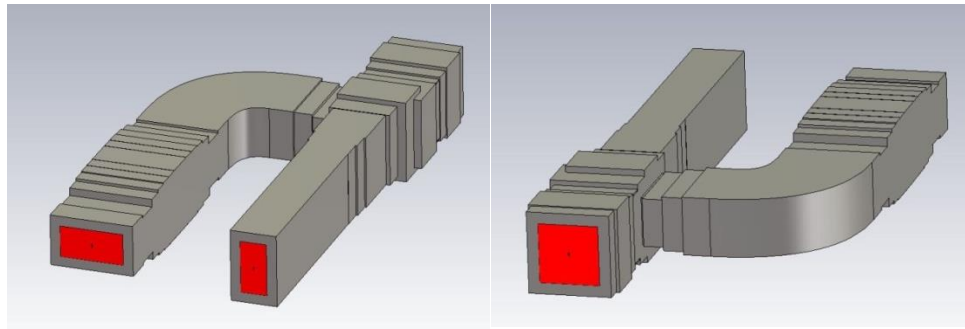
(c)

Figure 4.18. Simulation Results of the Designed OMT (a) S_{33} - S_{31} (Downlink/Vertical Pol.) (b) S_{22} - S_{12} (Uplink/Horizontal Pol.) (c) S_{23} - S_{32} (Isolation)

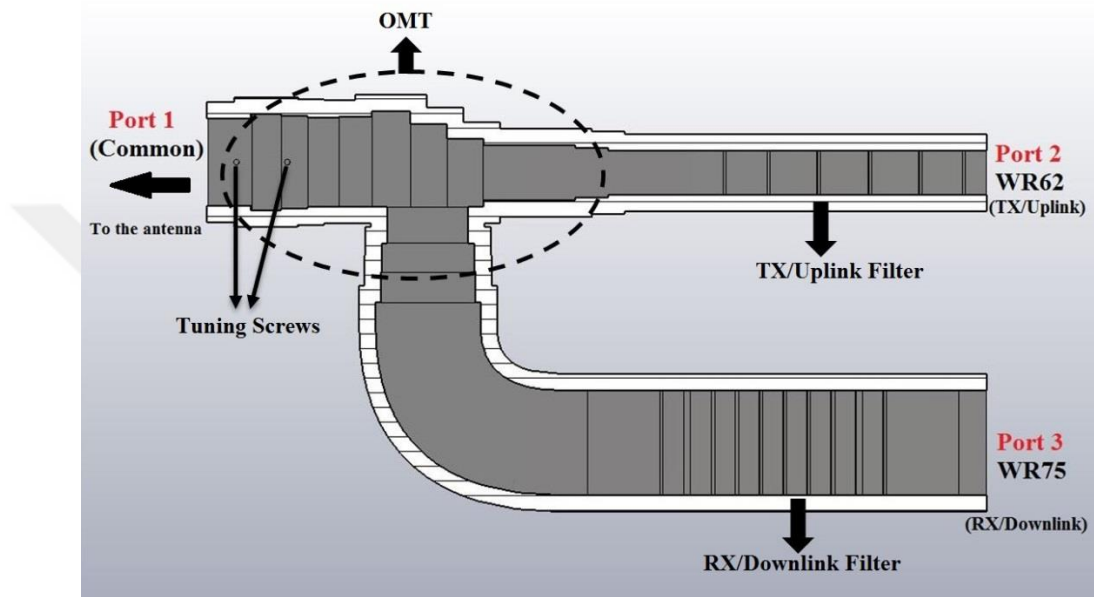
According to these results, the return loss value is higher than 10 dB for downlink band, and higher than 20 dB for uplink frequency bands. Besides, the other important parameter, which is $S_{3(1),2(1)}$ isolation value, is in sufficient levels.

4.3.3.2. Simulation Results for Dual-Polarized Diplexer

After the OMT design, the band-pass filters which are designed for H-plane and E-plane diplexers before are combined by WR-75 and WR-62 ports of the OMT. The completed dual-polarized diplexer structure is shown in Figure 4.19.



(a)



(b)

Figure 4.19. The designed Dual-Polarized Diplexer (a) Perspective View and (b) Inner Structure.

For the matching and setting the return loss value at 20 dB level 4 tuning screws are used and optimized ranging in length from 2 to 4 mm. The simulation results of designed dual-polarized diplexer are given in Figure 4.20.

According to these simulation results, the return loss values are higher than 20 dB again for both downlink and uplink frequency bands as expected. Also, the RX and TX reject values are almost in 75 dB levels.

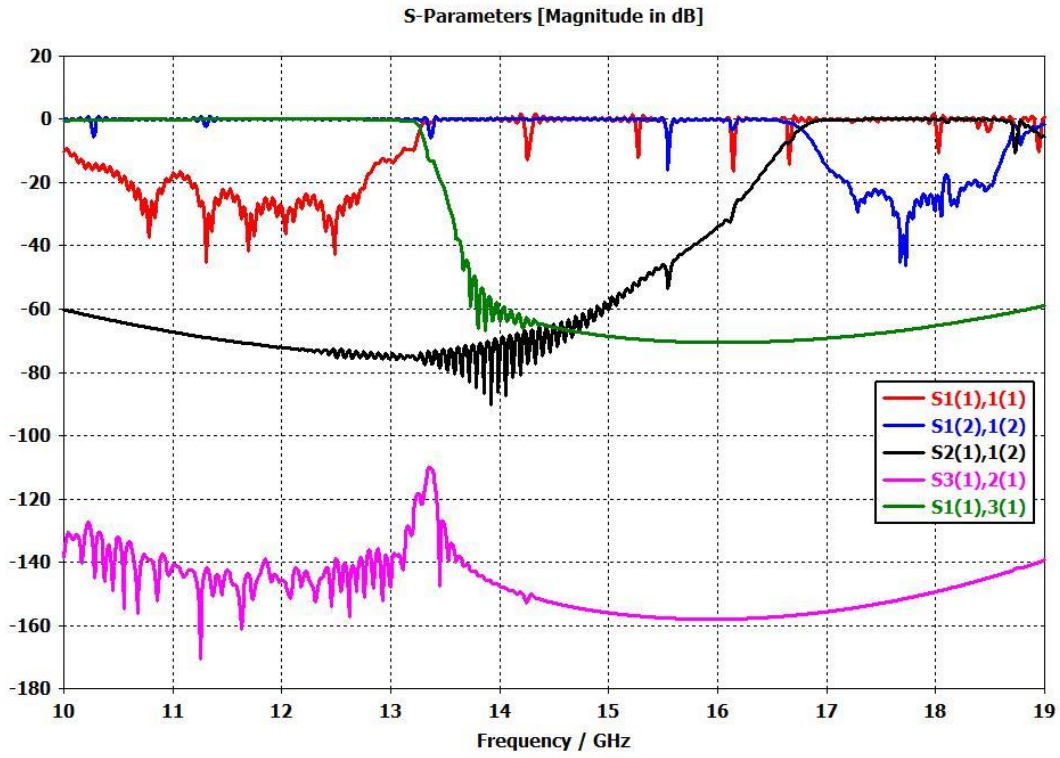


Figure 4.20. Simulation Results of the Designed Dual-Polarized Diplexer



CHAPTER FIVE

MANUFACTURING AND RESULTS

5.1. Manufacturing

For the fabrication of antenna and diplexer structures, a 3-D printer (Ultimaker 2+) is used, and PLA filament is selected as printing material. The important reason for choosing this material is due to fact that PLA is easier to be printed than ABS. This is because high temperature is required to print ABS material and 3-D printers require a closed area to maintain the heat. Another reason for the choice of PLA is being cheaper than ABS and environmentally friendly (Noorani, 2018).

The designed structures are printed as two identical (half) pieces, because they could be coated and made conductive after the printing is completed. Some printed pieces are shown in figure below (see Figure 5.1).

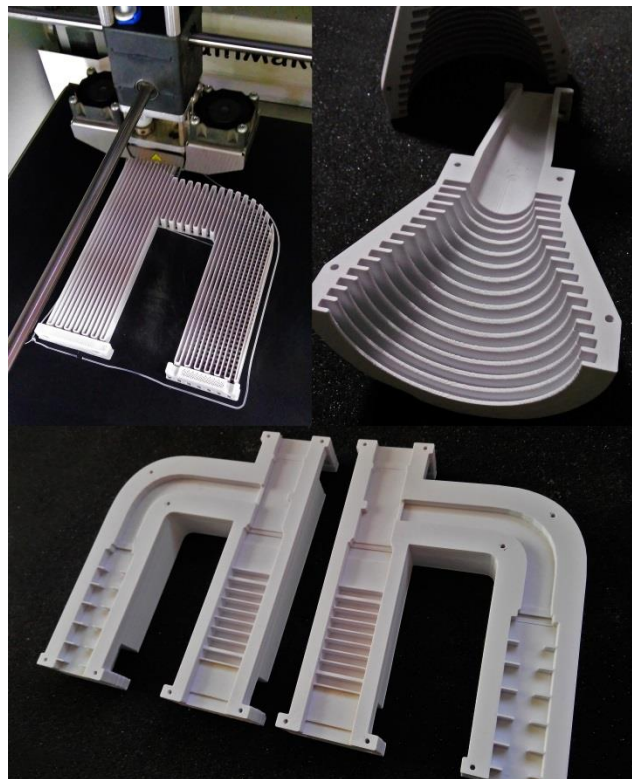
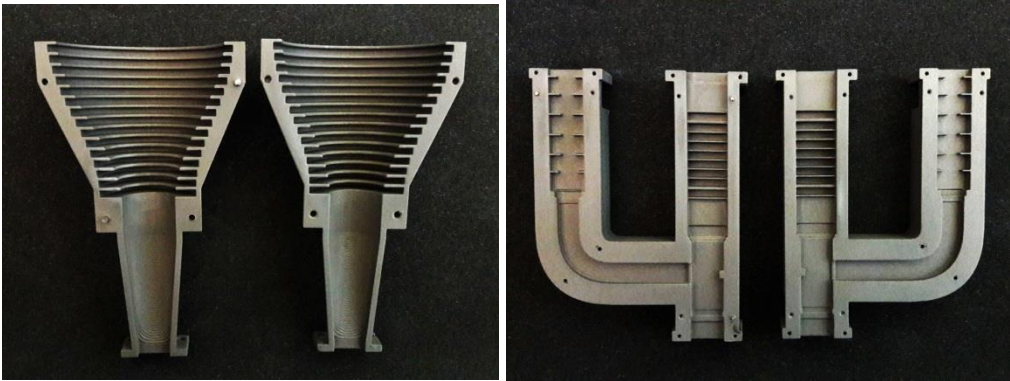


Figure 5.1. Printed Structures

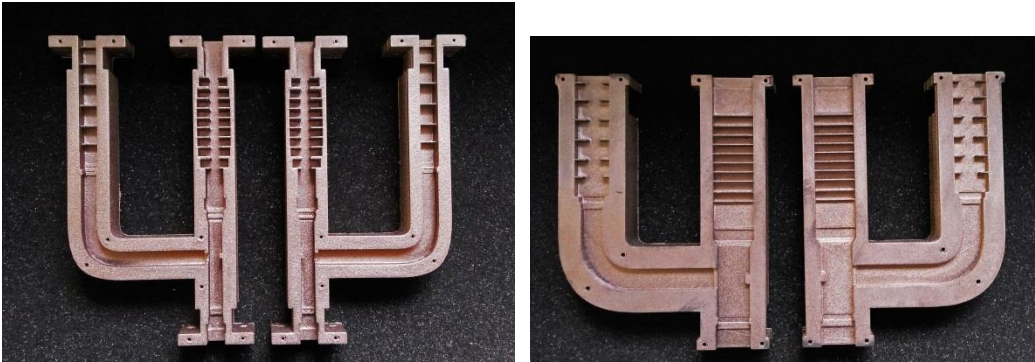
For the printing process 0.4 mm diameter nozzle is used by applying 0.2 mm layer height, %50 infill density and 50 mm/sec print speed precision settings. Total production time of the antenna and two diplexers (H-plane and E-plane) is about 48 hours, and total 67 m / 448 gr of PLA material is used for these structures.

After printing, the structures are coated by using two different conductive aerosol paint sprays, Super Shield-841 Nickel and Conductive Coating Pro (Silver Coated Copper). However, due to the poor conductivity of the nickel and the high loss level, silver conductive spray is used for diplexers. The printed structures after coating process are shown in Figure 5.2.



(a)

(b)

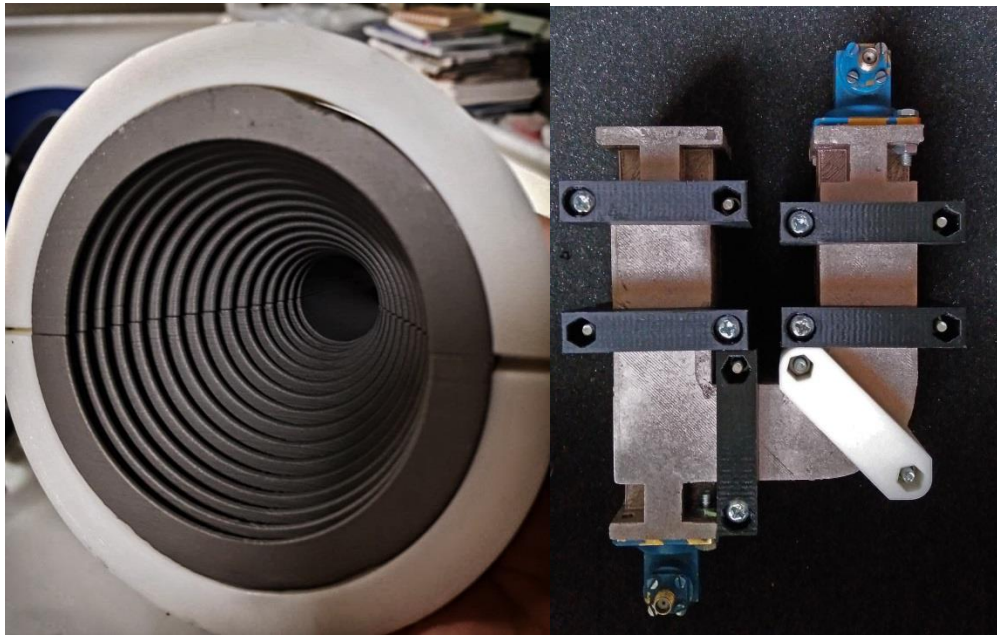


(c)

(d)

Figure 5.2. Coated Structures After Printing Process (a) Nickel Coated Corrugated horn antenna (b) Nickel Coated H-Plane diplexer (c) Silver Coated E-Plane Diplexer (d) Silver Coated H-Plane Diplexer

Finally, the fabricated half-pieces are assembled by combining them with a special adjustable clamp system as shown in figure below (see Figure 5.3).



(a)

(b)

Figure 5.3. (a) Assembled Antenna and (b) H-plane Diplexer Structures by Adjustable Clamp System

The purpose of the clamp system is to ensure that to provide fully combining of the two separate parts and to minimize losses from the gap. These parts are also printed by 3-D printer and assembled by us.

After the production and assembly steps are completed, measurement and comparison studies are started. These studies are described in the next section of this thesis.

5.2. Measurements

In order to make a fair comparison between the measurement results of the produced structures and simulation results, the simulation studies are repeated according to the properties of the materials used in conductive coating process instead of PEC material.

For this purpose, PLA ($\epsilon_r = 2.8$, $\tan \delta = 4.1 \times 10^{-2}$) is selected as material of the structures in the new simulations, and the coating thickness (about 0.1 mm) is also formed to represent conductive spray materials. The conductivity and surface resistance values (10-19 GHz) of these sprays are set as $\sigma = 24000$ S/m and $R_s = 2.5$ -3 ohm/sq. for nickel material by using the information in (Chieh, Dick, Loui and Rockway, 2014), and $\sigma=100000$ S/m and $R_s = 0.5$ -0.9 ohm/sq. for silver material in CST Microwave Studio.

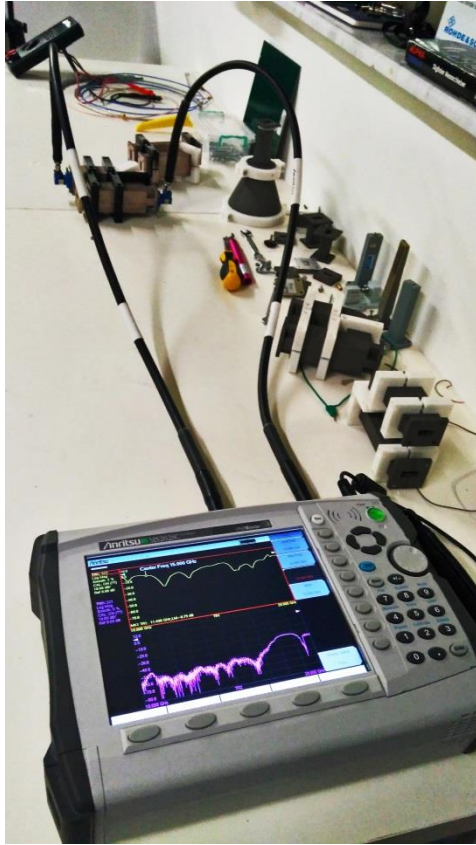
Through the information and formulas in equations (22) and (23), it is calculated that the skin depth of the low-conductivity spray material (Nickel) is at most $\delta_s = 17$ μm in the operating frequency band and the relative permeability coefficient is about $\mu_r = 3$ -4.

$$R_s = \frac{1}{\sigma \delta_s} \quad (22)$$

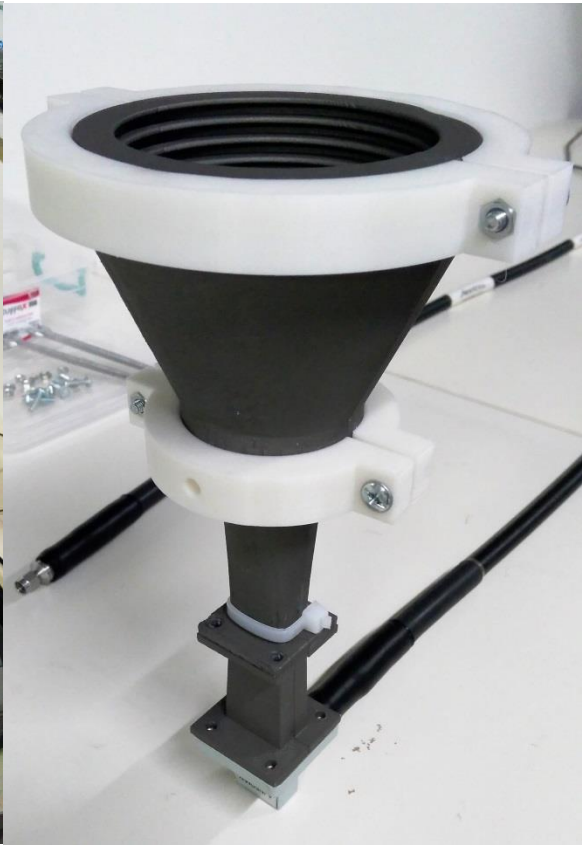
$$\delta_s = \sqrt{\pi f \mu \sigma} \quad (23)$$

As a results, the coating thickness (0.1 mm) of the material is found to be much higher than the highest skin depth value. Some images from measurements are given in Figure 5.4.

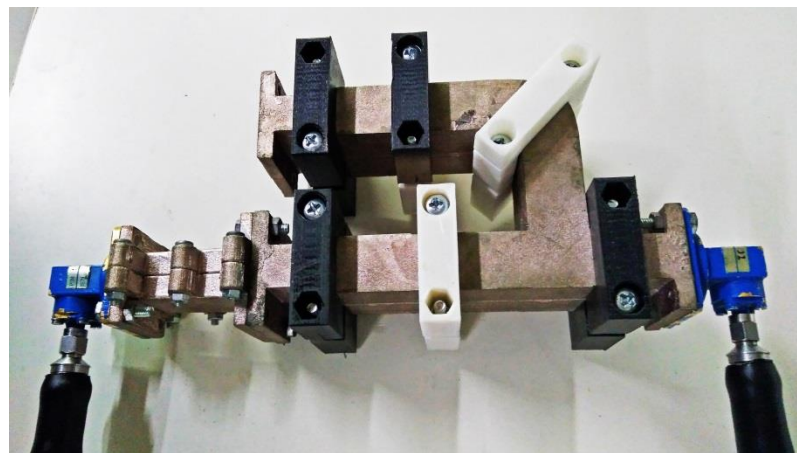
The S-parameter values and gains of prototype antenna and diplexers are measured at Yasar University Antenna and Microwave Laboratory. Besides, the radiation patterns of the antenna are measured at TUBITAK BILGEM Antenna Test and Research Center.



(a)



(b)

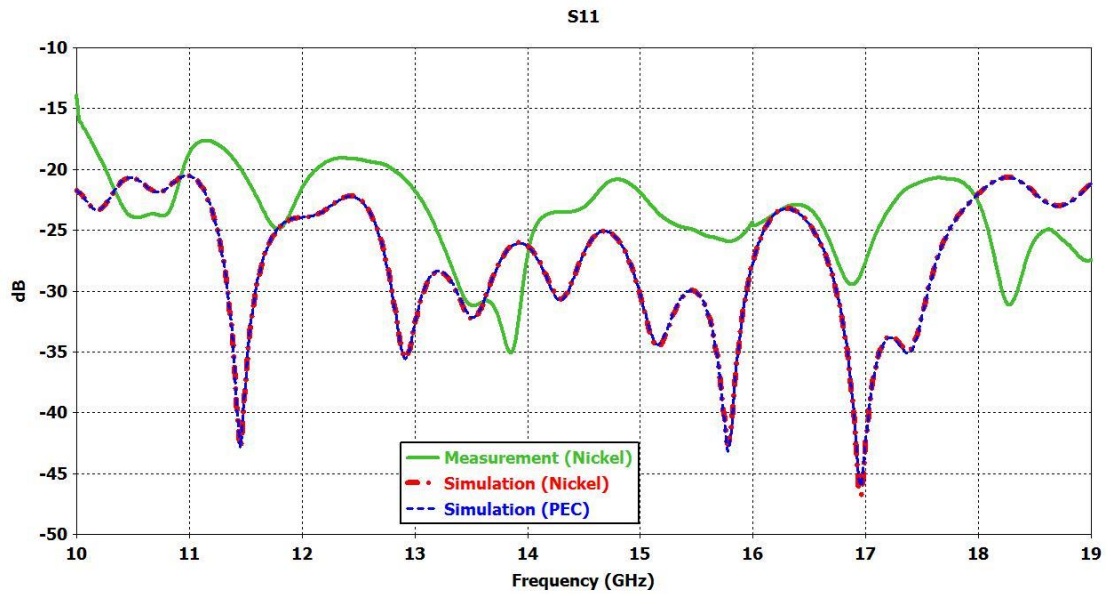


(c)

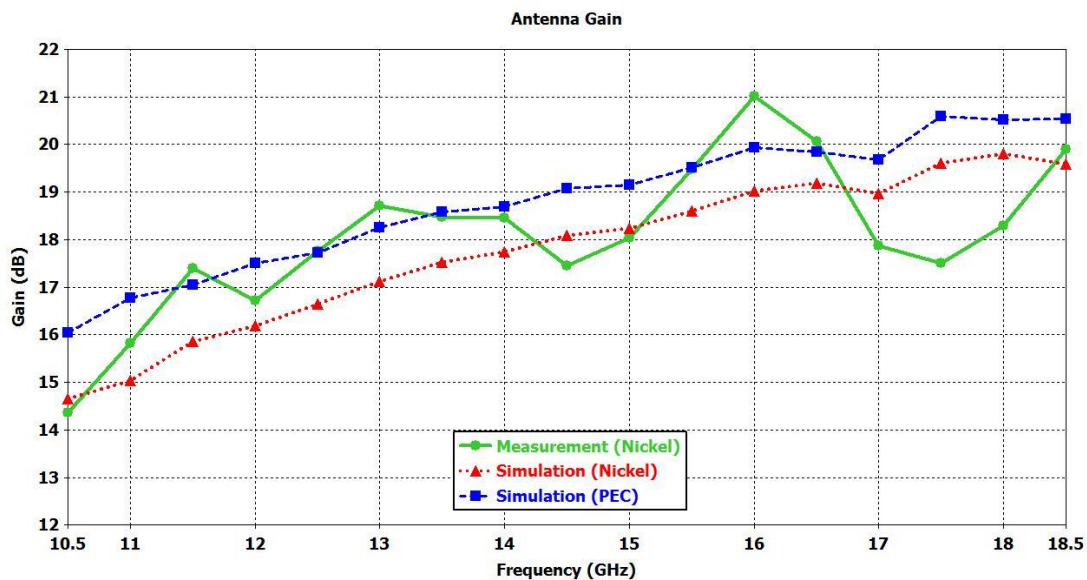
Figure 5.4. Measurement Setup (a) H-Plane Diplexer Measurement (b) Antenna Measurement (c) E-Plane Diplexer Measurement

5.3. Results for Conical Corrugated Horn Antenna

The return loss, gain and normalized pattern results of the manufactured antenna are given below in Figure 5.5 and Figure 5.6.



(a)

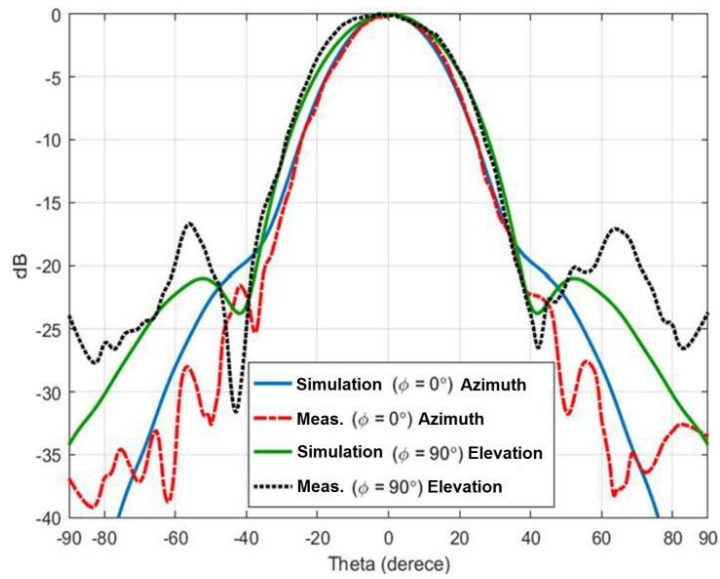


(b)

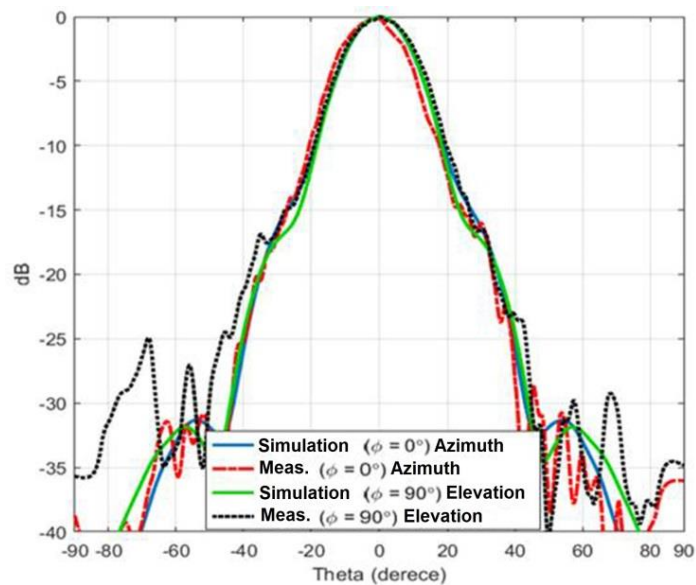
Figure 5.5. Return Loss and Gain Results (a) Return Loss Value (b) Gain

In Figure 5.5, the simulation and measurement results are in good agreement such that the measured return loss values are higher than almost 20 dB from 10.5 to 19 GHz and the measured gain values are between 14.5 and 20 dBi for 10.5-18.5 GHz.

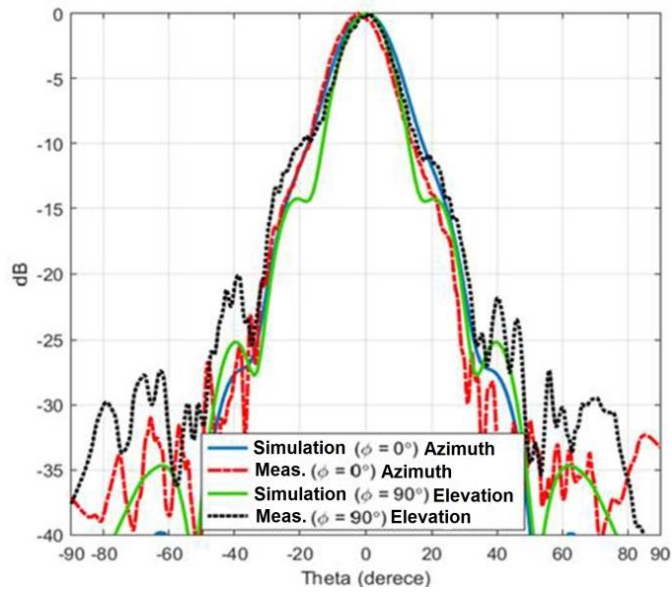
From the simulated gain results done with *PEC* and Nickel coating material for the antenna, it can be concluded that the loss effect of coating material is about 1-2 dB within the band.



(a)



(b)



(c)

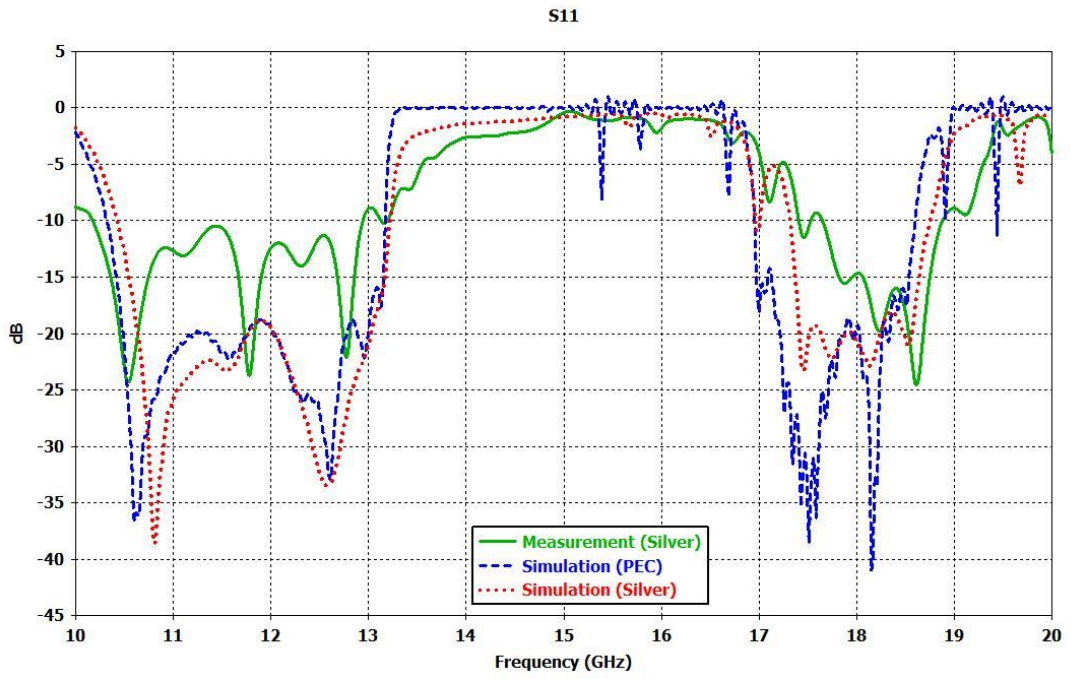
Figure 5.6. Normalize Radiation Patterns of Produced Antenna at (a) 10.5 GHz
(b) 14.5 GHz (c) 18 GHz

The normalized radiation diagrams of the designed antenna at 10.5, 14.5 and 18 GHz are given in Figure 5.6 for the azimuth and elevation planes. The measurement and simulation results are fairly consistent, and the measured directional values, which obtained by $26000/(\theta_E \theta_H)$ formula where θ_E and θ_H are the half-power beamwidths in the E- and H-planes in degrees (Stutzman and Thiele, 2013) are 14.23, 17.71 and 20.6 dBi at 10.5, 14.5 and 18 GHz, respectively, being highly close to the simulation results.

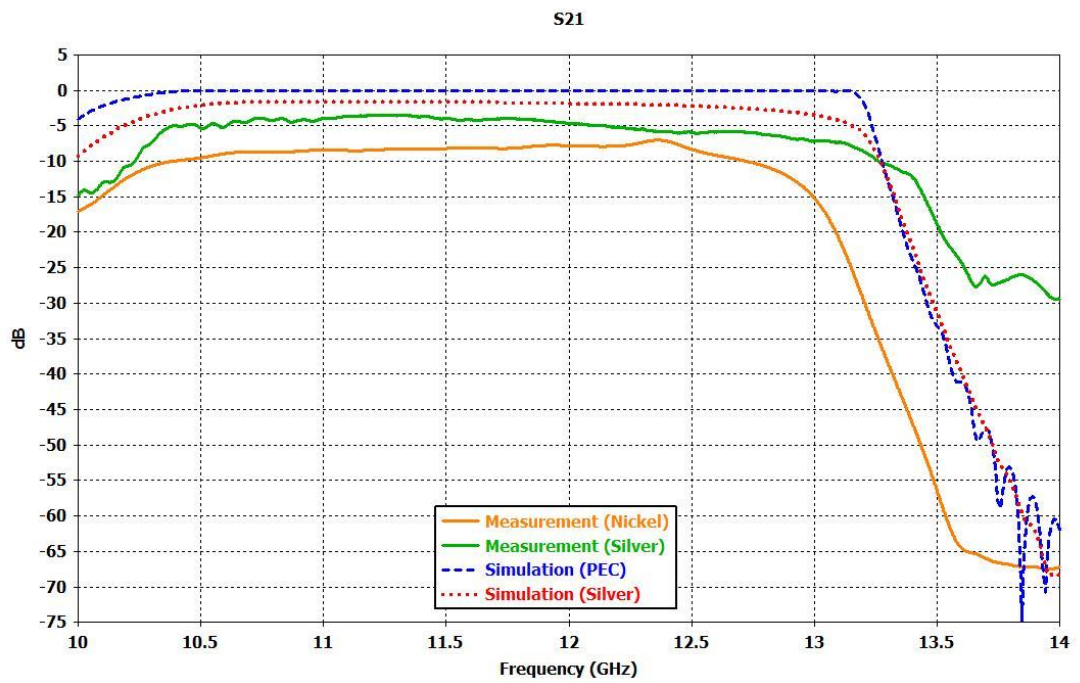
5.4. Results for Diplexers

5.4.1. H-Plane Diplexer Results

The return loss and insertion loss results of the fabricated H-plane diplexer are given in Figure 5.7. Also, to show the difference between nickel and silver coating sprays, both results of the nickel and silver coated H-plane diplexers are given in the graphs, S_{21} and S_{31} together.

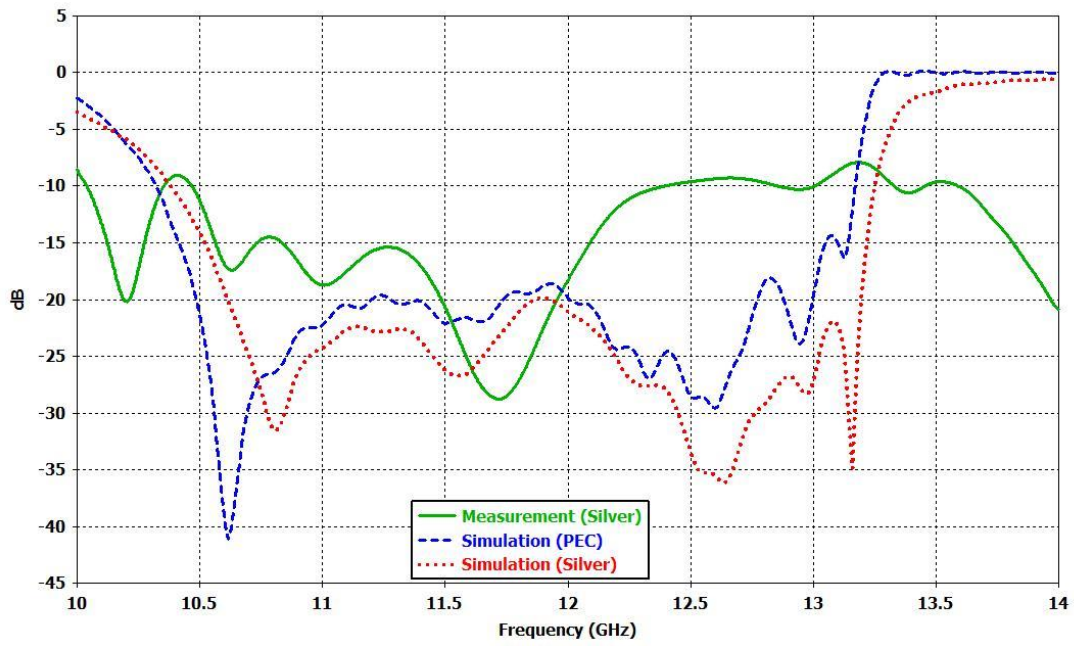


(a)



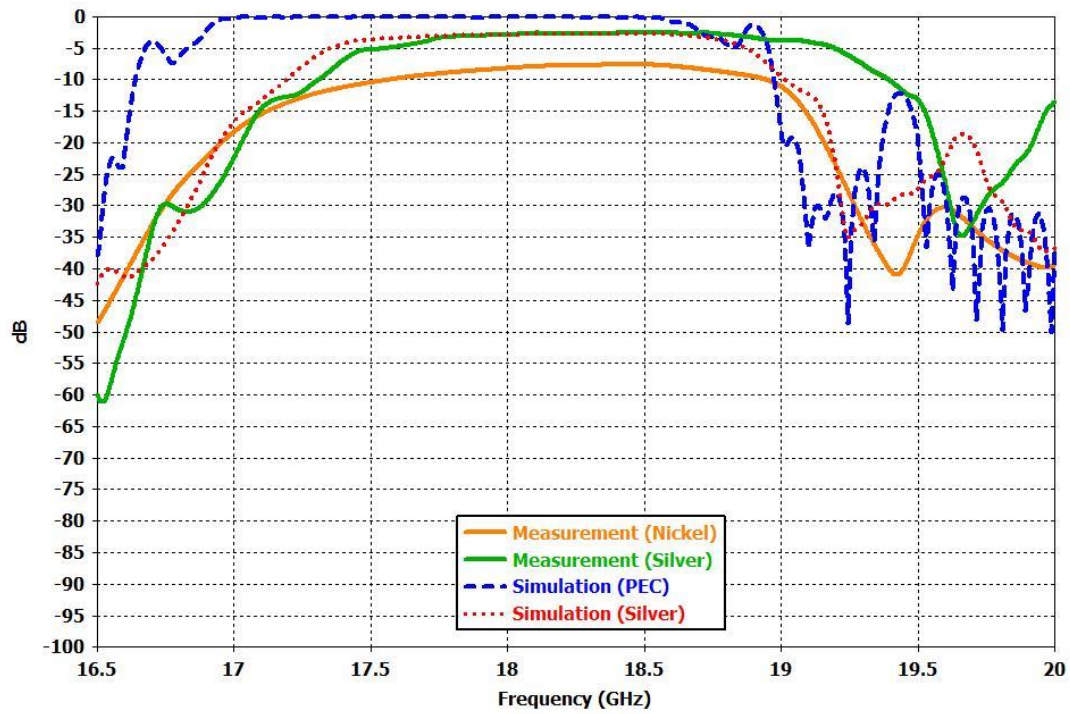
(b)

S22

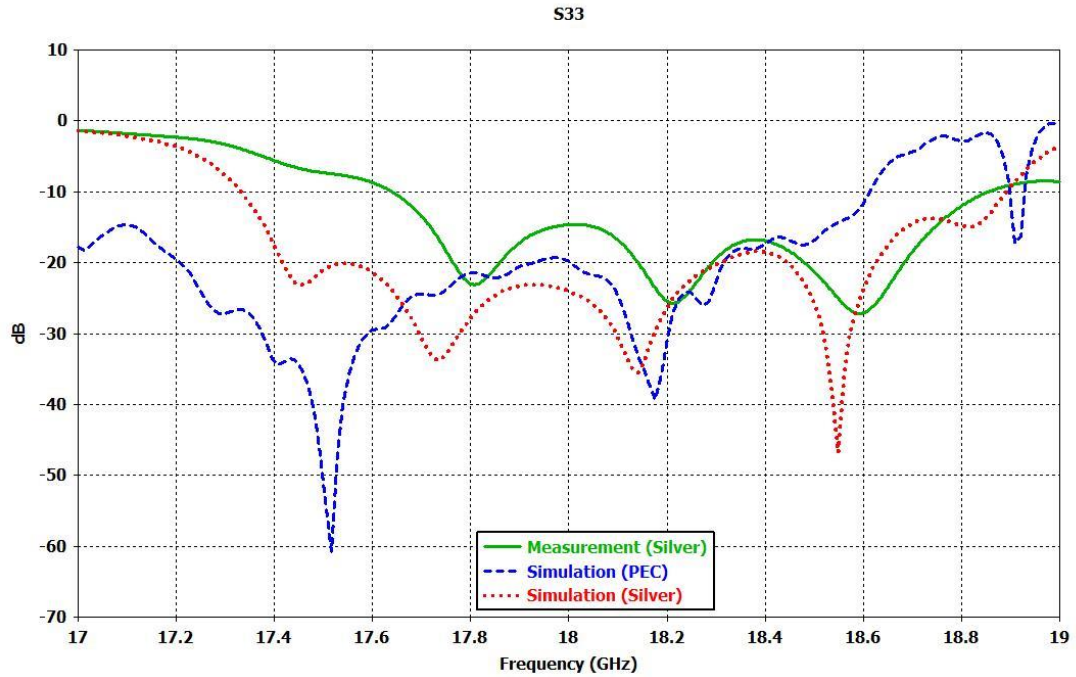


(c)

S31



(d)



(e)

Figure 5.7. Return Loss and Insertion Loss Results of the Fabricated H-Plane Diplexer (a) S_{11} (b) S_{21} (c) S_{22} (d) S_{31} (e) S_{33}

From the results in Figure 5.7, there is a shift towards the right side in desired frequency bands due to the coating thickness. Since the measured coating thickness is approximately 0.1 mm, this situation can be considered to be expected. Besides, thanks to the high conductivity of the silver material, it can be easily observed from the insertion loss graphs S_{21} and S_{31} that it is much less lossy compared to the nickel material. Along with that, a return loss level of about 15-20 dB is achieved for both downlink and uplink frequencies.

Figure 5.8 shows the isolation level between downlink and uplink ports. Although this value is seen as 65-70 dB in the graph, it is thought that the measurement can be up to 80-90 dB levels if more advanced calibration methods are used.

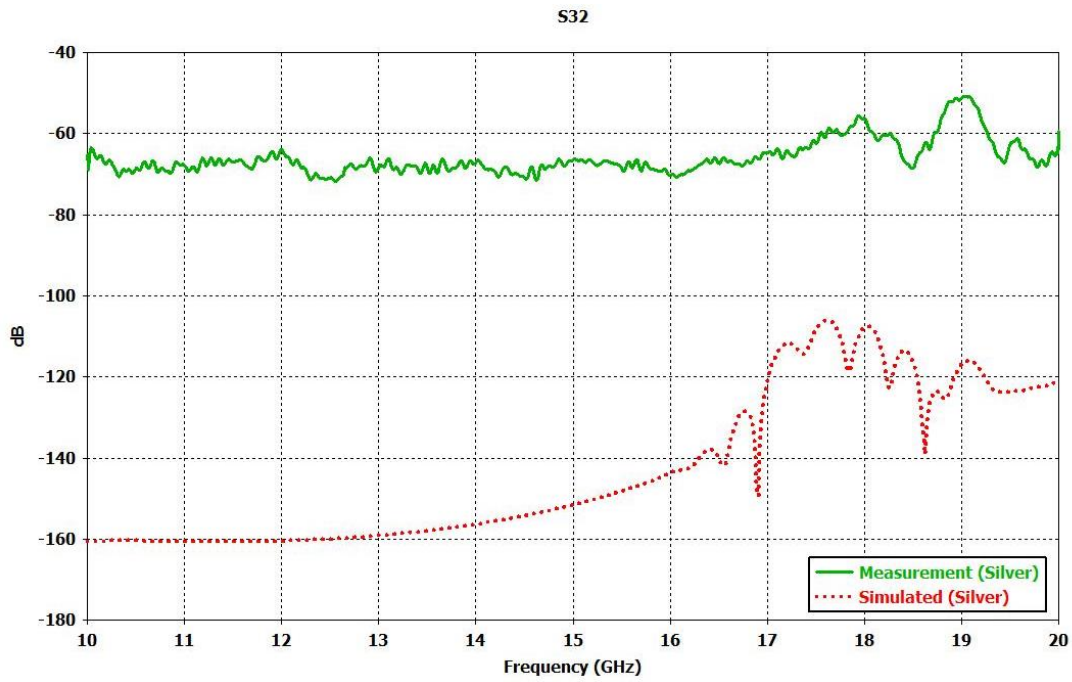
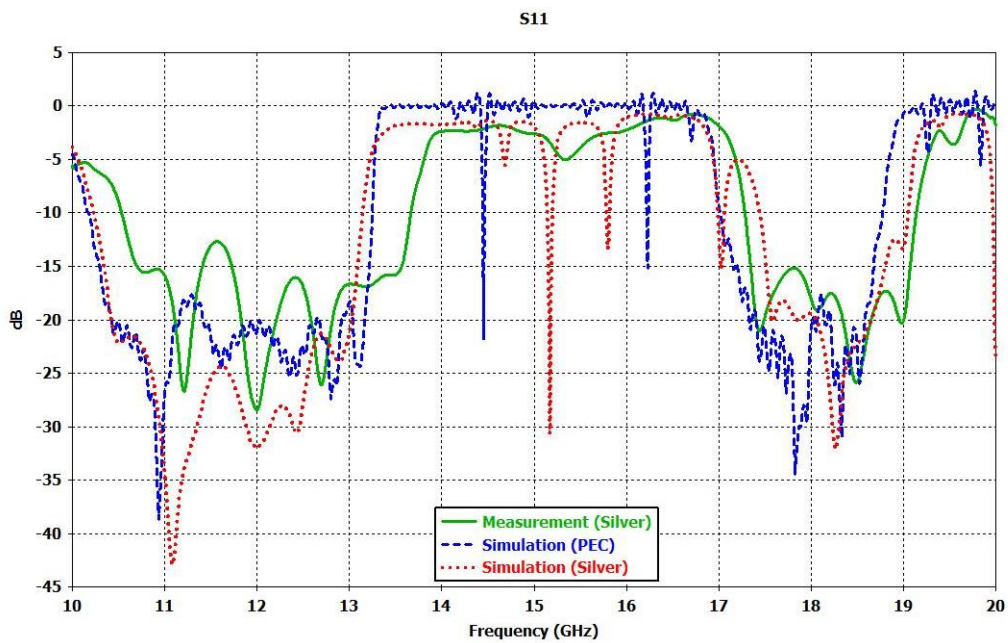


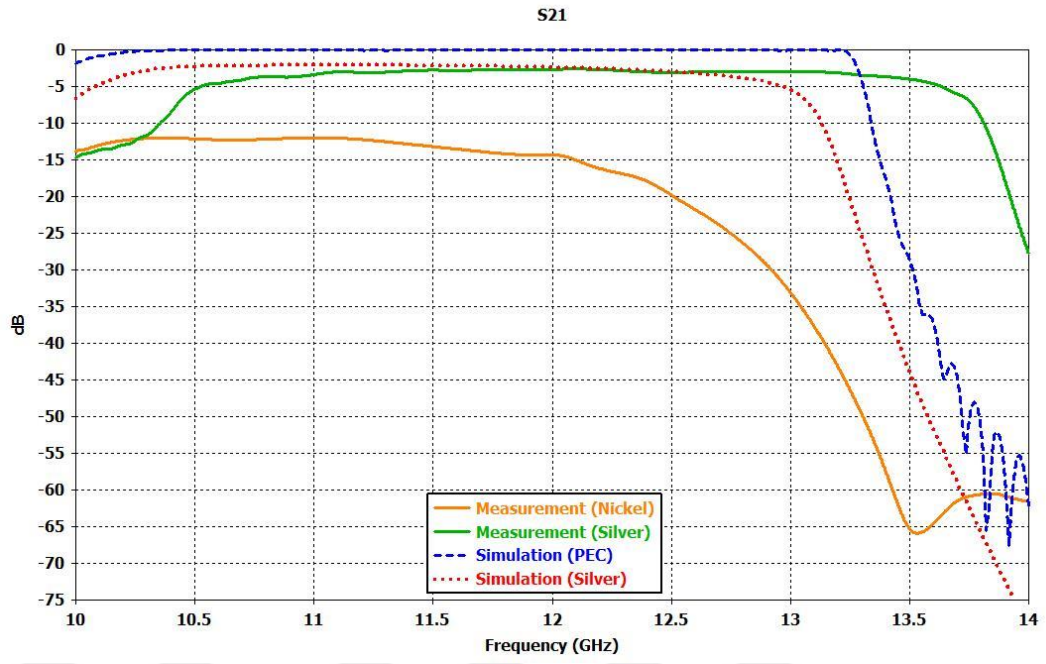
Figure 5.8. S_{32} (Isolation) Graph of the Fabricated H-Plane Diplexer

5.4.2. E-Plane Diplexer Results

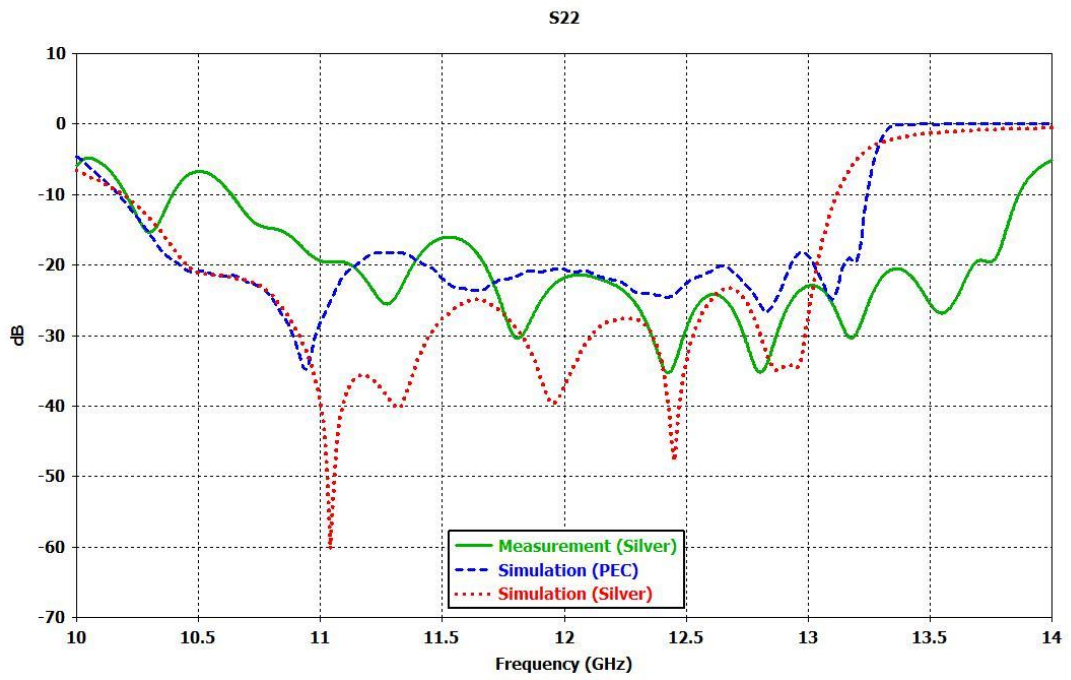
For the fabricated E-plane diplexer, similar measurement results are obtained with the H-plane which are given in previous section. The results are shown in figure below (see Figure 5.9).



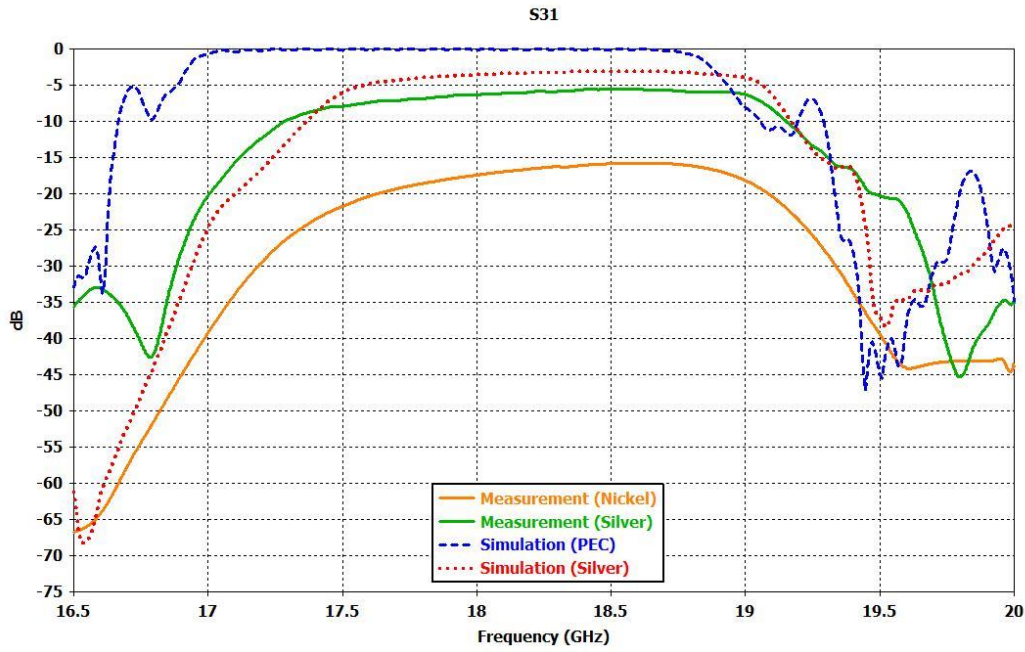
(a)



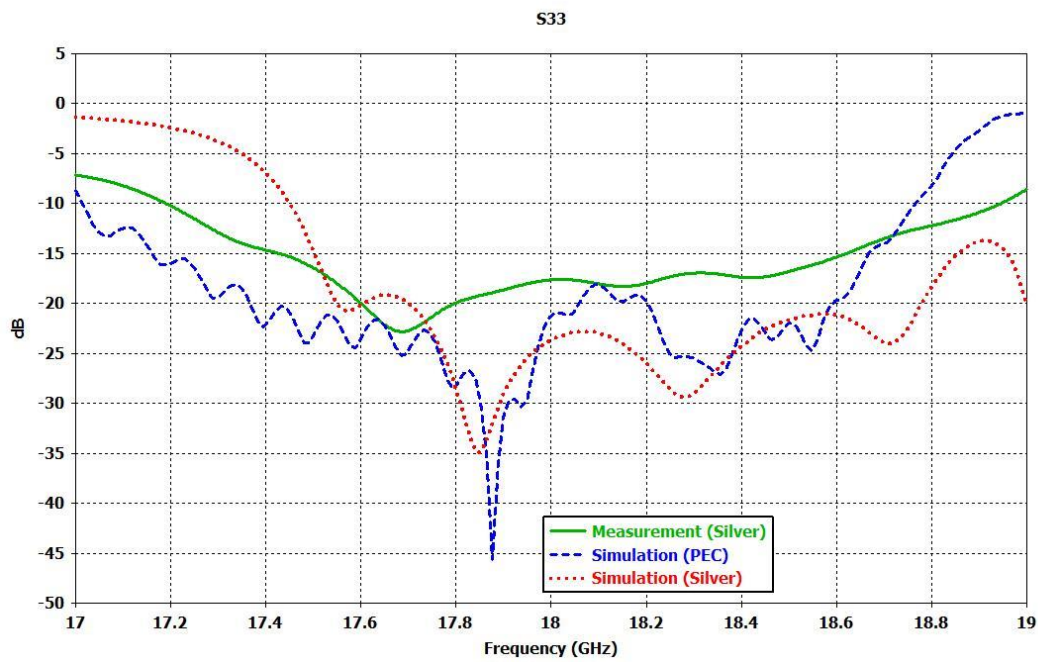
(b)



(c)



(d)



(e)

Figure 5.9. Return Loss and Insertion Loss Results of the Fabricated E-Plane Diplexer (a) S_{11} (b) S_{21} (c) S_{22} (d) S_{31} (e) S_{33}

By these results which are given in figure above, because of the coating thickness, there are shifting towards the right side in desired frequency bands again. Besides,

thanks to the high conductivity of the silver material, it can be easily observed from the insertion loss graphs S_{21} and S_{31} that it has lower loss compared to the nickel material. Along with that, a return loss level of about 15-20 dB is achieved for both downlink and uplink frequencies.

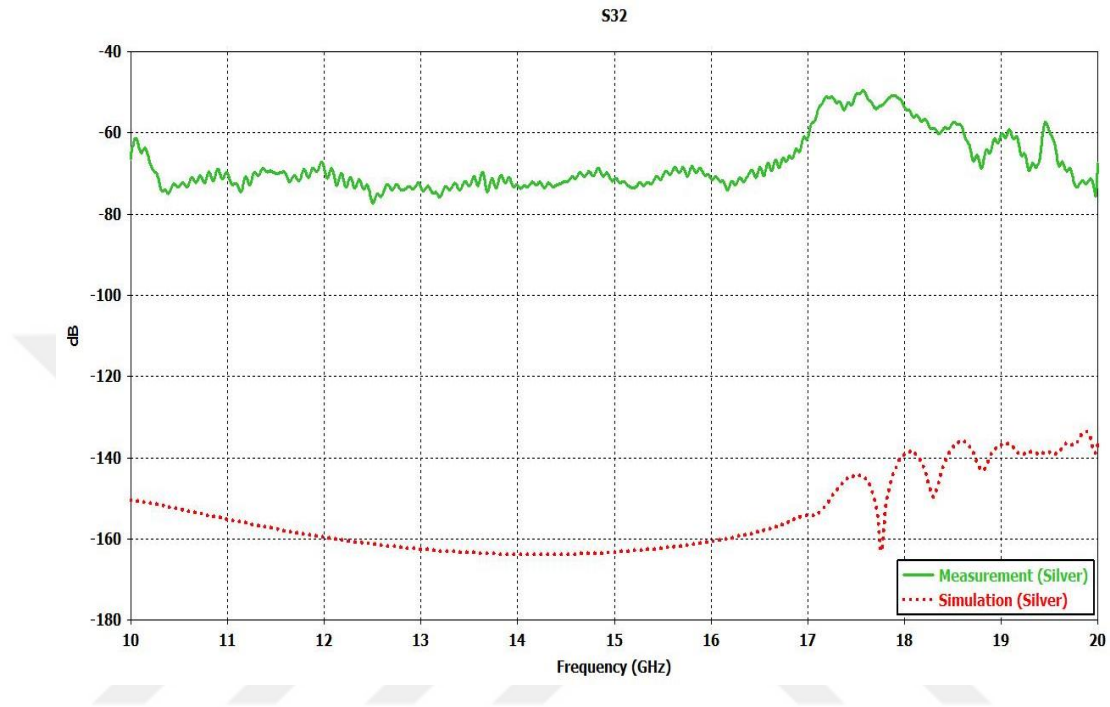


Figure 5.10. S_{32} (Isolation) Graph of the Fabricated E-Plane Diplexer.

Figure 5.10 shows the isolation level between downlink and uplink ports. Although this value is seen as 65-75 dB in the graph, it is thought that the measurement can be up to 85-90 dB levels if more advanced calibration methods are used.

5.5. Results for Overall System

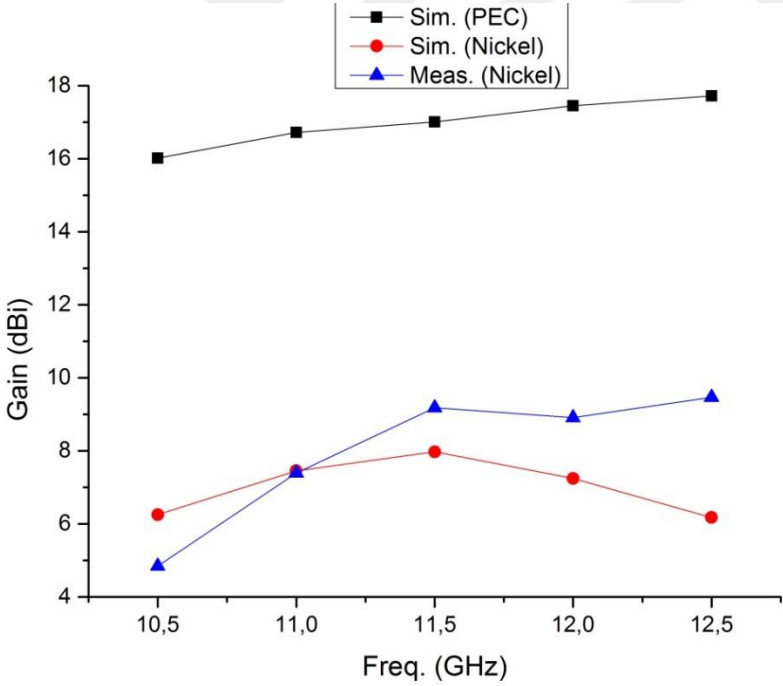
Finally, the antenna and diplexer (H-plane) is integrated as given in Figure 5.11 to form the feeding system. Here, the antenna is connected to common port (Port 1) of the diplexer. The return loss values of RX and TX ports (S_{22} and S_{33}) are found to be better than 15 dB similar to the results in Section 5.4.1.

For the gain measurements, both silver and nickel spray coated H-plane diplexers are used to compare the loss differences between these two materials.

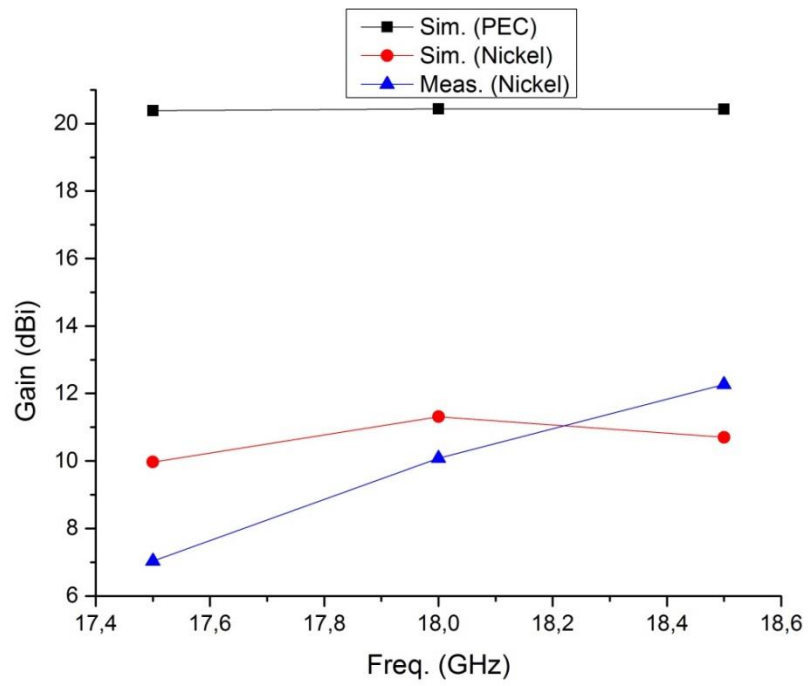
The gain results of the system with nickel and silver coated diplexers and PEC material are given in Figure 5.12 and Figure 5.13, respectively.



Figure 5.11. Integrated Feeding System Structure.

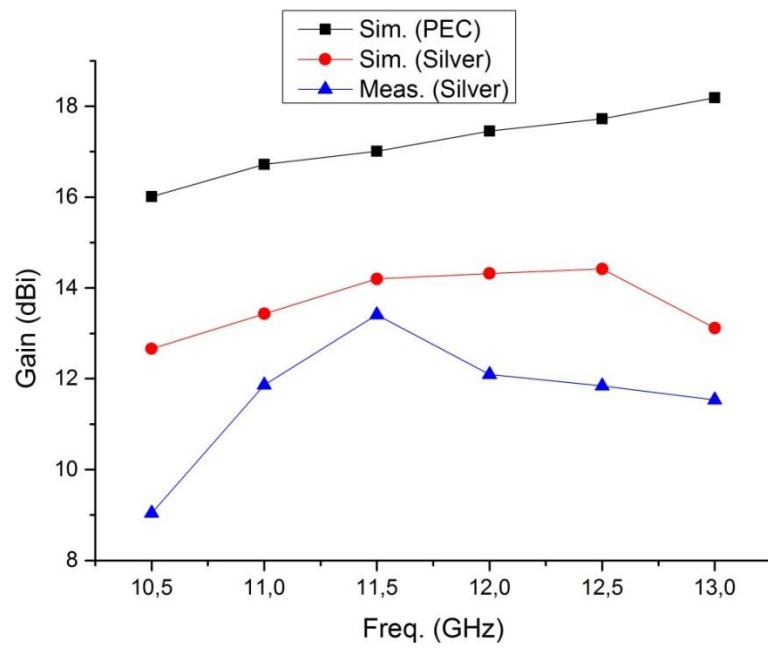


(a)

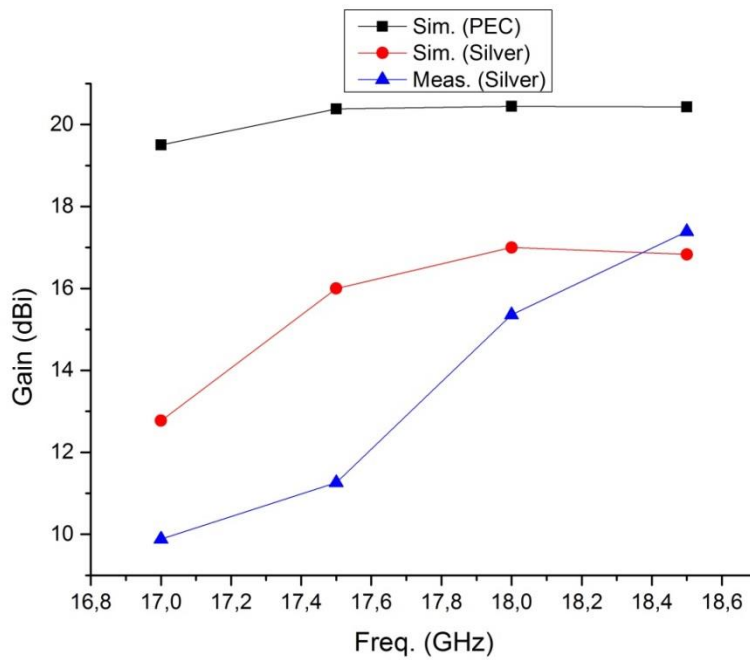


(b)

Figure 5.12. Gain Results of the Fabricated Feeding System with PEC Material and Nickel Coated Diplexer (a) RX side (b) TX side



(a)



(b)

Figure 5.13. Gain Results of the Fabricated Feeding System with PEC Material and Silver Coated Diplexer (a) RX side (b) TX side

The difference in conductivity of the materials is clearly visible in these gain results. Silver-coated results are more consistent than nickel-coated, and the difference between simulation and measurement results are thought to be due to the fact that the spray does not spread evenly over the entire surface in the coating process. Moreover, the reason of the similarity between the simulated gain at 17.5 GHz and measured gain at 17 GHz in Figure 5.13(b) is the shift, which is occurred owing to the coating thickness and observed in insertion loss graphs given in the previous sections.

CHAPTER SIX

CONCLUSIONS AND FUTURE RESEARCH

In this thesis, it is aimed to design a reflector antenna feeding system working in Ku Band for use in satellite communication and media broadcasting. Another important goal in the thesis is to use a cost effective method that can achieve fast results in the prototype production of the designed system. For this reason, 3-D printing and conductive spray coating method is preferred.

The designed feeding system consists of a conical corrugated horn antenna and a diplexer structure which supports the antenna. Three different types of diplexer (H-plane, E-plane and dual-polarized) are designed to use in different polarization depended application areas. In the system, 10.5-12.75 GHz frequency range is preferred as RX band and 17.3-18.4 GHz frequency range is used as TX band, and also diplexer is designed by combining of two band-pass filters which provide separation and isolation of these two channels. The designs are realized by optimizing the initial parameters that obtained from the theoretical researches in the literature by using CST Microwave Studio program in operating environment. After the desired results are achieved, the designed structures are produced using PLA material with Ultimaker 2+ 3-D printer. After production, two different conductive aerosol sprays (nickel and silver) are used for coating and measurements are carried out in Yasar University Antenna and Microwave Laboratory. It is observed that the high conductivity silver spray gives better results for diplexer structure. According to the results, a return loss value of 20 dB over the operating frequency (10-19 GHz) for the corrugated horn antenna is obtained with a gain value of 14.5-20 dBi. For the diplexer, both the TX and RX frequency bands are measured and provide a return loss value better than 15 dB and provide 60-75 dB rejection to each other. Insertion loss levels are observed as 4-5 dB lossy in both bands (RX / TX) compared to a PEC material, but the structure provides the desired band ranges. Finally, it is observed that the system results retain these values and provide the desired characteristics.

With all these results, if we consider the fact that the prototype production of such a system would be completed within 10-12 days with a high cost of CNC between 10000 and 15000 TL, it is possible to use the 3-D printer and conductive spray

coating method for about 1000 TL cost and 2.5 days can be said to be much more advantageous than CNC production. The only disadvantage of this study is to obtain lossy results with respect to the conductivity level of the used coating.

For future research and studies, it is also possible to produce antennas or waveguide structures for different applications by using this method. Furthermore, if these prototypes can be produced with a special coatable ABS material, which is very rare in the market, so that coating with a pure conductive material can be used in real applications according to the resulting power handling capability.



REFERENCES

- Antesky, <http://www.antesky.com/products/1.8m-Flyaway-antenna.html>, last access: 12.08.2018.
- Balanis, C. A. (2012). *Advanced Engineering Electromagnetics* (2nd ed.). Wiley.
- Balanis, C. A. (2005). *Antenna Theory Analysis and Design* (3rd ed.). Wiley.
- Bhutani, A., Schaefer, J., Pauli, M., Scherr, S., Goettel, B., Nierlich, M. & Zwick, T. (2016). 3D Metal Printed Ku/Ka Band Modified Turnstile Junction Orthomode Transducer. *Proceedings of the Asia-Pacific Microwave Conference*.
- Bianchi, G. & Sorrentino, R. (2007). *Electronic Filter Simulation & Design* (1st ed.). McGraw-Hill.
- Bongard, F., Gimersky, M., Doherty, S., Aubry, X. & Krummen, M. (2017). 3D-printed Ka-band Waveguide Array Antenna for Mobile SATCOM Applications. *11th European Conference on Antennas and Propagation (EUCAP)*. 579-583.
- Carmel b.k. Engineering, Israel, “conductive coating pro” [Online]. Available: <http://http://www.carmel-eng.co.il>
- Castro, A.T., Babakhani, B. & Sharma, S.K. (2017). Design and development of a multimode waveguide corrugated horn antenna using 3D printing technology and its comparison with aluminium-based prototype. *IET Microwaves, Antennas & Propagation*, vol. 11, 1977-1984. <http://doi.org/10.1049/iet-map.2016.0808>.
- Cheng, D. K. (1993). *Fundamentals of Engineering Electromagnetics* (1st ed.). Addison-Wesley.
- Chieh, J.C.S., Dick B., Loui S & Rockway J.D. (2014). Development of a Ku-Band Corrugated Conical Horn Using 3-D Print Technology. *IEEE Antennas and Wireless Propag. Lett.*, vol.13, 201-204. <http://doi.org/10.1109/LAWP.2014.2301169>
- Dimitriadis, A.I., Debogović, T., Favre, M., Billod, M., Barloggio, L., Ansermet, J.P. & Rijk, E. (2017). Polymer-Based Additive Manufacturing of High-Performance Waveguide and Antenna Components. *Proc. of the IEEE*, vol.105, 668-676. <http://doi.org/10.1109/JPROC.2016.2629511>.
- Dybdal, R. (2009). *Communication Satellite Antennas: System Architecture, Technology, and Evaluation* (1st ed.). McGraw-Hill.
- Elbert, B. R. (2004). *Satellite Communication Applications Handbook* (2nd ed.). Artech House.
- Elbert, B. R. (2008). *Introduction to Satellite Communication* (3rd ed.). Artech House.
- Elbert, B. R. (2000). *The Satellite Communication Ground Segment and Earth Station Handbook*. (1st ed.). Artech House.

- Genc, A., Basyigit, I.B., Goksu, T. & Helhel, S. (2017). Investigation of the performances of X-Ku band 3D printing pyramidal horn antennas coated with the different metals. *International Conference on Electrical and Electronics Engineering (ELECO)*, 1012-1016.
- Granet, C., & James, G.L. (2005). Design of corrugated horns: A primer. *IEEE Antennas Propag. Mag.*, vol. 47, 76–84.
- Ippolito Jr., L. J. (2008). *Satellite Communications System Engineering* (1st ed.). Wiley.
- Kolawole, M. O. (2014). *Satellite Communication Engineering* (2nd ed.). CRC Press.
- Laplanche, E., Tantot, O., Delhote, N., Périgaud, A., Verdeyme, S., Bila, S., Baillargeat, D. & Carpentier, L. (2017). A ku-band diplexer based on 3dB directional couplers made by plastic additive manufacturing. *47th European Microwave Conference (EuMC), Nuremberg*, 428-431.
- Maral, G., & Bousquet, M. (2010). *Satellite Communication Systems* (5th ed.). Wiley.
- Matthaei, G., Young, L. & Jones, E.M.T. (1980). *Microwave Filters, Impedance-Matching Networks, and Coupling Structures* (1st ed.). Artech House.
- Menargues, E., Garcia-Viguares, M., Debogovic, T., Capdevila, S., Dimitriadis, A.I., Rijk, E. & Mosig, J.R. (2017). 3D printed feed-chain and antenna components. *IEEE International Symposium on Antennas and Propagation & USNC/URSI National Radio Science Meeting, San Diego*, 1-2.
- Menargues, E., Favre, M., Dimitriadis, A.I., Capdevila, S., Debogovic, T., Mosig, J.R., Vorst, M.v.d. & Rijk, E. (2017). Polymer-based metal coated additive manufactured V- and W-band antenna feed chain components. *11th European Conference on Antennas and Propagation (EUCAP), Paris, France*. 584-588.
- MG Chemicals, Surrey, BC, Canada, “Super Shield nickel conductive coating 841 technical data sheet,” [Online]. Available: <http://www.mgchemicals.com>
- Midtbøen, V., Kjelgård, K.G. & Lande, T.S. (2017). 3D Printed Horn Antenna with for PCB Microstrip Feed UWB Radar Applications. *IEEE MTT-S International Microwave Workshop Series on Advanced Materials and Processes for RF and THz Applications (IMWS-AMP), Pavia, Italy*. 1-3. doi: 10.1109/IMWS-AMP.2017.8247374
- Milligan, T. (2005). *Modern Antenna Design* (2nd ed.). Wiley&Sons.
- Mirzaee, M., Noghianian, S., Wiest, L. & Chang, I. (2015). Developing flexible 3D printed antenna using conductive ABS materials. *IEEE International Symposium on Antennas and Propagation & USNC/URSI National Radio Science Meeting, Vancouver, BC, Canada*. 1308-1309.

- Musthofa, M.F.Y. & Munir, A. (2011). Design of rectangular to circular waveguide converter for S-band frequency. *Proc. 2011 International Conference on Electrical Engineering and Informatics, Bandung*. 1-5.
- Noorani, R. (2018). *3D Printing Technology, Applications, and Selection* (1st ed.). CRC Press.
- Olver, A.D., Clarricoats, P.J.B., Kishk, A.A. & Shafai, L. (1994). *Microwave Horns and Feeds* (1st ed.). IEEE Press.
- Pozar, D. M. (2012). *Microwave Engineering* (4th ed.). Wiley.
- Ragan, G. L. (1948). *Microwave Transmission Circuits* (1st ed.). McGraw-Hill.
- Rao, S., Sharma, S. K., & Shafai, L. (2013). *Handbook of Reflector Antennas and Feed Systems vol.1* (1st ed.). Artech House.
- Rao, S., Sharma, S. K., & Shafai, L. (2013). *Handbook of Reflector Antennas and Feed Systems vol.2* (1st ed.). Artech House.
- Rao, S., Sharma, S. K., & Shafai, L. (2013). *Handbook of Reflector Antennas and Feed Systems vol.3* (1st ed.). Artech House.
- Shang, X., Penchev, P., Guo, C., Lancaster, M.J., Dimov, S., Dong, Y., Favre, M., Billod, M. & Rijk, E. (2016). W -Band Waveguide Filters Fabricated by Laser Micromachining and 3-D Printing. *IEEE Trans. Microw. Theory Techn.*, vol. 64, 2572-2580. <http://doi.org/10.1109/TMTT.2016.2574839>.
- Silva, J.S., Garcia-Vigueras, M., Debogović, T., Costa, J.R., Fernandes, C.A. & Mosig, J.R. (2017). Stereolithography-Based Antennas for Satellite Communications in Ka-Band. *Proc. of the IEEE*, vol.105, 655-667. <http://doi.org/10.1109/JPROC.2016.2633898>
- Sorrentino, R. & Bianchi, G. (2010). *Microwave and RF Engineering* (1st ed.). Wiley.
- Stutzman, W. L., & Thiele, G.A. (2013). *Antenna Theory and Design* (3rd ed.). Wiley.
- Uher, J., Bornemann, J., & Rosenberg, U. (1993). *Waveguide Components for Antenna Feed Systems: Theory and CAD* (1st ed.). Artech House.
- Umar, A. (2004). *Mobile Computing and Wireless Communications* (1st ed.). NGE Solutions.
- Yao, H., Sharma, S., Henderson, R., Ashrafi, S. & MacFarlane, D. (2017) Ka band 3D printed horn antennas. *Texas Symposium on Wireless and Microwave Circuits and Systems (WMCS), Waco, TX*. 1-4. [doi:10.1109/WMCaS.2017.8070701](https://doi.org/10.1109/WMCaS.2017.8070701)
- Zhang, B. & Zirath, H. (2016). A Metallic 3-D Printed E-Band Radio Front End. *IEEE Microwave and Wireless Components Letters*, vol.26, 331-333.